Columbus crater and other possible groundwater-fed paleolakes of Terra Sirenum, Mars

J. J. Wray,[1] R. E. Milliken,[2] C. M. Dundas,[3] G. A. Swayze,[4] J. C. Andrews-Hanna,[5] A. M. Baldridge,[6] M. Chojnacki,[7] J. L. Bishop,[8] B. L. Ehlmann,[9] S. L. Murchie,[10] R. N. Clark,[4] F. P. Seelos,[10] L. L. Tornabene,[11] and S. W. Squyres[1]

Received 12 July 2010; revised 15 October 2010; accepted 3 November 2010; published 5 January 2011.

[1] Columbus crater in the Terra Sirenum region of the Martian southern highlands contains light-toned layered deposits with interbedded sulfate and phyllosilicate minerals, a rare occurrence on Mars. Here we investigate in detail the morphology, thermophysical properties, mineralogy, and stratigraphy of these deposits; explore their regional context; and interpret the crater's aqueous history. Hydrated mineral-bearing deposits occupy a discrete ring around the walls of Columbus crater and are also exposed beneath younger materials, possibly lava flows, on its floor. Widespread minerals identified in the crater include gypsum, polyhydrated and monohydrated Mg/Fe-sulfates, and kaolinite; localized deposits consistent with montmorillonite, Fe/Mg-phyllosilicates, jarosite, alunite, and crystalline ferric oxide or hydroxide are also detected. Thermal emission spectra suggest abundances of these minerals in the tens of percent range. Other craters in northwest Terra Sirenum also contain layered deposits and Al/Fe/Mg-phyllosilicates, but sulfates have so far been found only in Columbus and Cross craters. The region's intercrater plains contain scattered exposures of Al-phyllosilicates and one isolated mound with opaline silica, in addition to more common Fe/Mg-phyllosilicates with chlorides. A Late Noachian age is estimated for the aqueous deposits in Columbus, coinciding with a period of inferred groundwater upwelling and evaporation, which (according to model results reported here) could have formed evaporites in Columbus and other craters in Terra Sirenum. Hypotheses for the origin of these deposits include groundwater cementation of crater-filling sediments and/or direct precipitation from subaerial springs or in a deep (~900 m) paleolake. Especially under the deep lake scenario, which we prefer, chemical gradients in Columbus crater may have created a habitable environment at this location on early Mars.

Citation: Wray, J. J., et al. (2011), Columbus crater and other possible groundwater-fed paleolakes of Terra Sirenum, Mars, *J. Geophys. Res.*, *116*, E01001, doi:10.1029/2010JE003694.

1. Introduction

[2] The modern surface of Mars is frigid and desiccated at low latitudes, but many observations suggest that liquid water once played a substantial role in shaping the surface geology. The presence of hydrous minerals attests to water-rock interactions during the Noachian and Hesperian Periods [e.g., *Squyres et al.*, 2004b; *Bibring et al.*, 2006], a time that coincides with the formation of valley networks that suggest liquid water flowed across the surface [e.g., *Baker*, 1982; *Carr*, 1995; *Fassett and Head*, 2008a]. Although in some cases surface water may have been ephemeral [*Segura et al.*, 2002], evidence also exists for standing bodies of water that may have persisted for hundreds to tens of thousands of years or longer [e.g., *Moore et al.*, 2003; *Fassett and Head*, 2005; *Grant et al.*, 2008].

[1]Department of Astronomy, Cornell University, Ithaca, New York, USA.
[2]Department of Civil Engineering and Geological Sciences, University of Notre Dame, Notre Dame, Indiana, USA.
[3]Lunar and Planetary Laboratory, University of Arizona, Tucson, Arizona, USA.
[4]U.S. Geological Survey, Denver, Colorado, USA.
[5]Department of Geophysics, Colorado School of Mines, Golden, Colorado, USA.
[6]Jet Propulsion Laboratory, California Institute of Technology, Pasadena, California, USA.
[7]Department of Earth and Planetary Sciences, University of Tennessee, Knoxville, Tennessee, USA.
[8]SETI Institute, Mountain View, California, USA.
[9]Institut d'Astrophysique Spatiale, Université Paris Sud, Orsay, France.
[10]Johns Hopkins University Applied Physics Laboratory, Laurel, Maryland, USA.
[11]Center for Earth and Planetary Studies, National Air and Space Museum, Smithsonian Institution, Washington, D. C., USA.

0148-0227/11/2010JE003694

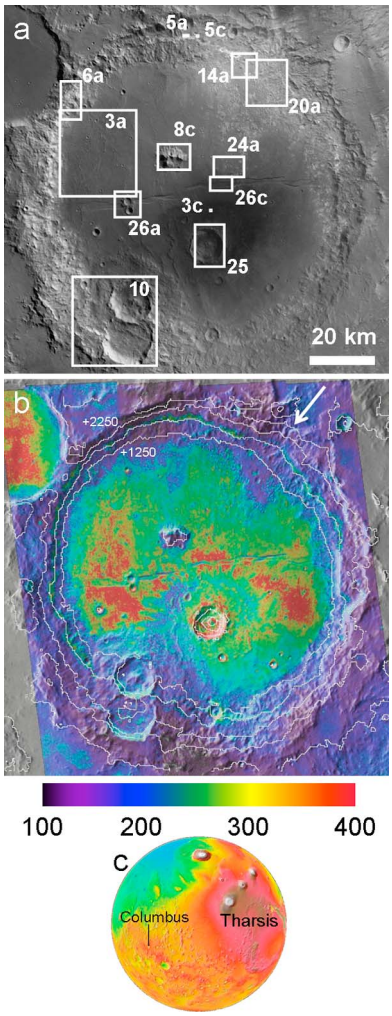

Figure 1. Two views of Columbus crater (29°S, 166°W). (a) HRSC nadir channel mosaic. Here and subsequently, numbered outlines indicate locations of future figures; north is up, unless indicated otherwise. (b) THEMIS daytime IR band 9 mosaic, colorized with THEMIS-derived thermal inertia (scale bar units are tiu). Superposed contours are MOLA elevations spaced 500 m apart, beginning at +250 m. Note medium-inertia (green) materials following the 1750 m contour around the crater walls. Arrow indicates small valleys on northeast wall, as described in the text (sections 2 and 5). (c) Location of Columbus crater on MOLA global topographic map.

[3] Impact craters are the most common type of basin on the Martian surface in which ancient water could have ponded. Hundreds of candidate crater paleolakes have been identified based on morphologic evidence such as inlet and/or outlet valleys, fan-shaped (possibly deltaic) deposits, and putative shoreline features [e.g., *Forsythe and Blackwelder*, 1998; *Cabrol and Grin*, 1999; *Fassett and Head*, 2008b]. Because of their potential for habitability and preservation of biosignatures in sediments deposited in a quiescent environment, paleolakes are considered high-priority targets in the astrobiological exploration of Mars [e.g., *Farmer and Des Marais*, 1999; *Ehlmann et al.*, 2008a].

[4] Minerals formed in paleolakes record ancient environmental conditions because evaporites and other precipitates can reflect both lake chemistry and the composition of atmospheric or other volatile reservoirs with which the lake water was in contact; for example, the relative partial pressures of CO_2 and SO_2 in the Martian atmosphere and their effects on surface water could have determined whether evaporites were carbonate-rich or sulfate-rich [*Bullock and Moore*, 2004]. The potential value of paleolake evaporites has prompted many searches for them, but while sulfates and chlorides have been identified in canyons, intercrater plains, and some craters [e.g., *Squyres et al.*, 2004b; *Gendrin et al.*, 2005; *Osterloo et al.*, 2008], the mineralogic results for classic morphologic paleolakes have been largely negative [*Ruff et al.*, 2001; *Squyres et al.*, 2004a; *Stockstill et al.*, 2005, 2007]. Recent orbital detections of phyllosilicates in a few paleolakes [*Ehlmann et al.*, 2008a; *Dehouck et al.*, 2010; *Milliken and Bish*, 2010; *Ansan et al.*, 2010] suggest that evaporite salts might be found using similar techniques.

[5] A spectral survey covering much of the southern highlands in search of new hydrated mineral exposures [*Wray et al.*, 2009a] identified a unique group of craters in northwest Terra Sirenum that contain Al-phyllosilicates (first reported in Cross crater by *Poulet et al.* [2007]) and hydrated sulfates in finely bedded deposits. The alteration mineral assemblages in these craters are reminiscent of those associated with terrestrial acid-saline lakes and groundwaters [*Benison et al.*, 2007; *Baldridge et al.*, 2009; *Story et al.*, 2010]. By analogy, the Terra Sirenum crater deposits may be lacustrine evaporites; even if not, their mineralogic and morphologic properties define a distinct class of aqueous deposit on Mars [*Murchie et al.*, 2009b]. Here we investigate in detail the morphology, thermophysical properties, mineralogy, and stratigraphy of these deposits; we then examine hypotheses for their origin to better determine their implications for ancient Martian environments. We focus first on Columbus crater (29°S, 166°W), where the greatest diversity of hydrated minerals is observed, and then look at nearby craters with similar deposits. Key data sets used in this study include the Mars Reconnaissance Orbiter (MRO)'s High Resolution Imaging Science Experiment (HiRISE) [*McEwen et al.*, 2007], Compact Reconnaissance Imaging Spectrometer for Mars (CRISM) [*Murchie et al.*, 2007], and Context Camera (CTX) [*Malin et al.*, 2007], as well as the High Resolution Stereo Camera (HRSC) [*Neukum and Jaumann*, 2004] on board Mars Express, the Thermal Emission Imaging System (THEMIS) [*Christensen et al.*, 2004a] on Mars Odyssey, and the Mars Orbiter Laser Altimeter (MOLA) [*Smith et al.*, 2001] and Thermal Emission Spectrometer (TES) [*Christensen et al.*, 2001a] on Mars Global Surveyor.

2. Morphology of Columbus Crater

2.1. General Characteristics

[6] Columbus crater lies in northwest Terra Sirenum in the southern highlands of Mars. Immediately surrounding Columbus are highly cratered plains of the Npl_1 unit [*Scott and Tanaka*, 1986], dated to the Middle Noachian Epoch [*Tanaka*, 1986]. Fluvial dissection is sparse here compared to other regions of the Noachian southern highlands [*Carr*, 1995; *Hynek et al.*, 2010], although this may be partly due to

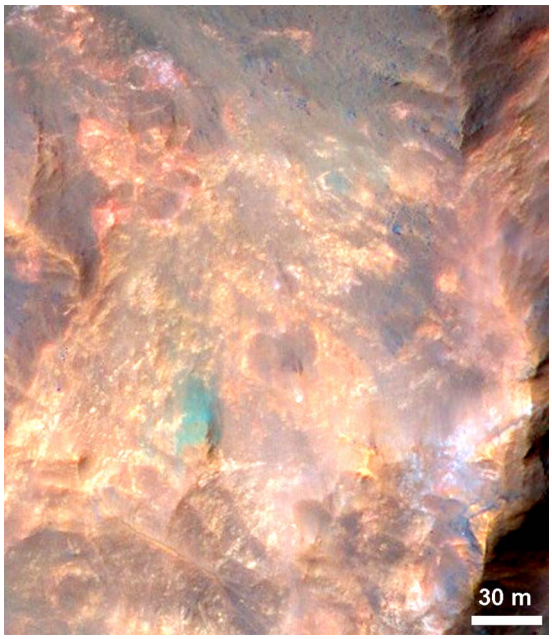

Figure 2. Megabreccia in hills on Columbus crater floor; from HiRISE ESP_016083_1505. Diverse colors likely indicate diverse rock compositions. Context shown in Figure 8c.

poor preservation, as the plains ~100 km to the east, south, and west of Columbus were largely resurfaced in the Late Noachian by materials in the $Np1_2$ unit of *Scott and Tanaka* [1986].

[7] Columbus itself has a well-preserved rim, with no breaches by valleys entering or exiting the crater (Figure 1). A few small valleys cut the northeast inner crater wall (Figure 1b), but their alcoves do not extend beyond the crater rim and they probably did not supply substantial fluvial sediment to the crater. The crater diameter is ~110 km, with a rim crest at 3000 ± 200 m (MOLA elevation relative to the geoid [*Smith et al.*, 1999]): well above the surrounding plains, which span 2200–2700 m in elevation. This rim height is typical for minimally degraded large craters of this size [*Garvin et al.*, 2003]; by contrast, Columbus's flat floor at 920 ± 30 m implies a current depth ~1.5 km less than fresh craters of this diameter, suggesting substantial infill by sedimentary and/or volcanic materials. Further evidence for significant infill and/or erosion of the crater interior is furnished by the lack of a central peak or peak ring. A single hill complex ~15 km NNW of crater center (Figure 1) could be a lone remnant of a peak ring (or an off-center peak), although its height (~700 m above the floor) exceeds that typical for central peaks in craters of this size (~440 m based on the relation of *Garvin et al.* [2003] for craters up to 100 km in diameter). These hills expose megabreccia (Figure 2), like many crater central uplifts on Mars [*McEwen et al.*, 2008].

[8] The flat portions of Columbus's floor have a relatively high thermal inertia (Figure 1b). We derived thermal inertia maps (~100 m/pixel) from THEMIS nighttime infrared (IR) images [*Fergason et al.*, 2006] using the thermal model of *Putzig and Mellon* [2007]. This method uses THEMIS band 9 (12.57 μm) nighttime brightness temperature images to derive best fit thermal inertia by interpolation with a seven-dimensional lookup table using season, time of day, latitude, thermal inertia, albedo, elevation, and visible dust opacity [*Putzig and Mellon*, 2007]. Columbus's eastern crater floor exhibits thermal inertia up to ~510 ± 30 $J \cdot m^{-2} s^{-0.5} K^{-1}$ (units hereafter abbreviated "tiu," after *Putzig and Mellon* [2007]). For comparison, thermal inertias >386 tiu were classified as "very high" by *Putzig et al.* [2005] and likely indicate high rock abundance and/or exposures of bedrock or other indurated surfaces. For example, in the Nili Patera caldera of Syrtis Major, thermal inertias of ~500 tiu are interpreted as indicative of a relatively fresh lava flow surface underlying minor amounts of unconsolidated material [*Fergason et al.*, 2006].

[9] High-resolution images of the Columbus crater floor reveal a rugged texture at decameter scales (Figure 3b), with good retention of small craters. Meter-scale boulders are also visible, further suggesting a cohesive surface material that breaks up to form the boulders; this material could be a strongly cemented sedimentary deposit or a lava flow. On

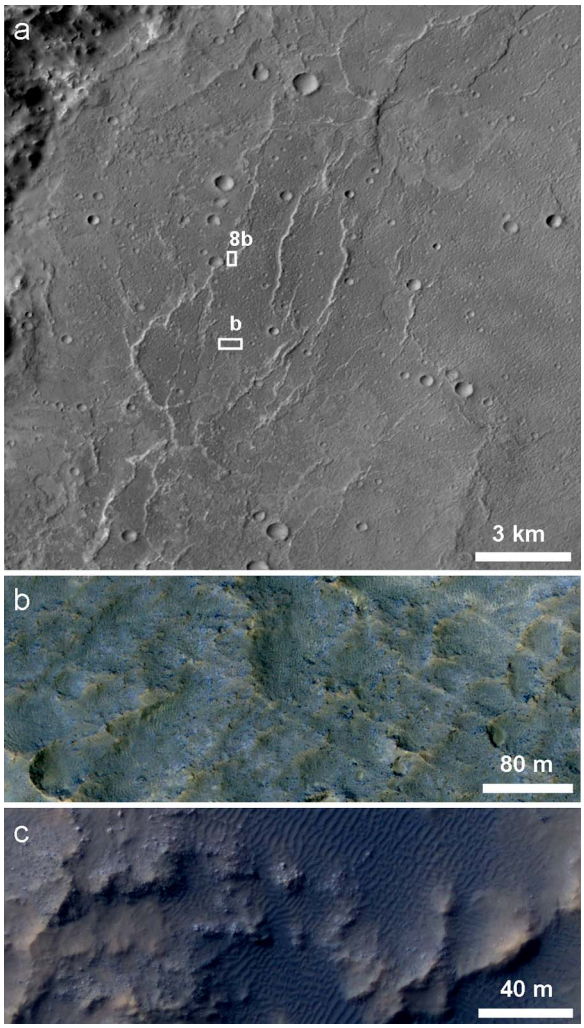

Figure 3. (a) Ridged western floor of Columbus crater; from CTX P03_002739_1505. (b) Dark rugged materials covering much of Columbus's floor, with meter-scale boulders just visible; from HiRISE PSP_004018_1505. (c) Sample of dark, lobate ejecta of D ~11 km crater on Columbus's floor; from HiRISE PSP_008356_1500. Dark materials occur in both aeolian bed forms and meter-scale blocks.

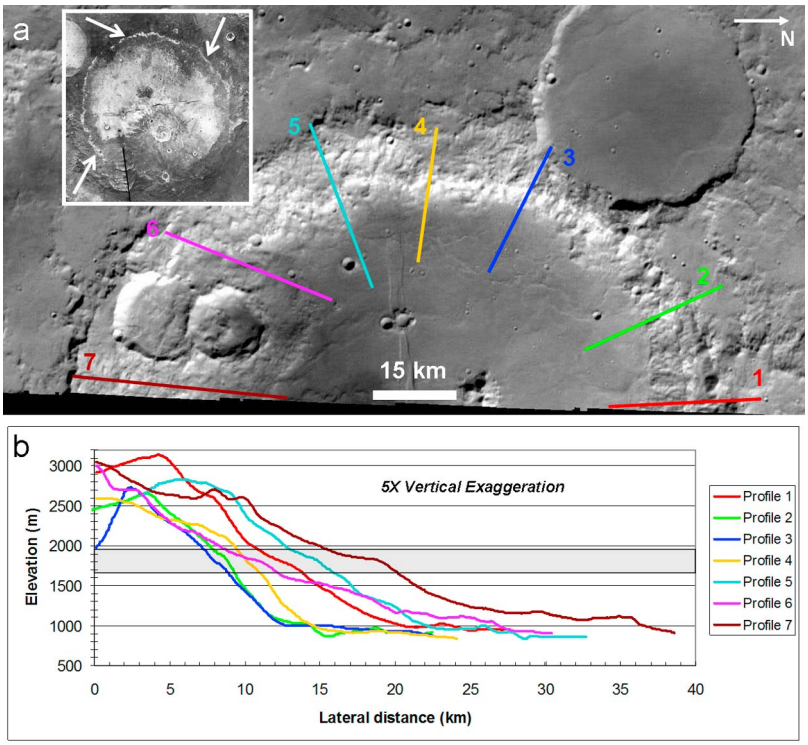

Figure 4. (a) Portion of HRSC h0538_0000 (red filter) covering the western half of Columbus crater. Inset is THEMIS nighttime IR mosaic of Columbus crater, showing a ring of light-toned deposits on the crater walls (arrows). (b) Crater wall elevation profiles, with colors and numbers corresponding to transects shown in Figure 4a. Gray zone marks elevation range of light-toned ring, at which many profiles show a convex-up break in slope.

the western crater floor, a series of ridges is observed (Figure 3a). These are generally segmented in planform and asymmetric in profile, with one steep scarp (most commonly west facing) and a broader, shallower rise on the other side. This morphology is characteristic of wrinkle ridges, as observed in layered materials (most commonly lava flows) on the Moon and terrestrial planets including Mars [*Mueller and Golombek*, 2004]. Wrinkle ridges are generally interpreted as blind thrust faults. On Mars, they are typically observed in Early Hesperian ridged plains, interpreted as low-viscosity lava flows [*Scott and Tanaka*, 1986]. Taken together, the wrinkle ridges and other textural and thermophysical characteristics of Columbus crater's floor are strongly suggestive of a lava flow, although we cannot rule out other possibilities such as lithified aeolian deposits. A 40 km diameter crater that cuts the northwest rim of Columbus (Figure 1) has a similarly flat floor with wrinkle ridges and a relatively high thermal inertia (~420 ± 30 tiu), suggesting that it contains similar deposits. The source of these putative lavas is not apparent, as is typically the case for ridged plains on Mars [*Greeley and Spudis*, 1981].

[10] Other notable characteristics of Columbus crater include a graben cutting east to west across the crater floor, and an 11 km diameter crater whose radial ejecta have darkened a large portion of Columbus's southern floor (Figure 1a). These dark materials (TES albedo ~ 0.11) form aeolian bed forms and have a thermal inertia (~250 tiu) consistent with medium sand [*Presley and Christensen*, 1997], but meter-scale blocks are also present (Figure 3c). This 11 km crater and a 14 km diameter crater on the southwest floor have lobate, single-layer ejecta, which are thought to result from fluidization of subsurface volatiles in the impact target materials [e.g., *Barlow and Perez*, 2003].

2.2. Light-Toned Layered Deposits

[11] Figure 1a shows outcrops of relatively light-toned materials scattered across the northeast quadrant of Columbus crater's floor, and in a discrete band approximately halfway down its walls: especially the northern and eastern walls. This band of material is more evident in Figure 1b (see also Figure 4a, inset), which shows its higher thermal inertia relative to adjacent crater wall materials, consistent with a more indurated surface. Thermal inertia of the light-toned materials is ~290 ± 40 tiu, within the range of values found for light-toned layered deposits in Terra Meridiani [*Arvidson et al.*, 2003] and Valles Marineris [*Fergason et al.*, 2006; *Mangold et al.*, 2008; *Chojnacki and Hynek*, 2008]. These values contrast with thermal inertias of ~130–190 tiu for the adjacent darker crater wall materials, which are likely surfaces dominated by loose fines.

[12] The light-toned deposits trace a nearly continuous ring around the eastern, northern, and western crater walls, at a near-constant elevation of 1800 ± 150 m (Figure 1b). At this elevation, crater wall profiles from an HRSC digital elevation model (DEM) show a convex-up break in slope at many (though not all) azimuths (Figure 4). The ring is interrupted by the *D* ~14 km crater on the southwest floor, and by the previously mentioned valleys on the northeast

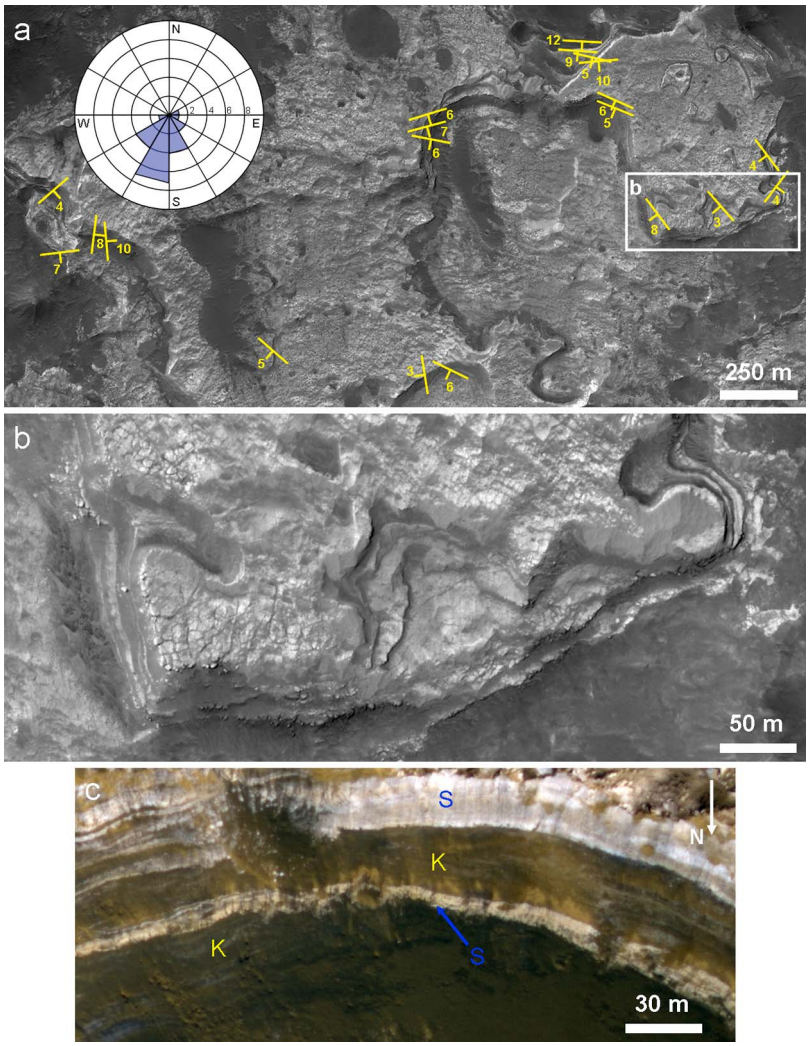

Figure 5. Light-toned layered materials on Columbus's northern wall, part of the deposit that rings the crater walls. (a) Portion of HiRISE PSP_005429_1510, with bedding strike and dip measurements (degrees) from HiRISE DEM superposed. Dip direction histogram "rose plot" (inset) highlights the predominance of southward dips. (b) Meter-scale bedding and meter-to-decameter-scale polygonal fracture patterns. (c) Light-toned beds and underlying darker beds of Columbus wall ring exposed in southern wall of small (D ~750 m) superposed crater; from ESP_013182_1515. S, sulfate-bearing; K, kaolinite-bearing [*Wray et al.*, 2009a, Figures DR6, DR7].

wall. On the southeast wall, it is poorly exposed at the resolution of Figure 1, but higher-resolution images (HRSC, CTX, HiRISE) reveal small exposures of light-toned outcrop here as well, albeit largely covered by darker surficial materials. This 360° ring of light-toned, indurated material is perhaps the most striking morphologic aspect of Columbus crater, and to our knowledge it is unique (or at least uniquely well preserved) among Martian craters.

[13] High-resolution images of Columbus's ring show stratification at meter scales (Figure 5). Beds are typically light-toned, but some darker beds are observed low in the section (Figure 5c) [see also *Wray et al.*, 2009a, Figure 4c]. Successive beds exposed in cross section appear approximately parallel, and to date we have observed no unambiguous angular unconformities, although this is typical for orbital observations even at HiRISE scale (~30 cm/pixel) and even where decimeter to meter-scale cross beds are known to exist from rover observations [e.g., *Grotzinger et al.*, 2005]. Further insight into bed geometries can be gleaned via strike and dip measurements from a high-resolution DEM. We use a DEM with 1 m grid spacing and vertical precision ~0.2 m produced from HiRISE images PSP_005429_1510 and PSP_005851_1510 via the techniques of *Kirk et al.* [2008]. These images cover a well-exposed portion of the Columbus wall ring (Figure 5a shows a subset), where some individual beds can be traced across >1 km of outcrop.

[14] We measured bed strike and dip angles from the DEM using multilinear regression to find the best fit plane through a set of points chosen manually along a bed. For each of twenty beds exposed within the area of Figure 5a, we selected between 8 and 28 points, which in all cases were well fit by a plane, with r^2 values of 99.5% or higher.

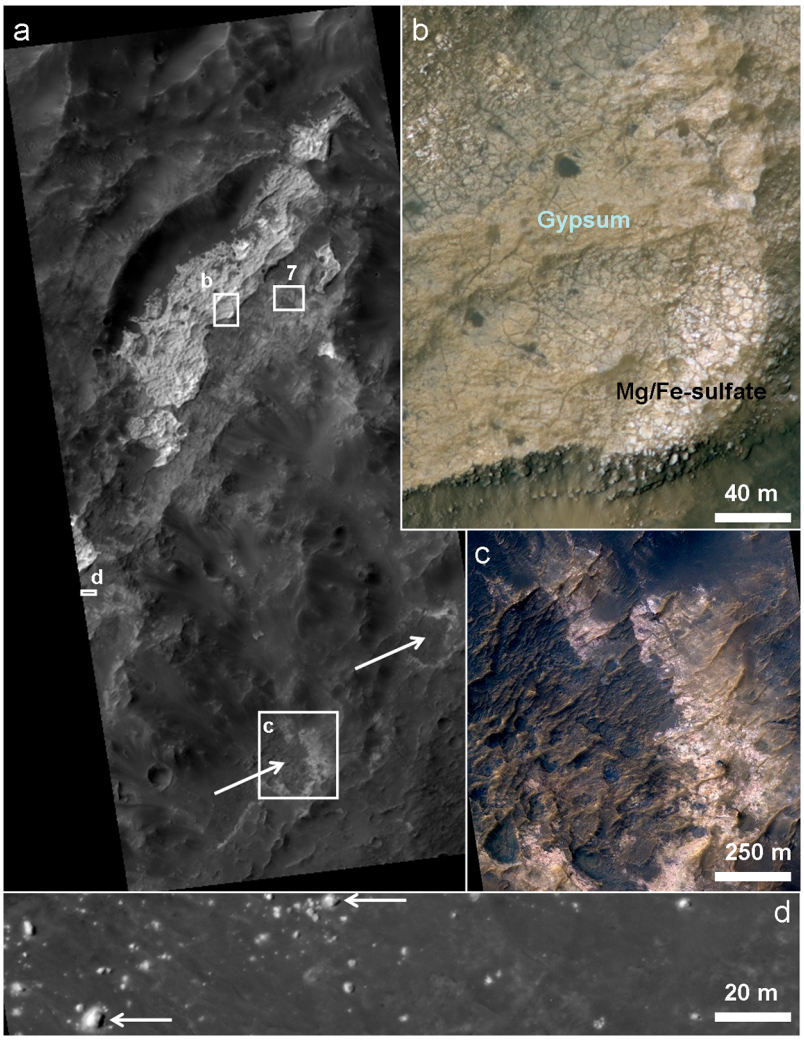

Figure 6. (a) HiRISE image ESP_013960_1510, showing a portion of the Columbus ring perched on a wall terrace as well as two bright-ringed pits (arrows) on the crater floor. (b) Textural and albedo contrast between different spectral (mineralogic) units within the ring. (c) Color diversity in the light-toned materials ringing a pit on Columbus's floor, which is filled with dark-toned materials. (d) Light-toned blocks downslope from Columbus's wall ring; note "halos" of bright-toned material surrounding many blocks (e.g., arrows).

Measured dip angles generally range from 3° to 10°, with a mean of 6.4° (median 6.3°) and typical uncertainties of ~1.0° (95% confidence level). Dip directions generally range from 125° to 235° clockwise from north, with most uncertainties <10°. Where multiple overlying beds can be measured on the same escarpment, their dips and dip directions are typically consistent with each other within the uncertainties, supporting the inference that bedding is conformable. The mean dip direction at this location is 183°, almost directly due south and toward the crater interior. These dip directions are measured from escarpments facing a range of azimuths (Figure 5a).

[15] DEM measurements also allow estimation of the total thickness of the Columbus wall ring deposits. Bed dips are used to calculate their true stratigraphic thickness (which is only equivalent to scarp height if bedding is horizontal), yielding an estimate of ~20 m total thickness of light-toned beds in the deepest exposures.

[16] Ring bed surfaces have a range of textures, but fracturing is common, typically yielding polygonal "tiles" a few to ~10 m across (Figures 5b and 6b). Polygon borders are typically darker than their interiors, probably due to shadowing and/or filling of fractures by fine-grained materials darker than the outcrop. However, bright polygon borders are observed in a few outcrops of the darker rocks immediately underlying Columbus's light-toned ring (Figure 7). Relative brightness may indicate that these polygon borders are intrinsically lighter-toned and/or relatively highstanding.

[17] Immediately downslope (toward the crater interior) from escarpments of Columbus ring materials, light-toned blocks up to several meters across are observed (Figure 6d). Many of these blocks are surrounded by "halos" of light-toned surface material, reminiscent of the "Gray Rock Soil" concentrations observed around "Gray Rocks" by the Imager for Mars Pathfinder [*Bell et al.*, 2002]. Those soils

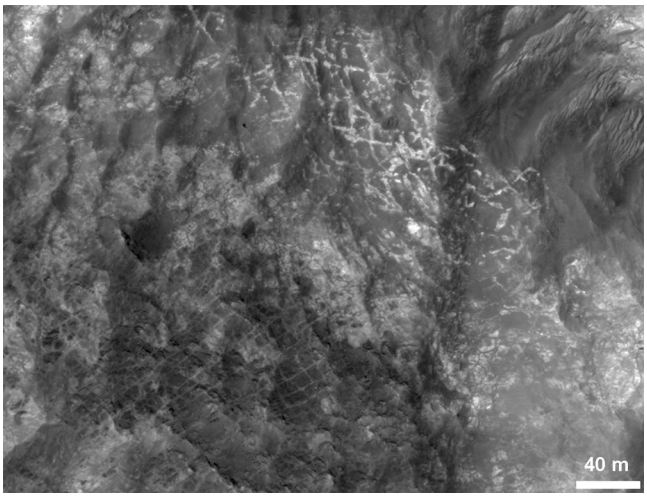

Figure 7. Light-toned material filling fractures in kaolinite-bearing outcrop underlying Columbus's wall ring; from HiRISE ESP_013960_1510. Location is shown in Figure 6a.

were inferred to be flakes or spalls from the rocks that they surround, subsequently comminuted and mixed with other aeolian fines. In the rocks of the Columbus ring, pervasive fractures may promote physical weathering and rockfall, after which blocks are worn away by aeolian erosion and further weathering.

[18] Light-toned materials are visible (Figure 1a) not only in the ring around Columbus's walls, but also on parts of the crater floor not covered by the possible lava flows discussed previously, particularly in the crater's northeast quadrant. Figure 8a shows a representative outcrop from this area, with dozens of meter-scale beds exposed in cross section. Strata exposed on the crater floor are typically darker-toned and show less relative contrast than strata in the ring along the crater wall. Boulders sourced from these beds are rare. As with the wall ring deposit, no clear angular unconformities between successive beds are visible, although it is difficult to trace individual beds over long distances due to debris cover and erosional topography.

[19] Light-toned materials on the western crater floor are most commonly exposed in (typically west facing) escarpments of wrinkle ridges (Figure 3a). Figure 8b shows an example, where light-toned materials crop out beneath darker materials. Other exposures of light-toned material on the crater floor are generally limited to the ejecta and walls of small superposed craters (see section 5), and to a narrow zone at the base of Columbus's crater walls where the younger lava flow may be thin to absent. For example, Figure 6a shows two bright-ringed pits on the northwestern crater floor edge, both filled with dark materials. Color diversity in the light-toned rocks exposed in these pits (Figure 6c) suggests that diverse lithologies may be present. One final location where light-toned materials are found is in the hills ~15 km NNW of the crater's center (Figure 8c). These hills, which have a fairly sharp crest line, appear to be predominantly composed of dark-toned material along with megabreccia (Figure 2). However, light-toned deposits that are morphologically (and mineralogically) similar to those in the Columbus wall ring are present at a range of elevations, up to the highest peak in the hills (Figures 8c–8d).

3. Mineral Identification and Distribution at Columbus

[20] To constrain the compositions of materials in Columbus crater (especially the light-toned deposits described in section 2.2) we used orbital infrared spectroscopy. For visible and near-infrared (NIR) wavelengths, multiple scattering dominates the reflected light signal from particulate and textured surfaces, and absorption band strengths often are not linearly proportional to mineral abundances [e.g., *Clark*, 1999]. This nonlinearity can allow minor mineralogic components to be detected, but it often prevents simple mineral abundance estimates via linear mixture modeling, as is commonly done at thermal infrared wavelengths. Although preliminary estimates of Martian secondary mineral abundances from NIR spectra are intriguing [*Poulet et al.*, 2008b], we limit our scope in this section to simply identifying these minerals using CRISM data; abundances are discussed in section 4 on the basis of thermal emission spectra.

[21] Most CRISM science observations fall into one of two categories: multispectral survey mapping or hyperspectral targeted imaging [*Murchie et al.*, 2007, 2009c]. In both cases, pixels having spectral absorptions characteristic of hydrated minerals can be mapped using spectral summary (i.e., mineral indicator) parameters [*Pelkey et al.*, 2007]. Figure 9a shows maps corresponding to olivine, Al-phyllosilicates, and hydrated sulfates derived from ~200 m/pixel multispectral mosaics. Olivine is present in the ejecta of small craters superposed on Columbus's floor (red tones in Figure 9a); in particular, the dark ejecta of the D ~11 km crater on the southern floor contain the strongest olivine signature observed by CRISM within several hundred kilometers of this location. Al-phyllosilicates (green tones) are present in the light-toned materials widespread across the northeast crater floor, at several locations on the crater walls, and in a narrow strip on the southeast floor at the foot of the crater wall. Weak signatures indicative of hydrated sulfates are detected in some locations on the crater floor (blue tones), but they are most apparent in the light-toned ring around the crater wall, including where this ring extends onto the floor of the D ~17 km crater shown in Figure 10. For more specific mineral identifications and correlations to surface morphology, we devote the remainder of this section to analysis of CRISM hyperspectral targeted observations.

3.1. Spectral Processing Methods

[22] CRISM I/F data were processed as described by *Murchie et al.* [2009c], including division by the cosine of the solar incidence angle and atmospheric removal via division by a scaled transmission spectrum derived from observations over Olympus Mons [*McGuire et al.*, 2009]. Spatial and spectral noise filtering [*Parente*, 2008] were also applied. Spectra from many pixels were averaged to improve the signal-to-noise ratio (SNR), and the resulting average spectra were divided by a spectral average from a dusty or otherwise spectrally "neutral" region in the same CRISM scene. This spectral ratio method suppresses resid-

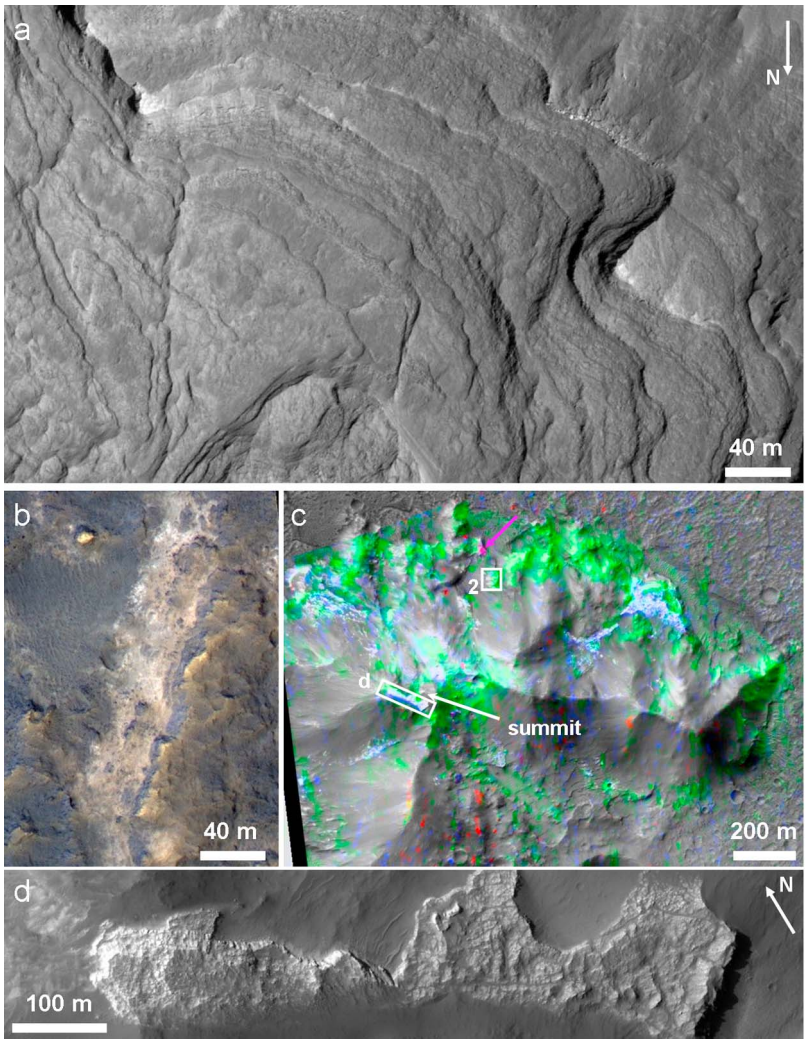

Figure 8. Light-toned deposits on Columbus crater floor. (a) Bedded outcrop on northeast crater floor; from HiRISE PSP_010281_1510. Location is shown in Figure 20a. (b) Light-toned material exposed in west facing escarpments of ridges on western crater floor; from HiRISE PSP_004018_1505. Location is in Figure 3a. (c) Light-toned deposits in hills on north/central crater floor; from CTX P12_005851_1505, colored with spectral parameter maps from CRISM FRT0001663B. Red is BD2100 [*Pelkey et al.*, 2007], green is BD2200 [*Ehlmann et al.*, 2009], and blue is SINDEX [*Roach et al.*, 2009]. Green materials contain kaolinite, blue materials contain polyhydrated sulfate, and magenta materials contain monohydrated sulfate (arrow). (d) Sample of light-toned deposits near summit of Columbus floor hill complex; from HiRISE ESP_016083_1505. Note morphologic similarity to deposits ringing Columbus's walls (e.g., Figure 5b).

ual artifacts of instrument calibration and atmospheric removal [e.g., *Mustard et al.*, 2008] while accentuating spectral signatures in the numerator spectrum that are unique relative to the denominator. Known artifacts that remain in some ratio spectra include a discontinuity near 1.65 μm due to a detector filter boundary and small features near 2.0 μm resulting from imperfect removal of atmospheric CO_2 bands [*Murchie et al.*, 2009c]; we have masked some of these known "bad bands" in the spectra plotted here.

[23] CRISM has a VNIR detector spanning ~0.4–1.0 μm and an IR detector spanning ~1.0–4.0 μm. Except for section 3.4, we focus on IR detector data because this wavelength range is less affected by ferric minerals in rock coatings and surficial dust [*Swayze*, 2004; *Cloutis et al.*, 2006], and it includes diagnostic absorptions for mafic minerals, carbonates, and hydrated or hydroxylated minerals including sulfates and phyllosilicates [e.g., *Ehlmann et al.*, 2009]. We devote most of our attention to the region from 1.0 to 2.6 μm, as beyond 2.6 μm CRISM data have lower SNR and several known instrument artifacts [*Murchie et al.*, 2009c]. In addition, wavelengths longer than 3 μm typically include a contribution from thermal emission that reduces absorption band strengths and we have not corrected the data for these thermal effects.

[24] We have processed and analyzed all CRISM targeted observations of Columbus crater acquired to date, including FRTs (18 m/pixel, covering 10 km × 10 km), HRLs (36 m/pixel, 10 km × 20 km) and one HRS (36 m/pixel, 10 km ×

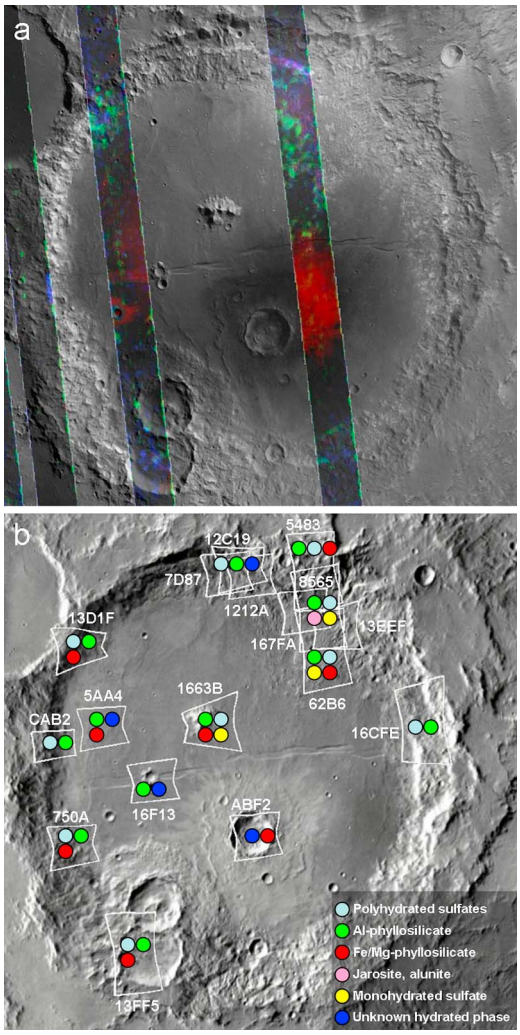

Figure 9. (a) CRISM multispectral mapping data from MRDR tile 553 overlain on HRSC nadir channel mosaic of Columbus crater. Red is OLINDEX, green is BD2210 [*Pelkey et al.*, 2007], and blue is SINDEX [*Roach et al.*, 2009], corresponding to olivine, Al-phyllosilicates, and hydrated sulfates, respectively. (b) CRISM targeted observation footprints mapped on THEMIS daytime IR mosaic of Columbus. Numbers correspond to observation IDs (e.g., "ABF2" is FRT0000ABF2), and colored dots indicate secondary minerals identified through analysis of each observation.

10 km). The locations of these observations are indicated in Figure 9b, along with the secondary minerals identified in each location. Minerals were identified by examining maps of the relevant spectral summary parameters defined by *Pelkey et al.* [2007], *Roach et al.* [2009], and *Ehlmann et al.* [2009], and then plotting CRISM spectra against laboratory spectra to confirm detections. For one CRISM observation with especially strong spectral signatures (FRT00007D87), we also used the USGS Tetracorder system [*Clark et al.*, 2003] to search for additional spectral phases that might have been missed by our manual approach.

[25] In the following subsections, we provide our rationale for each mineral identification and present representative spectra. We also describe where each mineral is found within the crater.

3.2. Aluminum Phyllosilicates

[26] As mentioned by *Wray et al.* [2009a] and *Murchie et al.* [2009b], the most commonly detected phyllosilicate type in Columbus crater is the kaolin group (Figure 11). This group of $Al_2Si_2O_5(OH)_4$ polymorphs includes kaolinite, halloysite, and the less common minerals dickite and nacrite. Kaolin group clay minerals are spectrally distinct from Al-smectite clays such as montmorillonite and beidellite: the former exhibit doublets near 1.4 and 2.2 μm, whereas the latter exhibit single absorptions at these wavelengths as well as the H_2O band near 1.9 μm [e.g., *Clark et al.*, 1990; *Bishop et al.*, 2008]. Halloysite can be difficult to distinguish from kaolinite when the latter is mixed with another hydrated mineral, but dickite and nacrite are distinguished by their more symmetric and narrower 2.2 μm doublet absorptions [*Ehlmann et al.*, 2009]. The kaolin group clay spectra in Columbus crater are most consistent with kaolinite or halloysite.

[27] Tetracorder analysis of FRT00007D87 identifies not only kaolinite, but also the Al-smectite montmorillonite in some outcrops. Montmorillonite, especially when mixed with kaolinite, can be challenging to distinguish from halloysite, poorly crystalline kaolinite, or other kaolinite-smectite mixtures, because all of these have a less distinct 2.2 μm doublet than well-crystalline kaolinite. Perhaps the most diagnostic effect of adding montmorillonite to kaolinite is the broadening of the long-wavelength edge of the

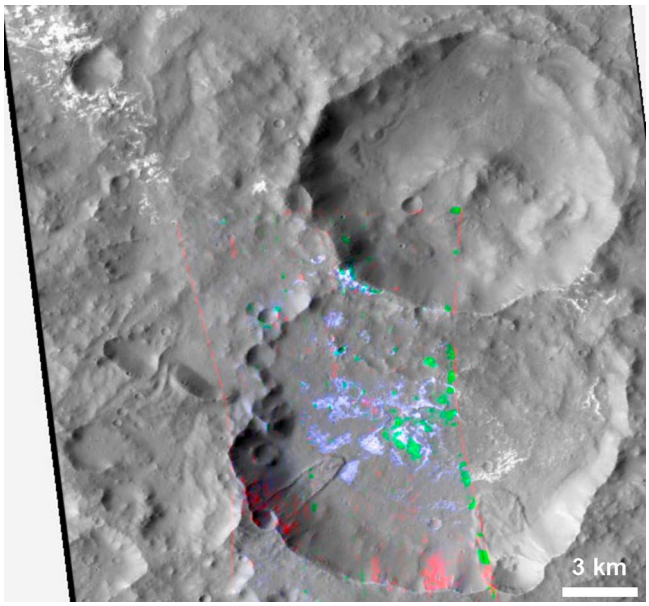

Figure 10. Two craters (D ~14 and ~17 km) superposed on Columbus; from CTX P04_002739_1505 colored with spectral parameter maps from CRISM HRL00013FF5. Red is D2300 [*Pelkey et al.*, 2007], green is BD2200, and blue is BD1900H [*Ehlmann et al.*, 2009]. Like all the light-toned deposits ringing Columbus's walls (e.g., upper left), deposits on the floor of the 17 km crater contain hydrated sulfates (blue) and kaolinite (green); Fe/Mg-phyllosilicate (red) is exposed in the crater's southern wall.

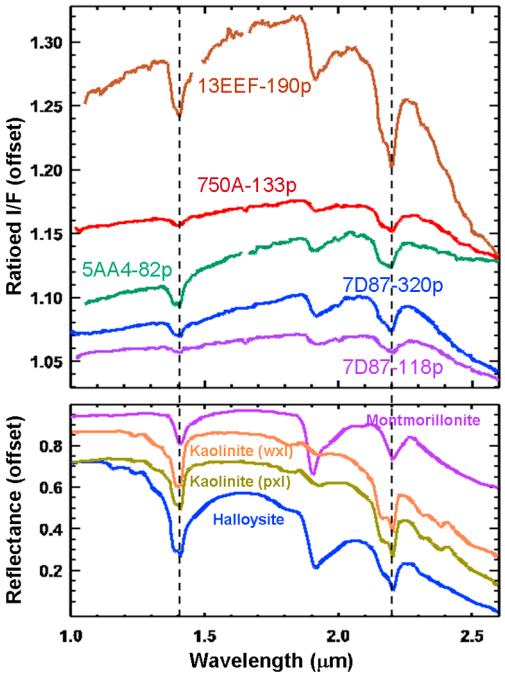

Figure 11. (top) CRISM spectra from Columbus crater and (bottom) lab spectra of Al-phyllosilicates. Here and in subsequent figures, CRISM spectra are labeled with abbreviated image IDs (e.g., 750A is FRT0000750A) and the number of pixels averaged in each spectral numerator. Vertical dashed lines are provided to aid visual comparisons of spectra. The bottommost CRISM spectrum has a 2.2 μm band shape largely consistent with montmorillonite but is most likely a mixture; other CRISM spectra are consistent with kaolinite group clays. Montmorillonite is sample SWy-1, well-crystalline (wxl) kaolinite is KGa-1, poorly crystalline (pxl) kaolinite is KGa-2, and halloysite is KLH503 from *Clark et al.* [2007].

2.2 μm absorption [*McKeown et al.*, 2010; *Clark et al.*, 2003, Figure 13a]. Spectra from locations in Columbus crater mapped by Tetracorder as montmorillonite-bearing indeed have a broad rise from 2.20 to 2.27 μm and a weak or absent 2.16 μm kaolinite doublet feature (bottom CRISM spectrum in Figure 11, top), consistent with montmorillonite being the spectrally dominant phase at these locations.

[28] Aluminum phyllosilicates are found in every CRISM observation of Columbus except for one covering the D ~11 km crater on the southern floor. Kaolinite is found on both Columbus's walls and floor. Figure 12 shows a perspective view of the northern crater wall, in which the green areas contain Al-phyllosilicates. These phyllosilicates are seen directly adjacent to (and, for the most part, stratigraphically beneath) Columbus's light-toned ring deposit, as well as several km upslope and downslope. At this particular location, where montmorillonite was mapped independently from kaolinite, the strongest kaolinite signatures are adjacent to the ring deposit, whereas the largest montmorillonite-bearing exposures occur farther from the ring. However, the two Al-phyllosilicates are typically mixed in Columbus crater, with evidence for a kaolinite component in all exposures.

[29] Many crater wall exposures of Al-phyllosilicate are morphologically unremarkable (e.g., dark materials beneath the light-toned layers in Figure 5b), but in some cases these exposures exhibit stratification (e.g., dark layers in Figure 5c) and/or fracture patterns (Figure 7). In rare instances, Al-phyllosilicates are interbedded with the lighter-toned rocks of the wall ring (Figure 5c) [see also *Wray et al.*, 2009a]. This interbedding likely reflects changing depositional environments or sediment sources, although it could alternatively result from in situ alteration that was strongly controlled by variations in porosity, permeability, and primary mineralogy between strata.

3.3. Polyhydrated Sulfates

[30] *Wray et al.* [2009a] and *Murchie et al.* [2009b] also reported hydrated sulfate detections in Columbus crater; specifically, *Wray et al.* [2009a] presented evidence for gypsum ($CaSO_4 \cdot 2H_2O$) and another polyhydrated phase consistent with Mg-sulfate (Figure 13). Gypsum can be uniquely identified by an absorption at 1.74–1.75 μm and

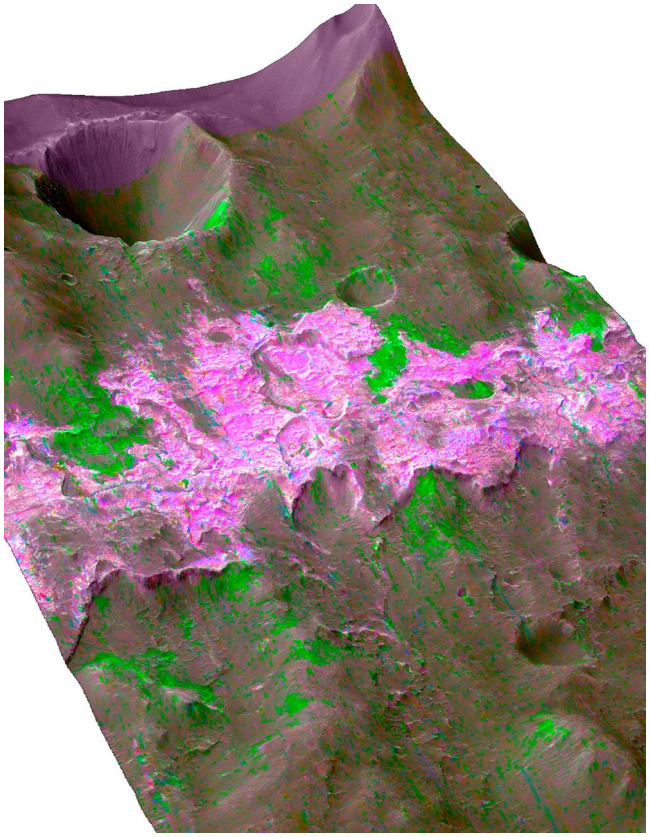

Figure 12. Perspective view of a portion of HiRISE PSP_005429_1510 (area near center is shown in Figure 5a) colored with spectral parameter maps from CRISM FRT00007D87 using the techniques described by *Delamere et al.* [2010, section 6.1] and projected on HiRISE DEM. Red is SINDEX [*Roach et al.*, 2009], green is BD2200, and blue is BD1900H [*Ehlmann et al.*, 2009]; purple/pink colors correspond to hydrated sulfates and green to Al-phyllosilicates. The latter are exposed in erosional windows, including along the edges of the light-toned, sulfate-bearing deposits. Crater at upper left is ~1.6 km in diameter.

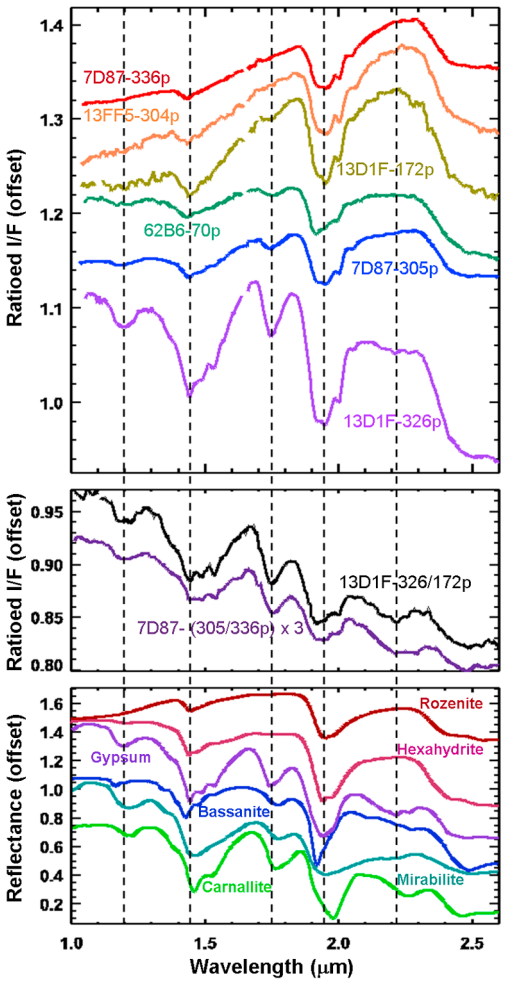

Figure 13. (top) CRISM spectra from Columbus crater and (bottom) lab spectra of polyhydrated salts; format similar to Figure 11. Spectra in the top panel show increasing strength of the 1.75 μm band (interpreted as due to gypsum) relative to the 1.94 μm band. No spectra from Columbus crater are consistent with pure gypsum, but in the middle panel we attempt to isolate the gypsum component by plotting in-trascene ratios between spectra shown in the top panel. These ratios (especially from FRT00013D1F) show the ~1.5 and ~2.2 μm triplet absorptions that are unique to gypsum among hydrated salts (see bottom panel). Rozenite ($FeSO_4 \cdot 4H_2O$) is BKR1JB626B and hexahydrite ($MgSO_4 \cdot 6H_2O$) is LASF57A from the CRISM spectral library. Gypsum ($CaSO_4 \cdot 2H_2O$) is HS333.3B, bassanite ($CaSO_4 \cdot 1/2H_2O$) is GDS145, mirabilite ($Na_2SO_4 \cdot 10H_2O$) is GDS150, and carnallite ($KMgCl_3 \cdot 6H_2O$) is NMNH98011 from *Clark et al.* [2007].

diagnostic triplets at 1.44, 1.49, 1.53 μm and 2.17, 2.21, 2.27 μm [*Crowley*, 1991; *Cloutis et al.*, 2006]. It has also been identified on Mars from orbit in the north polar region [*Langevin et al.*, 2005]. Previous reports of gypsum in equatorial canyons and chaos regions have been refuted by subsequent analyses [*Noe Dobrea et al.*, 2008a; *Kuzmin et al.*, 2009; *Bishop et al.*, 2009], but Ca-sulfates (not necessarily gypsum) have been found from orbit in Mawrth Vallis [*Wray et al.*, 2010] and possibly Noctis Labyrinthus [*Mangold et al.*, 2010], and by the Mars Exploration Rovers in both Meridiani bedrock [*Clark et al.*, 2005; *Glotch et al.*, 2006] and some rocks and soils of Gusev crater's Columbia Hills [*Squyres et al.*, 2006; *Yen et al.*, 2008].

[31] Other sulfates, including Mg-sulfates, have less diagnostic near-IR spectral characteristics. Spectra with absorptions only at 1.43, 1.93 μm and an inflection at ~2.4 μm (top two CRISM spectra in Figure 13, top) are commonly interpreted as polyhydrated sulfates [e.g., *Gendrin et al.*, 2005], with the 2.4 μm feature attributed to an S–O overtone and/or OH/H_2O-related absorption(s) [*Cloutis et al.*, 2006]. However, caution is warranted because some nonsulfate hydrated salts [*Crowley*, 1991; *Lane et al.*, 2008; *Hanley et al.*, 2010] and some zeolites (e.g., thomsonite) [*Ehlmann et al.*, 2009] have a similar feature at 2.4 μm. In the case of Columbus crater, the occurrence of this hydrated phase with gypsum and other sulfates described below suggests it is likely a polyhydrated sulfate, or possibly a hydrous chloride salt.

[32] NIR spectroscopy alone does not always allow unique identification of the cation(s) in polyhydrated sulfates, but this technique does provide some constraints. Ca and Na are unlikely because (like gypsum) bassanite ($CaSO_4 \cdot 1/2H_2O$) and mirabilite ($Na_2SO_4 \cdot 10H_2O$) have strong bands near 1.75 μm [*Crowley*, 1991] that are absent from spectra of Columbus's nongypsum polyhydrate. Eugsterite ($Na_4Ca[SO_4]_3 \cdot 2H_2O$) lacks a strong 1.75 μm band but absorbs at 2.48 μm [*Crowley*, 1991], a wavelength distinctly longer than the 2.4 μm band in our spectra. Mg and Fe are therefore the most geologically plausible candidate cations if this phase is indeed a sulfate. Either or both may be present, but we favor at least some Mg because all Fe-sulfates have a broad absorption centered near 1 μm (centered at 0.9–1.2 μm for Fe^{2+} or 0.8–0.95 μm for Fe^{3+}) [*Burns*, 1993; *Crowley et al.*, 2003; *Cloutis et al.*, 2006; *Lane et al.*, 2008]. These absorptions are not apparent in CRISM IR detector spectra (Figure 13), nor in VNIR detector spectra of Columbus's polyhydrate-bearing materials (section 3.4) [see also *Murchie et al.*, 2009b]. Furthermore, Mg-sulfates are the most abundant salts in Meridiani bedrock [*Clark et al.*, 2005] and in Martian soils and rock coatings at all landing sites prior to Phoenix [*Vaniman et al.*, 2004]; they have now also been identified in Phoenix soils [*Kounaves et al.*, 2010]. They are a major component of secondary mineral assemblages produced in laboratory experiments [*Tosca et al.*, 2004] and geochemical models [*Tosca et al.*, 2005] of olivine-bearing rock alteration under Mars-like conditions. Nevertheless, the lack of a strong ~1 μm absorption in CRISM spectra is not in itself sufficient to rule out Fe-sulfates; in fact, we identify Fe-sulfates elsewhere in Columbus crater (sections 3.5 and 3.6) even though no ~1 μm band is apparent in those cases. Therefore, we refer to this nongypsum sulfate generically as polyhydrated Mg/Fe-sulfate(s).

[33] The sulfate hydration state is also not well constrained by the CRISM spectra. We plot the spectrum of hexahydrite ($MgSO_4 \cdot 6H_2O$) in Figure 13, but it is quite similar to spectra of epsomite ($MgSO_4 \cdot 7H_2O$) pentahydrite ($MgSO_4 \cdot 5H_2O$), and starkeyite ($MgSO_4 \cdot 4H_2O$) [*Crowley*, 1991], making these sulfates difficult to distinguish with CRISM. However, the monohydrate kieserite is spectrally distinct [*Cloutis et al.*, 2006] and inconsistent with the CRISM spectra in Figure 13. Analogously, polyhydrated

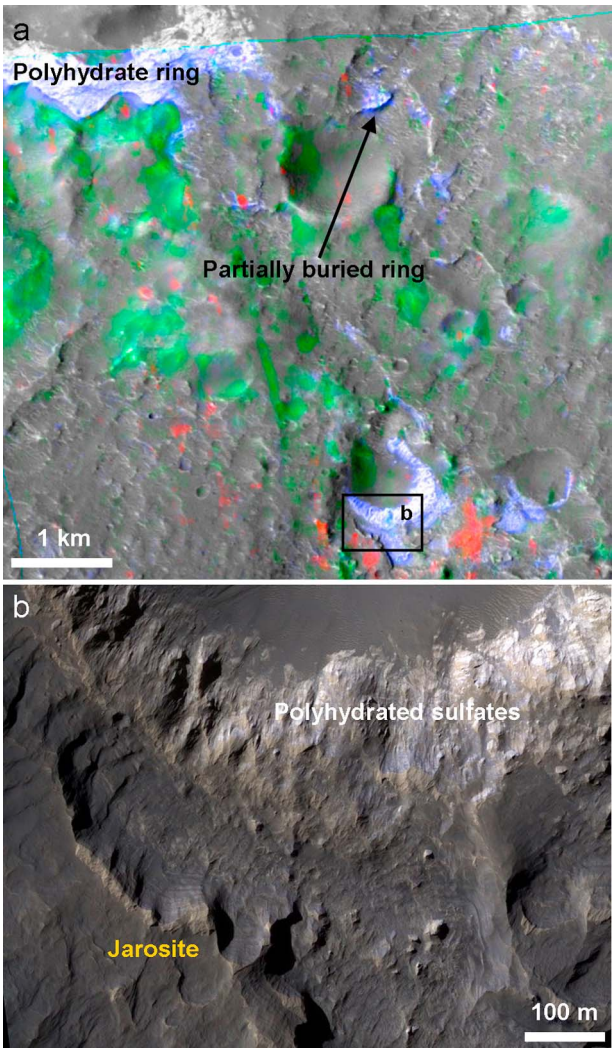

Figure 14. (a) Portion of northeast Columbus crater; from CTX P06_003306_1504 colored with spectral parameter maps from CRISM FRT000167FA. Red is 2.265 μm band depth, green is BD2200, and blue is BD1900H [*Ehlmann et al.*, 2009], corresponding to jarosite, Al-phyllosilicates, and polyhydrated sulfates, respectively. Several hundred meters of elevation separate the wall ring deposit at ~1750 m (MOLA) from (b) jarosite-bearing beds and polyhydrated sulfates on the crater floor (elevation ~1100 m); from HiRISE PSP_010281_1510.

Fe^{2+}-sulfates including melanterite ($FeSO_4 \cdot 7H_2O$) have spectra similar to rozenite ($FeSO_4 \cdot 4H_2O$) shown in Figure 13 [*Bishop et al.*, 2004], but the monohydrate szomolnokite is distinctive (section 3.5). In any case, these sulfates may have experienced hydration state changes since their formation [*Vaniman et al.*, 2004].

[34] Polyhydrated sulfates are identified in every CRISM observation of the Columbus crater walls and in some observations of the northeast crater floor. They are the spectrally dominant phase in the finely bedded, light-toned deposits ringing Columbus's walls (e.g., Figures 5a–5b), and in a few comparably bright-toned outcrops at lower elevations within the crater (e.g., Figures 8c and 14). The Mg/Fe-sulfate is ubiquitous in these materials, with varying contributions from gypsum. Spectral parameters can be used to map the two polyhydrates independently (Figure 15a). However, inspection of colocated images reveals no clear stratigraphic relationship between the relatively gypsum-rich outcrops and gypsum-poor outcrops. In some cases, the outcrops with gypsum appear relatively highstanding, darker, and more rugged than those without gypsum (Figure 6b).

3.4. Crystalline Ferric Oxide/Hydroxide

[35] The sulfate-rich layered rocks examined by the Opportunity rover in Meridiani Planum contain coarse-grained gray hematite [e.g., *Christensen et al.*, 2000, 2004b], and orbital spectroscopy suggests that crystalline ferric oxides are found in many sulfate-bearing deposits on equatorial Mars [e.g., *Bibring et al.*, 2007]. Yet, at visible wavelengths, Columbus's light-toned layered deposits are spectrally similar to Martian dust [*Murchie et al.*, 2009b], lacking the absorptions at 0.8–0.9 μm due to crystalline ferric oxides [e.g., *Morris et al.*, 2000] that have been identified by CRISM elsewhere on Mars [*Wray et al.*, 2008; *Murchie et al.*, 2009a; *McKeown et al.*, 2009; *Roach et al.*, 2010b]. Thermal emission spectra (section 4) also show no evidence for crystalline gray hematite in the Columbus layered deposits.

[36] However, crystalline ferric oxides/hydroxides are present in dark-toned debris immediately downslope from Columbus's light-toned ring (Figure 15a). Their spectra have an absorption centered at 0.92 μm (Figure 15b), consistent with ferric minerals including goethite or ferrihydrite [e.g., *Morris et al.*, 2000; *Bishop and Murad*, 2002]. Aeolian bed forms are observed at the locations with ferric oxides (Figure 15c). This concentration of ferric oxide in dark-toned debris adjacent to lighter sulfate-bearing outcrops is similar to the distribution of crystalline ferric oxides at many other locations on Mars [*Christensen et al.*, 2001b; *Soderblom et al.*, 2004; *Bibring et al.*, 2007; *Noe Dobrea et al.*, 2008a; *Weitz et al.*, 2008; *Mangold et al.*, 2008; *Le Deit et al.*, 2008; *Chojnacki and Hynek*, 2008; *Murchie et al.*, 2009a; *Bishop et al.*, 2009], except that a comparable ferric oxide signature is not observed in Columbus's light-toned deposits themselves.

3.5. Monohydrated Sulfate

[37] Monohydrated sulfates such as kieserite ($MgSO_4 \cdot H_2O$) and szomolnokite ($FeSO_4 \cdot H_2O$) are distinguished from more hydrated sulfates by a broad absorption that is deepest near 2.1 μm. Natural samples of kieserite have the band minimum at 2.13 μm, while for szomolnokite it occurs at 2.09–2.10 μm [*Crowley et al.*, 2003; *Cloutis et al.*, 2006; *Bishop et al.*, 2009]. However, pure synthetic kieserite has been observed to have a shorter-wavelength minimum coincident with that observed for szomolnokite, potentially making it difficult to distinguish between these minerals [*Milliken*, 2006]. Only a few other minerals have a similarly broad absorption near 2.1 μm, including some NH_4-bearing minerals [e.g., *Bishop et al.*, 2002a], but these lack the 2.4 μm absorption typical of monohydrated sulfate spectra and/or have additional absorptions not observed in hydrated sulfates (Figure 16). With band minima at ~2.11 and ~2.40 μm, the Columbus crater spectra in Figure 16 appear most consistent with monohydrated sulfate.

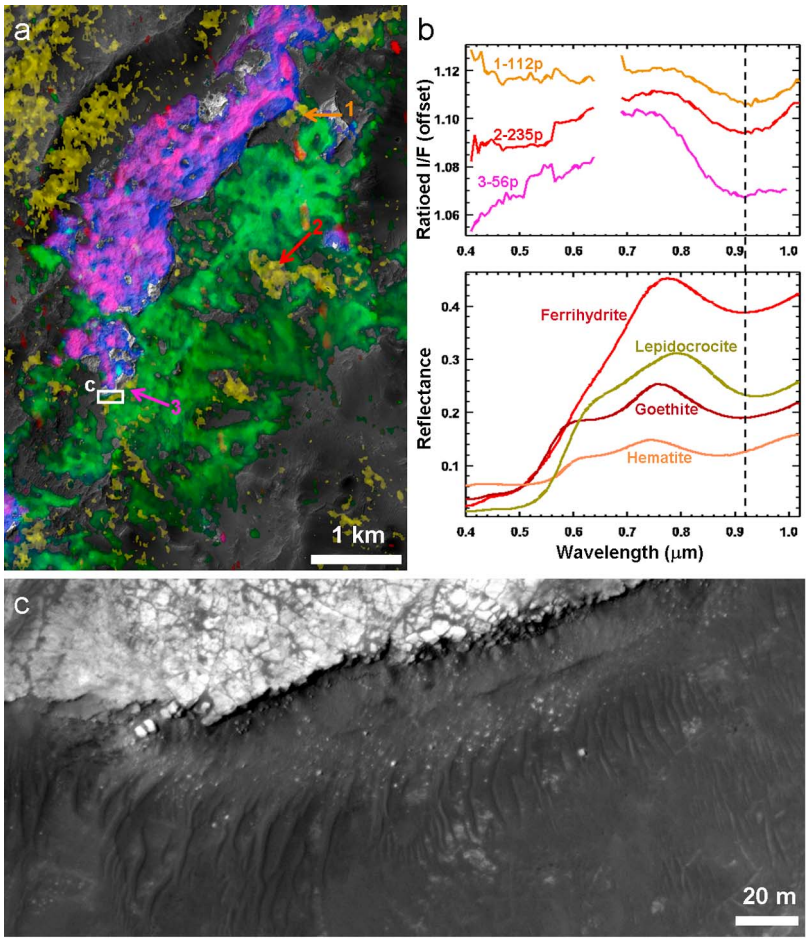

Figure 15. (a) A subset of HiRISE ESP_013960_1510 (Figure 6a) colored with spectral parameters from CRISM FRT00013D1F. Red is BD1750, yellow is BD920 [*Pelkey et al.*, 2007], green BD2200, and blue is BD1900H [*Ehlmann et al.*, 2009]. Gypsum-bearing materials appear pink/purple, Mg/Fe-polyhydrate appears blue, Al-phyllosilicates appear green, and ferric oxides appear yellow. The ferric oxide map is imperfect, as yellow areas northwest of the light-toned ring (upper left) do not actually have a spectrum consistent with this phase. Numbered arrows indicate source locations for (b) ratio spectra from CRISM FRT00013D1F (top, with number of pixels averaged in spectral numerator indicated), with lab spectra of crystalline ferric oxides (bottom) shown for comparison. Ferrihydrite ($5Fe_2O_3 \cdot 9H_2O$) is C1092F55, lepidocrocite (γ-FeOOH) is 892F51, goethite (α-FeOOH) is C1GO01, and hematite (Fe_2O_3) is F1CC17B from CRISM spectral library. (c) Sample area with ferric oxide signature adjacent to light-toned bedrock, showing darker-toned aeolian bed forms.

[38] A weaker, narrow absorption at 2.22–2.23 μm is also observed in the spectra of Figure 16 (top), especially in the bottommost spectrum. A comparably narrow absorption at 2.23–2.24 μm has been observed in light-toned layered deposits on the plains west of Juventae Chasma [*Milliken et al.*, 2008; *Bishop et al.*, 2009], in Aram Chaos [*Lichtenberg et al.*, 2010], and in Cross crater (G. A. Swayze et al., manuscript in preparation, 2010). This absorption has been attributed to Fe^{3+}-OH in the hydroxylated ferric sulfate $Fe(OH)SO_4$, a phase that has been formed in the laboratory at temperatures >200°C via dehydration of ferric sulfates such as hydronium jarosite [*Swayze et al.*, 2008a] or (ferri) copiapite [*Milliken et al.*, 2008; *Bishop et al.*, 2009], or via oxidation and dehydration of ferrous sulfates such as melanterite or szomolnokite [*Morris et al.*, 2009; *Lichtenberg et al.*, 2010]. In Cross crater (a mere ~400 km from Columbus crater in northwest Terra Sirenum (see also sections 3.6 and 6.1)) the 2.23 μm band has been found to date only in association with monohydrated sulfate (G. A. Swayze et al., manuscript in preparation, 2010), consistent with where it is found in Columbus crater. If the monohydrate in both craters is (at least partially) szomolnokite, then the 2.23 μm band could imply partial oxidation and dehydration of szomolnokite to form $Fe(OH)SO_4$.

[39] The strongest monohydrate + $Fe(OH)SO_4$ signature yet observed in Columbus crater (bottom spectrum in Figure 16, top) is found in a D ~200 m crater on Columbus's northeast floor (Figure 17a). Radial rays attest to the relative freshness of this impact crater, and exposures within the crater reveal that it excavated light-toned layered deposits. Several thin beds appear green in HiRISE enhanced color images (Figure 17b), but their exposures are too narrow to be resolved by CRISM. While this color is rare in Columbus crater and in

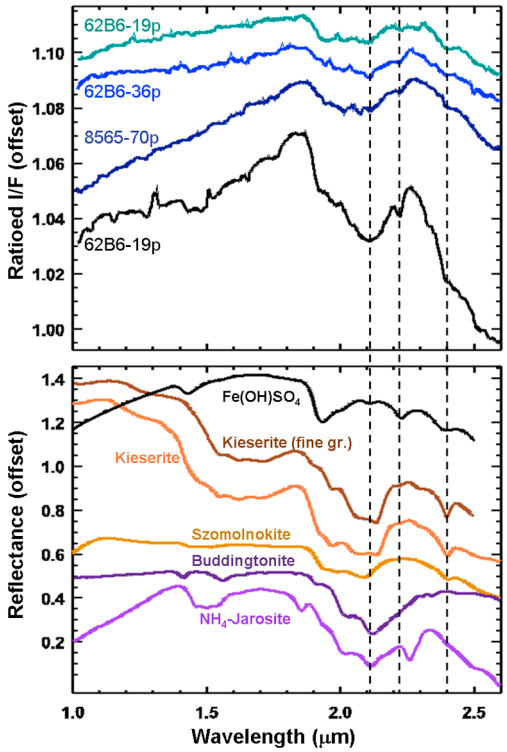

Figure 16. (top) CRISM spectra from Columbus crater and (bottom) lab spectra of monohydrated sulfates and NH_4-bearing minerals; format similar to Figure 11. Columbus crater spectra appear more consistent with monohydrated sulfates (plus an additional phase that absorbs at 2.22–2.23 μm, possibly $Fe(OH)SO_4$) than with NH_4-bearing minerals such as buddingtonite ($NH_4AlSi_3O_8$, a feldspar) or ammoniojarosite ($NH_4Fe_3[SO_4]_2[OH]_6$). $Fe(OH)SO_4$ is from copiapite dehydrated at 300°C, from *Bishop et al.* [2009]. Fine-grained kieserite ($MgSO_4 \cdot H_2O$) is KIEDE1.b, buddingtonite is GDS85, and ammoniojarosite is SCR-NHJ from *Clark et al.* [2007]; other kieserite is F1CC15 and szomolnokite ($FeSO_4 \cdot H_2O$) is BKR1JB622A from CRISM spectral library.

HiRISE enhanced color images of Mars in general, we have observed it in other locations where ferric sulfates are detected from orbit (Aram Chaos and the plains surrounding Valles Marineris). HiRISE IRB color composites [*McEwen et al.*, 2010] display IR (~875 nm), RED (~700 nm), and BG filter (~500 nm) images [*McEwen et al.*, 2007] in the red, green, and blue channels, respectively; therefore, a green hue indicates high RED I/F relative to the IR and BG, as would be expected for a ferric mineral such as $Fe(OH)SO_4$ due to its strong electron charge transfer absorption at <530 nm and spin-forbidden crystal field transition absorption at 800–970 nm [*Milliken et al.*, 2008; *Lichtenberg et al.*, 2010] reducing reflectance in the BG and IR filters, respectively. Thus the green color is consistent with our CRISM-based inference of a ferric mineral such as $Fe(OH)SO_4$.

[40] Most monohydrate exposures in Columbus are found on the northeast crater floor, although one outcrop has been identified at the base of the hills on the central floor (Figure 8c). Monohydrate-bearing outcrops exhibit internal stratification (Figures 8a and 17c) and, in comparison to beds within the polyhydrate-bearing crater wall ring (Figure 5), monohydrate beds are somewhat darker-toned, with weaker albedo contrasts between successive beds. The fracture patterns observed in the polyhydrate ring are less common in monohydrate-bearing outcrops, which in some cases display a "scalloped" or "reticulate" texture (Figure 17d) reminiscent of that seen on some wind-eroded surfaces elsewhere on Mars [*Bridges et al.*, 2010]. This texture is specifically associated with monohydrated sulfate in other regions [*Chojnacki and Hynek*, 2008; *Karunatillake et al.*, 2009; *Lichtenberg et al.*, 2010]. These morphologic characteristics are shared by the majority of light-toned outcrops on Columbus's floor, many of which are unresolved or heretofore unobserved by CRISM.

3.6. Jarosite and Alunite

[41] The acid sulfate jarosite ($KFe_3[SO_4]_2[OH]_6$) was first identified on Mars in Meridiani Planum by Opportunity [*Klingelhöfer et al.*, 2004] and subsequently identified by CRISM in other regions [*Milliken et al.*, 2008; *Metz et al.*, 2009; *Farrand et al.*, 2009; *Weitz et al.*, 2010]. A related acid sulfate, alunite ($KAl_3[SO_4]_2[OH]_6$), has been identified by *Swayze et al.* [2008b] in Cross crater: again, only ~400 km from Columbus. Here we present evidence for jarosite and possible alunite in Columbus crater.

[42] Jarosite has a nearly unique absorption at ~2.265 μm, with additional absorptions at ~1.5, 1.85, 2.51, and 2.62 μm [*Crowley et al.*, 2003; *Bishop and Murad*, 2005; *Cloutis et al.*, 2006; *Swayze et al.*, 2008a]. K-jarosite has an additional band at ~2.21 μm that is weak to absent in Na- and H_3O-jarosites [*Cloutis et al.*, 2006; *Swayze et al.*, 2008a]. We observe one location in Columbus crater whose spectrum exhibits all of these absorptions except the ~1.5 μm band(s), and also has a ~1.93 μm band attributed to H_2O (common in lab spectra of jarosites formed at low temperature). The 1.85, 2.51, and 2.62 μm absorptions are near the noise level but are present in both CRISM observations covering the location of interest (Figure 18). The 2.21 μm band observed in the CRISM spectra is most consistent with K-jarosite, similar to the Mawrth Vallis jarosite reported by *Farrand et al.* [2009]; however, in all K-jarosite lab spectra the 2.21 μm band is significantly weaker than the 2.265 μm band, so their comparable strength in the spectrum from HRL00008565 (Figure 18) may indicate an additional absorber at ~2.2 μm (e.g., Al-phyllosilicate). Additional hydrous minerals could also contribute to the observed 1.93 μm band, but to the extent that this band is due to H_2O in jarosite, its strength suggests a relatively low formation temperature and minimal subsequent recrystallization [*Swayze et al.*, 2008a]. Similarly, a low-temperature formation has been inferred from the spectrum of alunite in Cross crater [*Swayze et al.*, 2008b] and for jarosite found on the plains surrounding Valles Marineris [*Milliken et al.*, 2008].

[43] To our knowledge, the only common mineral other than jarosite with an absorption at ~2.27 μm is gibbsite ($Al[OH]_3$) [*Cloutis and Bell*, 2000]. While a mixture of gibbsite + montmorillonite could account for the major absorptions in our Figure 18 CRISM spectra, such a mixture would not reproduce the weak feature we observe at 1.85 μm. Gibbsite also has a very different spectral shape

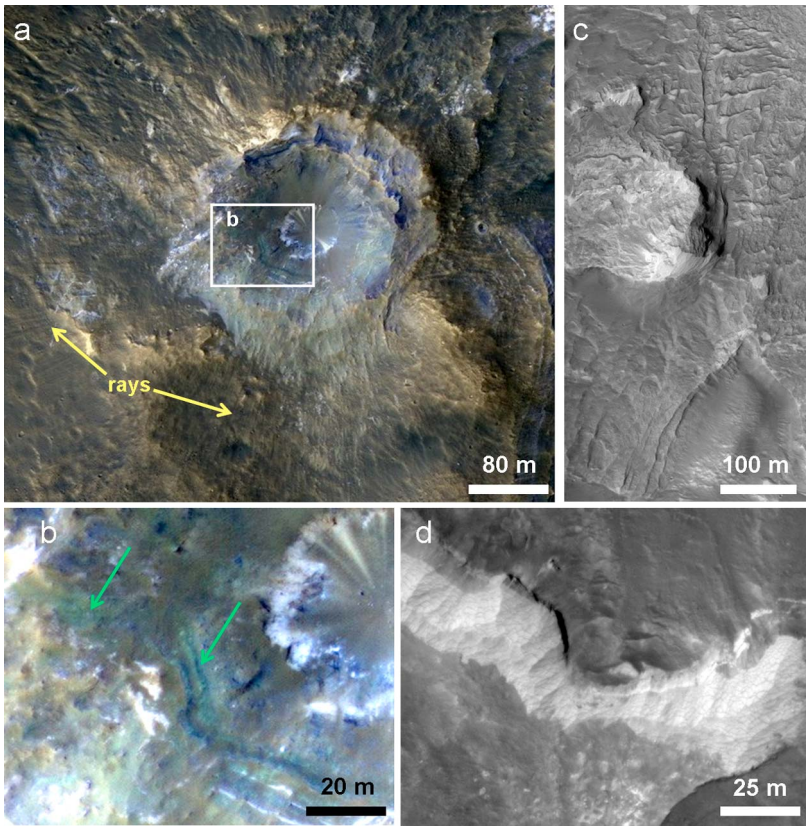

Figure 17. Columbus crater outcrops with spectral evidence for monohydrated sulfate; see Figure 20a for locations. (a) Relatively fresh impact crater (note radial rays) with strongest monohydrated sulfate signature yet observed in Columbus crater (bottom spectrum in Figure 16, top); from HiRISE ESP_014039_1510. (b) Subset of Figure 17a, showing layers with relatively green enhanced color hue (arrows), possibly due to crystalline ferric minerals including sulfates. (c) Bedded outcrop with monohydrated sulfate (70 pixel spectrum in Figure 16); from PSP_003306_1510. (d) Outcrop with possible "reticulate" texture; from ESP_014039_1510.

from 2.1 to 2.5 μm, and strong bands near 1.5 μm that are not observed in these CRISM spectra. The presence of many other sulfates in Columbus crater as well as alunite in nearby Cross crater further supports the identification of jarosite in Columbus. Alternatively, an acid-sulfate environment could have induced partial acid weathering of Fe/Mg-clay minerals (see section 3.7), resulting in silica formation and the appearance of a 2.21/2.28 μm doublet [*Madejová et al.*, 2009]. Again, however, this would not explain the weak feature at 1.85 μm in our CRISM spectra, which is most consistent with jarosite. The one exposure of jarosite found to date is on Columbus's northeast floor; it exhibits internal bedding and lies adjacent to a circular depression containing lighter-toned polyhydrate-bearing outcrops (Figure 14).

[44] Alunite is distinguished by a strong, broad absorption centered at 2.17 μm, with additional bands at 1.43–1.44, 1.47–1.49, 1.76, 2.32, and 2.51–2.53 μm (those with a range of positions are at longer wavelengths in Na-alunite than in K-alunite) [*Bishop and Murad*, 2005; *Cloutis et al.*, 2006]. In Cross crater, alunite has been identified as the spectrally dominant phase in some outcrops, and in others it is mixed with kaolinite [*Swayze et al.*, 2008b]. In Columbus crater, several relatively small (up to ~1 km wide) outcrops have spectra consistent with a contribution from alunite (Figure 19), although the signatures are not as strong as in Cross crater, and all are probably mixtures with Al- (and possibly Mg-) phyllosilicates. To varying degrees, these spectra contain absorptions at the six positions described above for alunite, and the band centers at 1.44 and 1.49 μm in some spectra are most consistent with Na-alunite. The relative weakness of the 1.76 and 2.32 μm absorptions and the presence of a band at ~1.93 μm (if the latter is due to H_2O in alunite) are most consistent with laboratory spectra of alunite formed at low temperature, similar to the alunite in Cross crater [*Swayze et al.*, 2008b].

[45] It is worthwhile to consider whether the CRISM spectra in Figure 19 could alternatively be explained by mixtures of minerals identified elsewhere in Columbus. For example, gypsum mixed with kaolinite could explain bands at 1.44, 1.49, and 1.75 μm (gypsum) and a shoulder at 2.32 μm (kaolinite). However, the 2.2 μm doublet of kaolinite (or singlet of montmorillonite) cannot account for the 2.17–2.18 μm band minimum in some CRISM spectra shown in Figure 19. Aside from alunite, the phyllosilicates pyrophyllite [*Clark et al.*, 1990] and beidellite [*Kloprogge*, 2006; *Bishop et al.*, 2010] have bands centered at 2.17 and 2.18 μm, respectively. Beidellite has been previously iden-

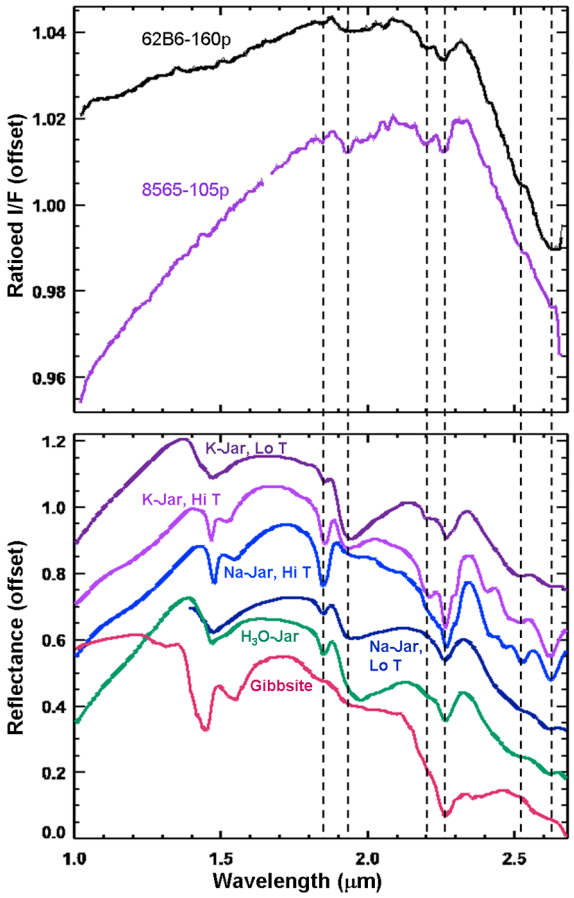

Figure 18. (top) CRISM spectra from Columbus crater and (bottom) lab spectra of jarosites; format similar to Figure 11. Gibbsite ($Al[OH]_3$) is also plotted because it shares a ~2.27 μm band but lacks other characteristics of jarosites. CRISM spectra were extracted from essentially the same area, but from two different (overlapping) observations. Low-temperature (90°C) K-jarosite is sample GDS98, high-temperature (200°C) K-jarosite is GDS99, high-T Na-jarosite is GDS101, low-T Na-jarosite is GDS100, H_3O-jarosite is SJ-1, and gibbsite is WS214 from *Clark et al.* [2007].

tified elsewhere on Mars [*Noe Dobrea et al.*, 2010]. However, the absorptions in beidellite and especially in pyrophyllite are too narrow to account for the broad band observed in some of our CRISM spectra, even if mixed with kaolinite and/or gypsum (Figure 19). Furthermore, linear mixtures of gypsum, kaolinite, and beidellite do not have absorptions with the same proportionate strengths or precise wavelengths as in alunite or as observed in the CRISM data, although intimate mixtures may have slightly different spectral properties. From spectral evidence combined with the proximity of Columbus crater to the most definitive alunite detection on Mars [*Swayze et al.*, 2008b], we infer that an alunite component is plausible for some outcrops in Columbus.

[46] The outcrops with a possible alunite component are on the northeast floor of Columbus crater and on the northeast wall just below the polyhydrate-bearing ring (Figure 20a). Morphologically, these outcrops are distinguished by their smoothness at meter scales (Figures 20b–20c); in contrast to other hydrated mineral-bearing outcrops in Columbus, these strata appear more massive and lack fractures. Bedding is exposed along the edges of the alunite-bearing outcrops, but it is unclear whether all of these beds contain alunite. Outcrops of alunite-bearing material in Cross crater appear similarly smooth at meter scales (G. A. Swayze et al., manuscript in preparation, 2010).

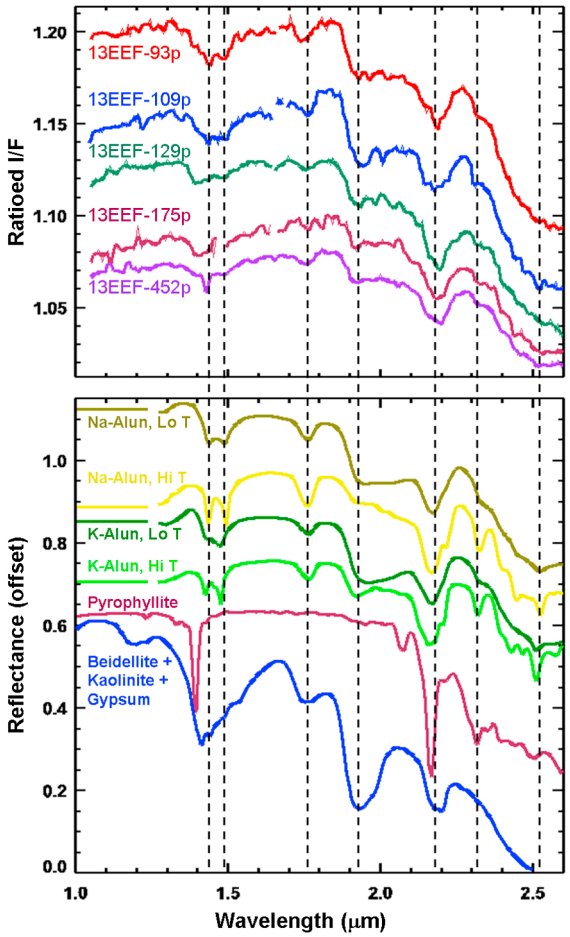

Figure 19. (top) CRISM spectra from Columbus crater and (bottom) lab spectra of alunites; format similar to Figure 11. Pyrophyllite and a linear mixture including beidellite are also plotted because these Al-phyllosilicates also absorb at 2.17–2.18 μm. However, pyrophyllite's narrow absorptions at 1.39 and 2.17 μm are inconsistent with our CRISM spectra; the slightly broader 1.41 and 2.18 μm bands of beidellite are marginally more consistent, but linear mixtures excluding alunite still fail to reproduce the exact band positions and relative strengths observed in CRISM data. Low-temperature (150°C) Na-alunite is sample GDS95, high-temperature (450°C) Na-alunite is RES-3, low-T K-alunite is GDS97, high-T K-alunite is RES-2, pyrophyllite is PYS1A (fine gr), and the mixture is equal parts beidellite(+montmorillonite) GDS124, kaolinite CM7, and gypsum HS333.3B, all from *Clark et al.* [2007].

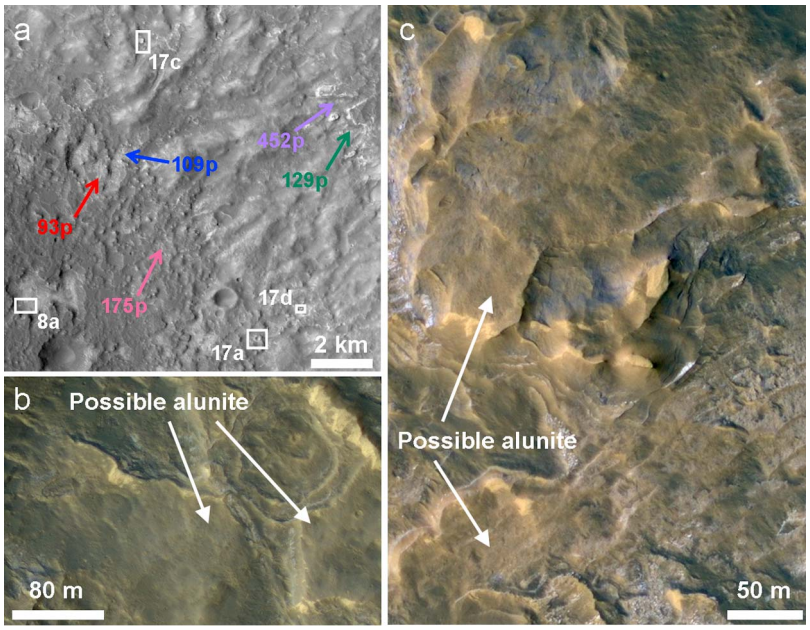

Figure 20. (a) Source locations for possible alunite spectra in Figure 19; from CTX P06_003306_1504. The 452 and 129 pixel spectra are from outcrops adjacent to Columbus's bright polyhydrate wall ring. Locations of monohydrate-bearing outcrops from previous figures are also shown. (b and c) Smooth-textured outcrops on Columbus crater floor with possible alunite component; from PSP_003306_1510. Area shown in Figure 20b corresponds to the 175 pixel spectrum in Figure 19, and area shown in Figure 20c corresponds to the 109 pixel spectrum.

3.7. Iron/Magnesium Phyllosilicates

[47] Although Al-phyllosilicates are the spectrally dominant alteration phase in most CRISM scenes in Columbus crater, Fe/Mg-phyllosilicates are the most common alteration product detected from orbit in most other regions on Mars [e.g., *Bibring et al.*, 2006; *Mustard et al.*, 2008]. Fe/Mg-phyllosilicates have absorptions at 2.28–2.35 μm, which in smectites occur shortward of 2.32 μm (the exact position depending on Fe versus Mg content) and with a ~1.9 μm H_2O band [e.g., *Clark et al.*, 1990; *Bishop et al.*, 2002b; *Swayze et al.*, 2002]. To date, we have identified ~10 relatively small areas on the walls and floor of Columbus that are spectrally consistent with Fe/Mg-phyllosilicates, possibly including smectites (Figure 21). Specifically, Fe/Mg-phyllosilicates are exposed in the southern wall of the *D* ~17 km crater shown in Figure 10 (CRISM HRL00013FF5), in hectometer-scale resistant knobs on Columbus's northwest wall (FRT00013D1F), in materials eroding from the hills on the central floor (FRT0001663B), and in areas up to a few kilometers wide on the crater floor (e.g., HRL000062B6). Some of these materials may predate the formation of Columbus crater, but the crater floor deposits likely represent infilling materials that postdate the impact event.

[48] The spectra that we classify as Fe/Mg-phyllosilicates are diverse, with varying relative strengths of the 1.9 and 2.3 μm bands; the position of the latter band ranges from 2.29 to 2.32 μm. A 1.39 μm band is observed in some cases, consistent with Mg-rich phyllosilicates [*Clark et al.*, 1990; *Bishop et al.*, 2002b]. In most cases, a mineral identification more specific than "Fe/Mg-phyllosilicate" is not possible.

3.8. Other Hydrated Phases

[49] Still other locations on the walls and floor of Columbus crater have spectral absorptions at ~1.4 and ~1.9 μm consistent with hydrated minerals, but they lack other strong, diagnostic absorptions that would enable specific identification (Figure 22). In some cases, weak features in the 2.2–2.3 μm range are likely due to metal-OH vibrational absorptions. In particular, spectra from the *D* ~11 km crater on Columbus's southern central floor (CRISM FRT0000ABF2) exhibit weak features at 2.19–2.20 and 2.27–2.28 μm (Figure 22). These wavelengths are slightly too short and too long, respectively, for jarosite (section 3.6). They are somewhat reminiscent of the 2.21/2.27 μm doublet feature observed by *Roach et al.* [2010a] in spectra from Valles Marineris, although the features we observe are much weaker. *Roach et al.* [2010a] attributed this doublet to either a mineral mixture or a poorly crystalline Fe/SiO_2-bearing phase similar to that described by *Tosca et al.* [2008b], formed via acid weathering of Fe-bearing clays [*Madejová et al.*, 2009].

3.9. Phases Not Observed: Carbonate, Chloride, Zeolite, Prehnite

[50] As described above, Columbus crater contains a wealth of phyllosilicate and sulfate minerals not commonly observed on Mars. However, several types of secondary minerals detected elsewhere on Mars by CRISM and THEMIS have not been found to date in Columbus crater. These include salts such as carbonates [*Ehlmann et al.*, 2008b] and chlorides [*Osterloo et al.*, 2008] as well as hydrated silicates that form under alkaline (zeolites) and/or

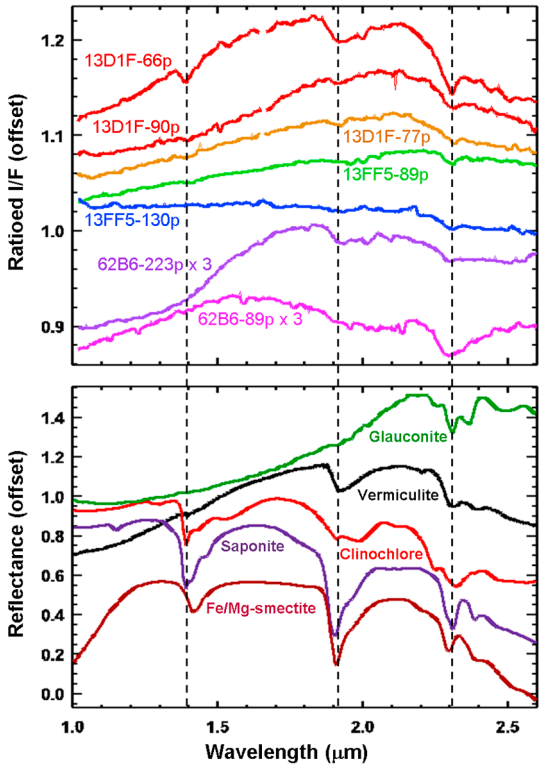

Figure 21. (top) CRISM spectra from Columbus crater and (bottom) lab spectra of Fe/Mg-phyllosilicates; format similar to Figure 11. Vermiculite is sample LAVE01 from CRISM spectral library; glauconite (K, Fe-mica) is HS313.3B, clinochlore (chlorite) is GDS159, and saponite (Mg-smectite) is SapCa-1.AcB from *Clark et al.* [2007]; Fe/Mg-smectite (scaled x8 for ease of comparison) is GDS759A from Flagstaff Hill, California. No single lab spectrum is an excellent match to the CRISM spectra.

high-temperature conditions (prehnite) [*Ehlmann et al.*, 2009]. The potential absence of these minerals in Columbus crater would be consistent with an alteration environment of relatively low temperature and low-to-neutral pH. However, nondetection of a mineral via orbital spectroscopy does not necessarily imply the absence of that mineral [e.g., *Kirkland et al.*, 2003].

4. Constraints on Modal Mineralogy

[51] Thermal emission spectra of Columbus crater enable an independent assessment of the surface mineralogy. In particular, the ~100 m/pixel THEMIS data set is ideal for studying the small-area outcrops in Columbus crater. We have analyzed the highest-quality THEMIS observation of Columbus available to date, I07746002 (Figure 23a), which covers a ~30 km swath across the crater, including the well-exposed sulfate-bearing ring of material on the northern crater wall.

[52] Emissivity spectra of the dark materials covering most of Columbus's floor (Figure 23b) are similar to that of TES Surface Type 1 (ST1; Figure 23c), the dominant spectral unit in the Martian southern highlands [*Bandfield et al.*, 2000] that is generally interpreted as representing a basaltic composition. Spectra of the plains outside Columbus and of ejecta surrounding the D ~11 km crater on the southern central floor are also consistent with basalt, but with a stronger absorption at ~11 μm (THEMIS band 7). This feature, which is especially strong in the D ~11 km crater ejecta, suggests higher olivine abundance in the ejecta relative to the rest of Columbus's floor [e.g., *Hamilton and Christensen*, 2005]. This is consistent with the detection of olivine in this small crater's ejecta by CRISM (Figure 9a).

[53] Decorrelation stretch (DCS) images show that the sulfate-bearing ring is spectrally distinct from the adjacent wall materials (Figure 23a). Where this spectral distinction is strongest ("wall lower" spectrum in Figure 23b), the slope from 9.4 to 11 μm (1070 to 910 cm^{-1}) is greater than that seen in ST1, suggesting a greater abundance of high-silica phases that could include phyllosilicates (Figure 23c). In addition, the "wall lower" spectrum has an absorption at 8.6 μm (band 4, 1170 cm^{-1}), consistent with the presence of sulfates. In particular, absorptions at this relatively short wavelength are most consistent with water-poor sulfates, e.g., kieserite or sanderite ($MgSO_4 \cdot 2H_2O$), but not the more hydrated Mg-sulfates [*Baldridge and Christensen*, 2006; *Lane*, 2007]. Ca-sulfates including gypsum (which CRISM detects in Columbus's polyhydrate ring) would also be consistent with this 8.6 μm feature [*Christensen et al.*, 2004a, Figure 7a]. In either case, this feature provides independent support for our CRISM detections of sulfates in Columbus crater.

[54] Linear mixing models of higher spectral resolution thermal emission data can be used to estimate mineral abundances with ~5–15% precision [e.g., *Ramsey and Christensen*, 1998; *Feely and Christensen*, 1999]. The TES instrument is ideal for this, although its ~3 km resolution is coarse compared to most outcrops in Columbus. We modeled a TES spectrum extracted from the "wall lower" location in Figure 23 using the standard ASU mineral library including smectites [*Rogers et al.*, 2007], supplemented with Mg-sulfate spectra measured by *Baldridge and Christensen* [2006]. The results yield an estimate of roughly 40% phyllosilicates by volume, 16% hydrated sul-

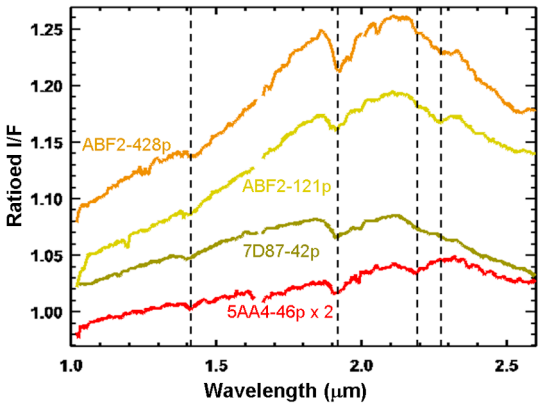

Figure 22. CRISM spectra from Columbus crater with ~1.4 and ~1.9 μm bands suggestive of hydrated minerals, but with few other diagnostic absorptions. Weak features in the 2.2–2.3 μm range may be due to metal-OH vibrations in poorly crystalline minerals.

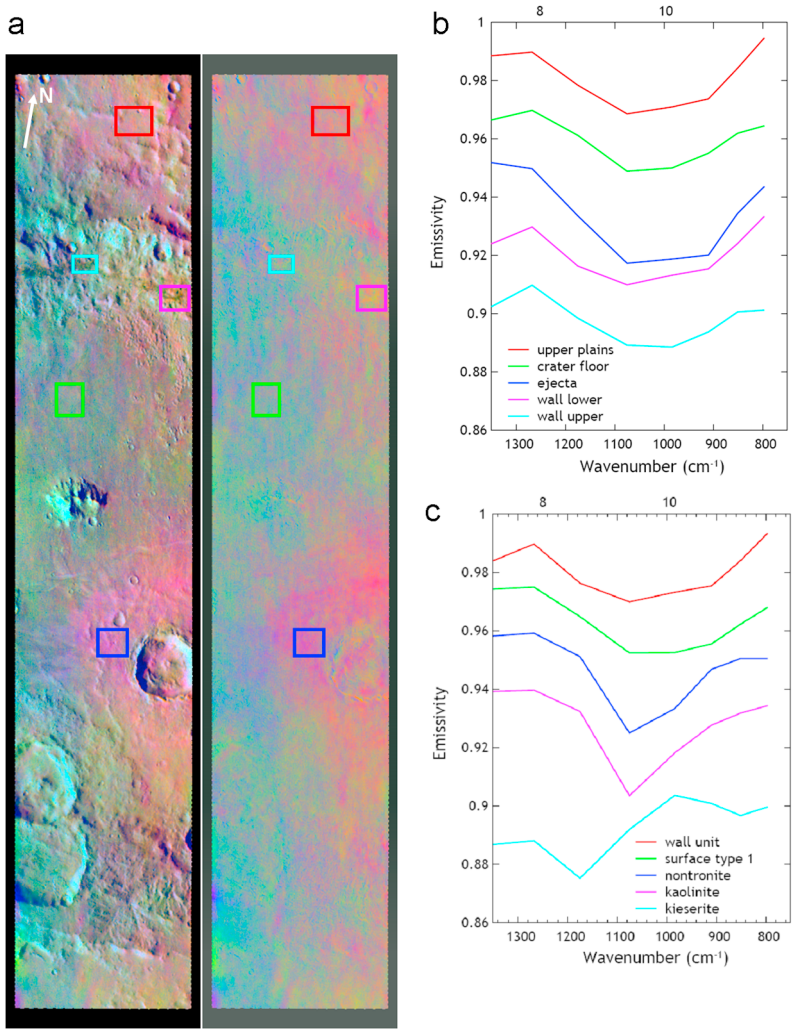

Figure 23. (a) Daytime IR DCS band 9-6-4 image covering central ~30 km swath across Columbus crater, from THEMIS I07746002. Left image is radiance, right image is emissivity. (b) Spectra extracted from boxed areas in Figure 23a. (c) "Wall lower" spectrum from Figure 23b (magenta box in Figure 23a) compared to spectra of TES Surface Type 1, phyllosilicates, and a sulfate.

fates, 15% olivine, and the balance in feldspars. The modeled sulfate abundance does not substantially exceed the TES detection limit of ~10–15% [*Christensen et al.*, 2001a]. However, the modeled spectrum was extracted from an area that includes several distinct spectral units at CRISM resolution (sulfate-bearing versus clay-bearing versus nonhydrated), so abundances of sulfates and phyllosilicates are likely higher within the light-toned outcrops specifically.

5. Stratigraphy and Chronology at Columbus

[55] Sections 2 and 3 have described the diversity of deposits in Columbus crater. Here we describe their stratigraphic relationships and use crater counting to estimate the ages of some events in Columbus's geologic history. The diverse hydrated minerals in Columbus crater may have formed during numerous alteration events spanning significant time or during a single, geologically brief period of aqueous activity. Exposures in the walls of small craters (e.g., Figure 5c) and other steep scarps provide some insights, including the significant observation of polyhydrated sulfate-bearing beds alternating with kaolinite-bearing beds [*Wray et al.*, 2009a, Figures 4c, DR6, DR7]. However, in many cases the stratigraphic relations are less clear; for example, Figure 14 shows polyhydrated sulfates on the crater wall, jarosite-bearing beds on the crater floor, and additional polyhydrated sulfates at still lower elevations in a depression adjacent to the jarosite. But does this topographic distribution indicate a period of jarosite formation separating two distinct periods of polyhydrate formation? Or did the jarosite form first, followed by a single period of polyhydrate formation on the crater walls and in local depressions on the crater floor? Or could the jarosite have formed diagenetically after the polyhydrates were precipitated/deposited, as in some acid saline lakes on Earth [*Benison et al.*, 2007]? These questions are difficult to resolve based on orbital imagery alone, preventing us from constructing a simple stratigraphic

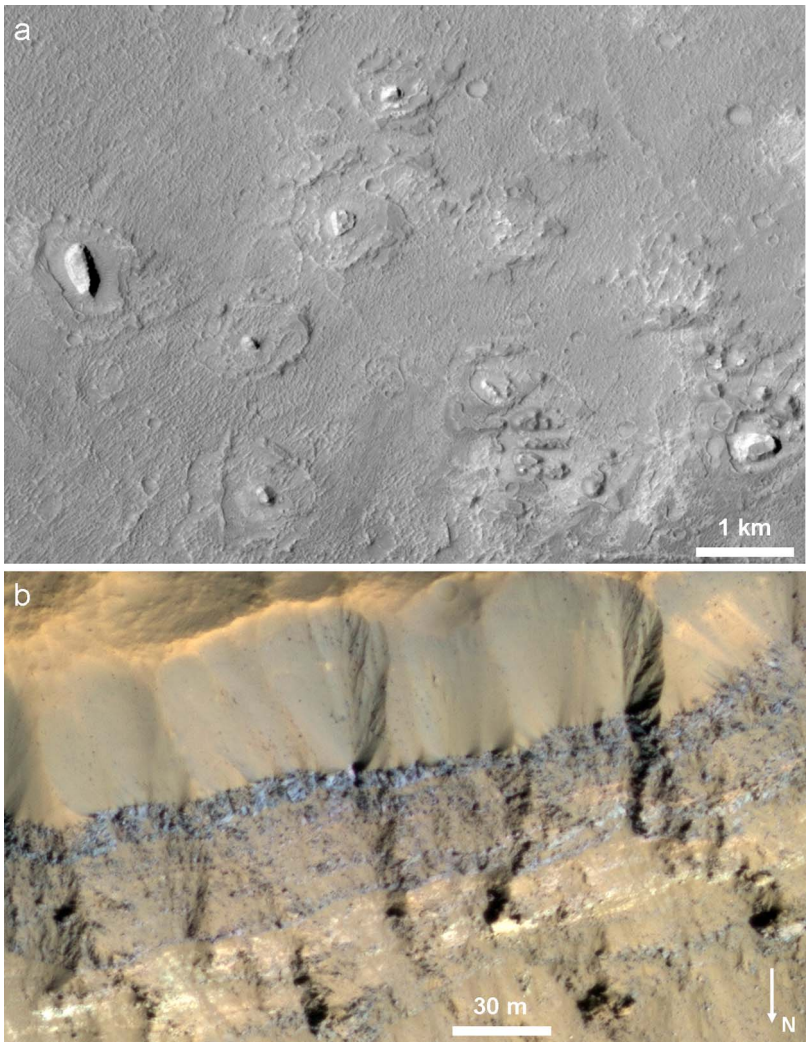

Figure 24. Stratigraphic relations on Columbus crater floor. (a) Mesas of light-toned layered materials on the eastern floor, embayed by darker ridged material interpreted as lava; from CTX P05_003095_1518. (b) Stratigraphy of Columbus crater floor exposed in the wall of a superposed D ~11 km crater; from HiRISE PSP_008356_1500. Light-toned layered deposits underlie darker, rubbly, olivine-bearing layers. Location shown by black box in Figure 25.

column to compare to theoretical evaporite sequences [e.g., *Tosca et al.*, 2008a; *Altheide et al.*, 2010a].

[56] One constraint on the timing of aqueous activity is provided by Figure 10, which shows a D ~17 km crater superposed on Columbus's southwest wall. The crater's flat floor and strongly degraded rim contrast with the similarly sized crater to its northeast, which retains its central peak, implying that the 17 km crater's interior has experienced significant infilling and/or erosion; the materials exposed on its modern floor therefore postdate the crater. The crater floor is at the elevation of the polyhydrate ring, and polyhydrated sulfates are indeed found in layered deposits on its floor. This implies that aqueous activity postdated the formation of the 17 km crater; therefore, at least some aqueous activity must have occurred some time after the formation of Columbus crater (i.e., not all aqueous activity predated or coincided with crater formation).

[57] Other observations show that the dark deposit covering much of Columbus's floor (which we have argued to be consistent with lava (section 2.1)) postdates the light-toned deposits containing hydrated minerals. As described in section 2.2, the probable lava overlies light-toned materials on the northwest crater floor (Figure 8b), and CRISM FRT00005AA4 shows these light-toned materials to be hydrated (Figure 22). Images of the northeast crater floor show the lava embaying mesas of light-toned material (e.g., Figure 24a). In addition, the D ~11 km crater on Columbus's southern central floor exposes decameters of stratigraphy in its upper walls, with light-toned beds overlain by darker, relatively blue beds (Figure 24b). Boulders are eroding from the darker beds, which have a rougher texture and (according to CRISM) an enhanced olivine signature; we interpret these darker beds as lavas, possibly olivine-bearing basalt flows. By contrast, erosion of the lighter-toned beds appears to yield finer-grained, hydrated

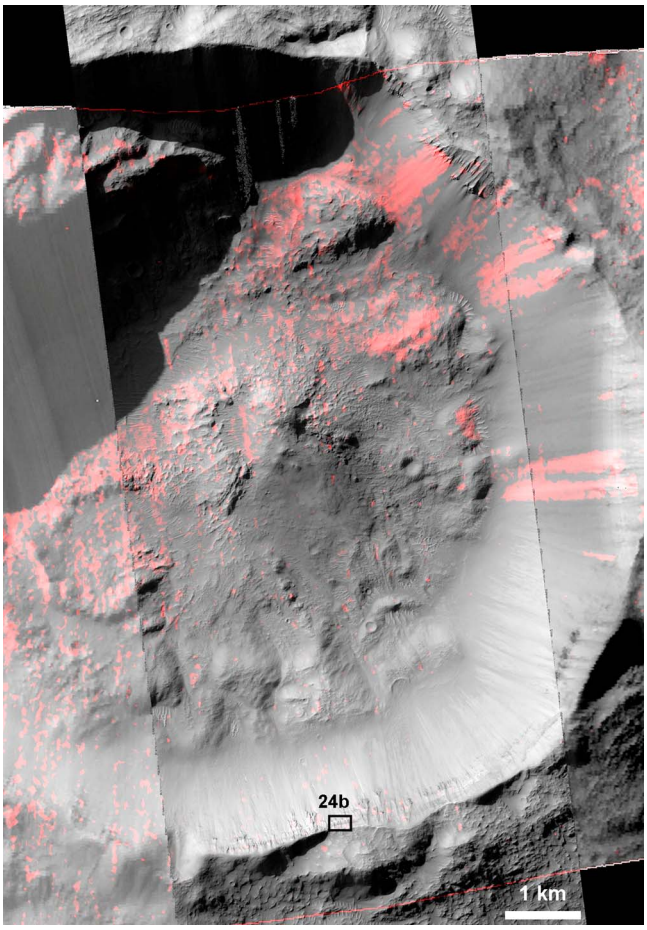

Figure 25. Hydrated materials (red) inside D ~11 km crater on the floor of Columbus crater. Hydrated colluvial deposits extend down crater walls from beds exposed in upper walls. Background is HiRISE PSP_008356_1500 and CRISM FRT0000ABF2 IR albedo (IRA from *Pelkey et al.* [2007]); hydration mapped using BD1900H [*Ehlmann et al.*, 2009].

material that is transported downslope to form scree deposits (Figure 25). These and other probable colluvial materials mantle the lower crater walls and conceal the >1 km thickness of underlying deposits inferred to occupy Columbus's floor (section 2.1). Overlying the dark-toned beds in Figure 24b is a somewhat lighter-toned, smooth-textured deposit with sparse boulders <1 m in diameter and a relatively weak olivine (or other ferrous mineral) spectral signature. These characteristics are consistent with those of the Late Hesperian-aged "Electris deposits" of Sirenum Fossae as described by *Grant et al.* [2010], who interpreted them as probable aeolian loess. From an HRSC DEM, we estimate a crater wall slope of ~20° at the location of Figure 24b, so the lateral extent of the deposits indicates a vertical thickness of ~10 m hydrated layered deposits, ~15 m olivine-bearing lava, and ~20 m Electris-like deposits at this location. While we cannot exclude the alternative that some of these layers are stratigraphically inverted ejecta from the D ~11 km crater itself, they occur some ~200 m below the crater rim crest and their stratigraphy is consistent with that observed elsewhere in Columbus.

[58] As discussed in section 2.1, a graben cuts the floor of Columbus crater approximately in half (Figure 1). The ENE–WSW orientation of this graben is similar to that of the larger Memnonia and Sirenum Fossae to the north and south of Columbus, respectively. These graben systems are in turn part of a hemisphere-wide collection of structures oriented radially to Tharsis, which formed over a large span of Martian history [*Plescia and Saunders*, 1982; *Anderson et al.*, 2001]. Some graben in Terra Sirenum may date to the Noachian "stage 1" of tectonic activity, but many likely date to the Late Noachian/Early Hesperian, overlapping wrinkle ridge formation in the Early Hesperian Epoch ("stage 3" of *Anderson et al.* [2001]).

[59] The graben in Columbus crater appears to predate the light-toned layered deposits, as revealed by the stratigraphy surrounding a D ~2.5 km crater on the western floor (Figure 26a). Mesas surrounding this crater consist of light-toned layered deposits overlain by darker materials (Figure 26b) and extend to a height of ~100 m above the surrounding plains, twice the typical rim height for a fresh crater of this size [*Garvin et al.*, 2003]. These mesas are therefore probably not composed solely of crater ejecta; instead, the uppermost dark materials may be ejecta that armored underlying light-toned layered deposits against an erosional process that stripped the deposits from adjacent terrain [e.g., *McCauley*, 1973]. Neither the D ~2.5 km crater nor the mesas surrounding it are visibly deformed by the graben, suggesting a sequence of (1) graben formation, (2) layered deposit formation, (3) formation of the 2.5 km crater, and (4) erosion of adjacent layered deposits. Lava deposition is inferred to postdate these events because the probable lavas embay the erosional remnant mesas. Lava would be expected to fill and bury a preexisting graben, so the fact that the graben remains visible may be explained by its later reactivation following lava flow emplacement, as evidenced by the graben's disruption of some small craters on the lava flow surface (Figure 26c).

[60] As mentioned in section 2.1, a few poorly developed valleys are visible on the northeast wall of Columbus (Figure 1b). The crater walls and floor near the mouths of these valleys host a dark-toned deposit with relatively low thermal inertia (~230 ± 10 tiu) and a spectrum dominated by broad bands near 1 and 2.1–2.2 μm, consistent with a basaltic composition [e.g., *Mustard et al.*, 1997]. This dark deposit overlies the light-toned deposits on this part of the crater floor and has partially buried the sulfate-bearing ring on the crater walls (Figure 14a). These superposition relationships suggest that gradation of the crater wall likely occurred here after the period during which aqueous minerals and light-toned deposits formed in Columbus. The dark-toned deposit may have preferentially armored light-toned deposits on this part of the crater floor against erosion. Columbus crater lies at the southern edge of the latitude band (18–29°S) in which *Moore and Howard* [2005] identified alluvial fans dating to the Noachian-Hesperian boundary in 18 middle-sized to large craters. The dark deposit in northeast Columbus could be a highly degraded alluvial fan. A deltaic interpretation seems less plausible given the lack of clear stratal geometries or clay minerals; for comparison, two of the most likely deltaic deposits

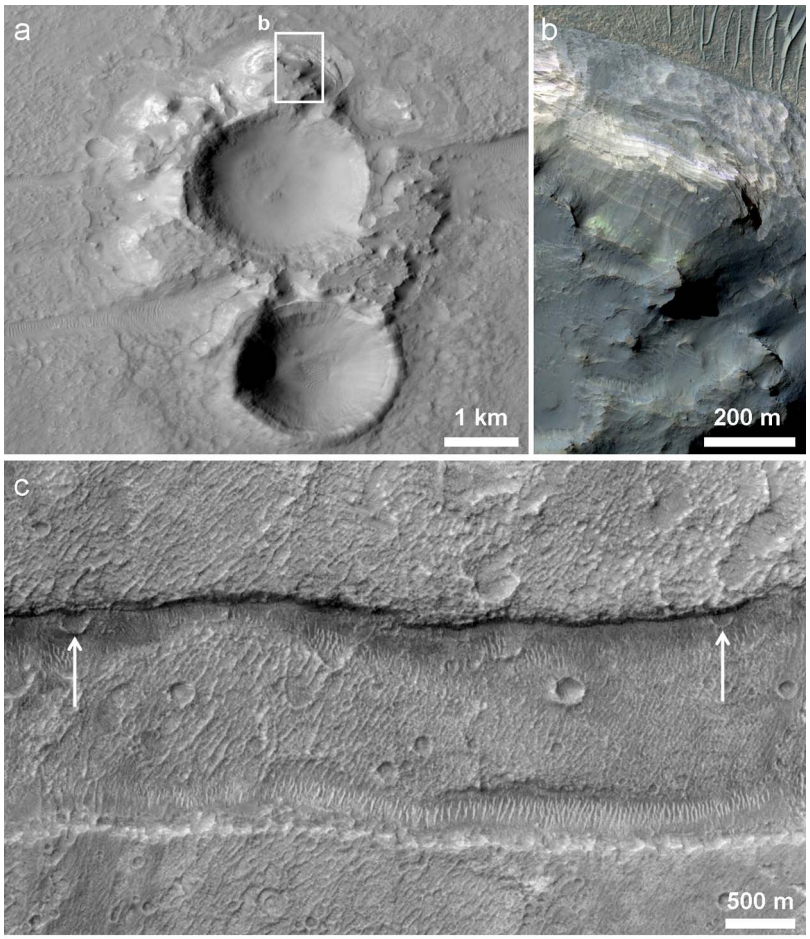

Figure 26. (a) A ~2.5 km impact crater superposing the graben in Columbus crater; from CTX P03_002739_1505. The *D* ~2 km crater immediately to the south is fresher and probably younger, as indicated by its greater depth (note shadows) and more pronounced rim crest. (b) Dark-toned materials overlying light-toned layered deposits in the mesas surrounding the *D* ~2.5 km crater; from HiRISE ESP_016861_1505. (c) Graben segment on Columbus eastern floor, disrupting two small craters (arrows); from CTX P12_005851_1505.

identified on Mars contain phyllosilicates and exhibit clear bedding [*Ehlmann et al.*, 2008a; *Milliken and Bish*, 2010].

[61] For an estimate of the absolute age of Columbus and its interior deposits, we now consider counts of superposed impact craters. Columbus's interior and proximal ejecta represents a small area for counting craters (~17,000 km^2), so the formal statistical uncertainties (which are proportional to $1/\sqrt{(n)}$, where n is the number counted) are large. In the notation of *Tanaka* [1986], in which the measured crater densities are scaled to an area of 10^6 km^2, Columbus has N(16) = 120 ± 85 craters > 16 km in diameter per 10^6 km^2, and N(5) = 420 ± 160. These values are most consistent with a Middle Noachian age for Columbus, although a Late Noachian age (that of the Upper Noachian units described by *Tanaka* [1986]) is within the uncertainties. As stated in section 2.1, the cratered plains unit in which Columbus occurs has similarly been dated to the Middle Noachian. We also counted separately only those craters that clearly superpose (i.e., postdate) Columbus's light-toned layered deposits, yielding densities of N(5) = 280 ± 160 and N(2) = 1210 ± 340, consistent with a Late Noachian age (although Early Hesperian is within the uncertainties). Finally, the probable lava flow on the floor of Columbus has crater densities N(5) = 130 ± 130, N(2) = 920 ± 350, and N(1) = 3410 ± 670, consistent with an Early Hesperian age like most ridged plains on Mars. For each of these (Columbus crater, layered deposits, and lava), 1–3 craters were counted in the largest size category and 7–26 craters in the smaller size categories.

[62] In summary, Columbus crater likely formed in the Middle-to-Late Noachian, and it accumulated >1 km of fill prior to a distinct period of light-toned deposit formation and aqueous activity during the Late Noachian. A probable lava flow subsequently covered most of the crater floor during the Early Hesperian, and it was modified during this period by compressional and extensional tectonics likely related to Tharsis loading. Sediment accumulation continued at a lower rate during the Late Hesperian and possibly later, emplacing a mantle of likely aeolian origin on at least some portions of the crater interior. In the more recent Amazonian, the dominant geologic processes have likely been mass wasting and aeolian erosion of the intracrater deposits, as

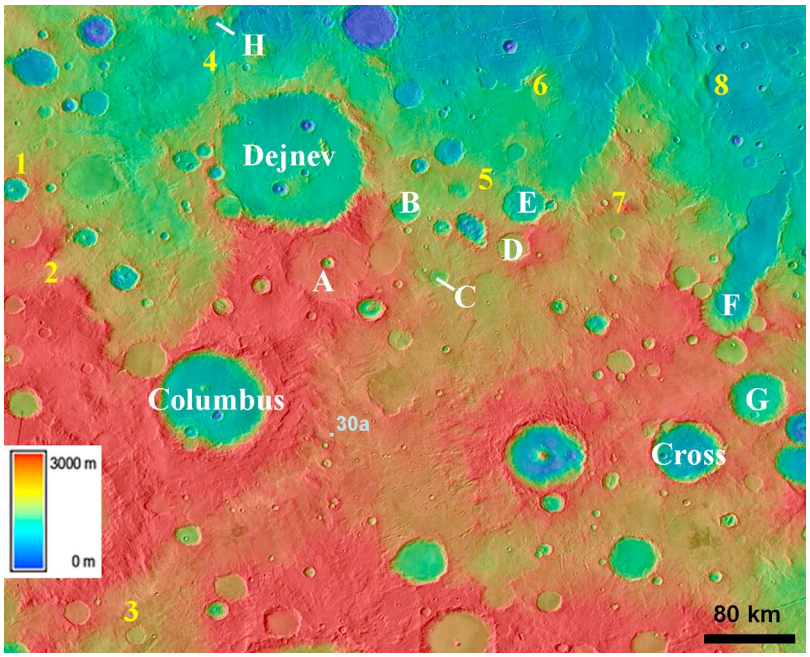

Figure 27. THEMIS daytime IR mosaic of northwest Terra Sirenum (190–205°E, 22.5–34°S) colorized with MOLA elevations. Named impact craters and those designated A–H exhibit a ~2.2 μm Al/Si-OH absorption in CRISM multispectral data and/or contain light-toned layered deposits. Numbered locations correspond to possible Al/Si-OH detections on intercrater plains. Chloride and Fe/Mg-phyllosilicate exposure shown in Figure 30a is also indicated.

well as impact events that have exposed older deposits in the walls and ejecta of fresh craters such as that in Figure 25.

6. Other Aqueous Deposits of Northwest Terra Sirenum

[63] As reported by *Murchie et al.* [2009b] and *Wray et al.* [2009a], CTX images and CRISM multispectral data hint that several craters near Columbus in northwest Terra Sirenum may host similar layered deposits, and this region's intercrater plains also contain aqueous mineral deposits. Here we describe these deposits as regional context for our Columbus crater observations.

6.1. Intracrater Deposits

[64] The most striking feature of northwest Terra Sirenum in CRISM multispectral data is the presence of a ~2.2 μm Al- or Si-OH absorption in materials occupying most of the region's large craters (Figure 27). In particular, this spectral feature is found in the region's most degraded (and therefore probably oldest) craters, which have flat floors, degraded rims, and superposed impact craters. By contrast, a D ~80 km crater ~300 km east of Columbus with fresh-appearing ejecta has no detectable hydrated minerals. Of the northwest Sirenum craters other than Columbus, so far the greatest mineralogic diversity has been found in Cross crater, which hosts alunite, kaolinite, and montmorillonite or hydrated silica in finely bedded deposits on its walls and floor [*Swayze et al.*, 2008b]. Cross crater is the focus of a manuscript in preparation by G. A. Swayze et al. (2010), so we focus on other craters here.

[65] Of the nine craters identified with a ~2.2 μm band in CRISM multispectral data, three are named (Columbus, Cross, Dejnev) and to the other six we assign letters (craters A–F) for convenience (Figure 27). Two other craters (G and H in Figure 27) lack CRISM coverage but have light-toned floor deposits morphologically similar to those on the floor of Columbus (see CTX P18_008237_1505 and HiRISE ESP_017573_1570, respectively). Craters A, D, E, and Dejnev have recently been observed by CRISM in hyperspectral mode, and all craters exhibiting the 2.2 μm absorption have been imaged by HiRISE. Light-toned layered deposits are observed in most of these craters (Figure 28). These deposits are especially widespread across the floor of crater E (Figure 28a), where they have likely been significantly eroded to yield the scattered mesas observed on the modern crater floor. Each hectometer-scale mesa exposes dozens of meter-scale beds in cross section (Figure 28e). The morphology and color of beds in crater F and Dejnev (Figures 28c and 28d) are reminiscent of beds on the floor of Columbus crater, including those that contain monohydrated sulfate. In HiRISE enhanced color images, the green appearance of some beds in crater B (Figure 28b) suggests a crystalline ferric mineral might be present (possibly ferric sulfate; see discussion in section 3.5), but this possibility has not yet been tested with CRISM hyperspectral data.

[66] As in Columbus and Cross craters, kaolinite is identified in hyperspectral images of craters A, D, E, and Dejnev (Figure 29). We have also found Fe/Mg-phyllosilicate in each of these locations except in crater D, and montmorillonite is detected in crater E. Somewhat surprisingly, these minerals generally are not found within the light-toned

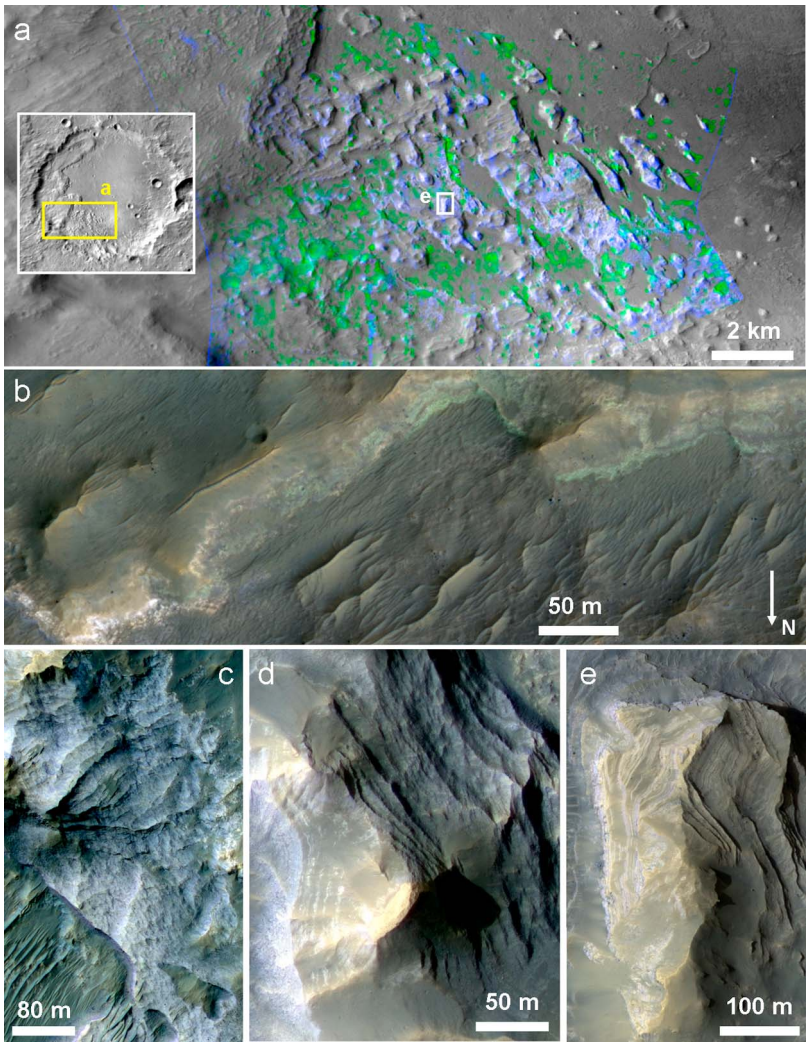

Figure 28. Light-toned layered deposits in craters near Columbus. (a) Portion of western wall and floor of crater E in Figure 27 (see inset for context); from CTX P03_002330_1539, colored with parameter maps from CRISM FRT000106E4. Green is BD2200 [*Ehlmann et al.*, 2009] and blue is BD3000 [*Pelkey et al.*, 2007], tracking Al-phyllosilicates and H_2O-bearing materials, respectively. Light-toned mesas are hydrated, and darker areas between mesas near image center are spectrally consistent with montmorillonite. (b) Colorful layers on floor of crater B; from HiRISE ESP_015951_1535. Green materials may contain ferric sulfate. (c) Layered deposits in crater F; from ESP_016109_1525. (d) Layered deposits at base of southern wall of Dejnev crater; from ESP_011560_1535. (e) Mesa on floor of crater E, exposing dozens of meter-scale layers; from ESP_011639_1535.

layered units of Figures 28c–28e. Instead, kaolinite and Fe/Mg-phyllosilicate most commonly occur in massive materials on the crater walls, and montmorillonite (possibly mixed with kaolinite) is found in the somewhat darker, rough-textured (but layered) floor of crater E (Figure 28a). Some detections of kaolinite in crater E (CRISM FRT000106E4) appear to correspond to light-toned layered deposits, but the higher spatial resolution of HiRISE is needed to confirm this. Stratigraphic relations between the kaolinite and Fe/Mg-phyllosilicates are not always clear, but in the case of crater E the latter are found eroding from the uppermost southeast crater wall (analogous to Figure 10 from Columbus), whereas Al-phyllosilicates are seen deeper within the crater.

[67] What, then, is the mineralogy of the light-toned beds on these crater floors? In crater E, spectra of most layered outcrops contain no obvious absorptions from 1.0 to 2.6 μm; however, these outcrops have stronger ~3 μm bands than other materials in the same CRISM scene (Figure 28a). Absorptions at ~3 μm are ubiquitous on Mars, though variable in strength; they are attributed to adsorbed or structural H_2O and/or OH in surface materials [*Jouglet et al.*, 2007; *Milliken et al.*, 2007]. Many nominally anhydrous minerals have a ~3 μm absorption in spectra obtained under terrestrial laboratory conditions [*Clark et al.*, 2007]. Still, this absorption is typically stronger for hydrated minerals such as phyllosilicates, including those on Mars [*Jouglet et al.*, 2007; *Milliken et al.*, 2007], but in crater E the ~3 μm band is weaker in the montmorillonite-bearing crater floor materials

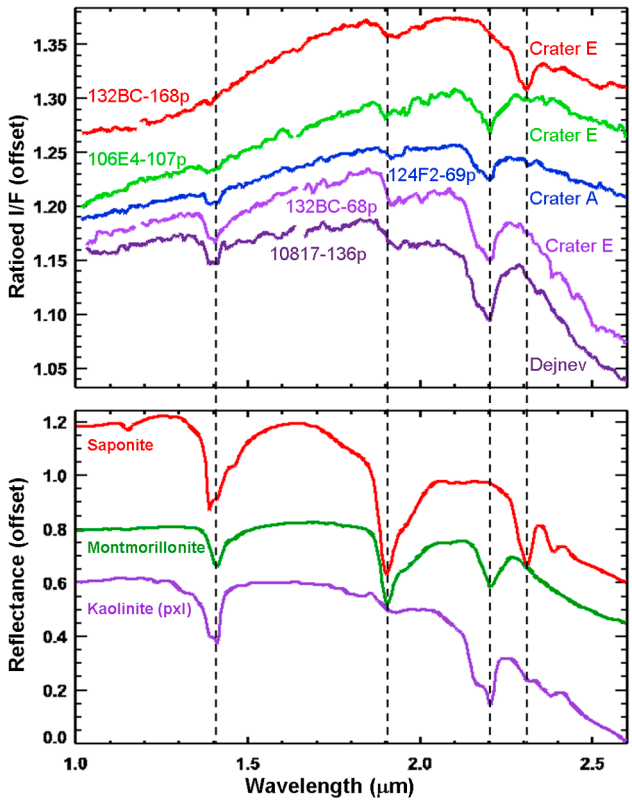

Figure 29. (top) CRISM spectra from northwest Terra Sirenum craters and (bottom) lab spectra of phyllosilicates; format similar to Figure 11. Saponite is SapCa-1.AcB, montmorillonite is SWy-1, and poorly crystalline (pxl) kaolinite is KGa-2 from *Clark et al.* [2007].

and stronger in the layered mesas. The mesas have a higher albedo, a property that is also positively correlated with ~3 μm band depth in I/F spectra on a global scale, possibly because the greater absorptivity of darker materials results in higher daytime temperatures, driving off adsorbed water [*Jouglet et al.*, 2007]. Alternatively, *Milliken et al.* [2007] showed that the hydration–albedo correlation can result from nonlinear absorption processes, and that high albedo regions do not contain more water than dark regions once these effects are accounted for by converting spectra to single scattering albedo. Regardless, the precise mineralogy and nature of hydration in the layered mesas of crater E (and Dejnev) are currently unconstrained.

6.2. Intercrater Deposits

[68] Whereas Al-phyllosilicates and sulfates are the dominant secondary minerals in the craters of northwest Terra Sirenum, Fe/Mg-phyllosilicates (smectites) and chloride salts are more common on the intercrater plains, as in other regions of the southern highlands [*Osterloo et al.*, 2008; *Murchie et al.*, 2009b; *Wray et al.*, 2009a; *Glotch et al.*, 2010]. *Baldridge et al.* [2009, Figure 2c] identified putative chlorides in a shallow basin just ~10 km south of Columbus crater's southwestern rim, and Figure 30a shows another location ~60 km east of Columbus where THEMIS identifies chloride in bright outcrops; these outcrops overlie materials in which CRISM (FRT0000B59A) detects Fe/Mg-phyllosilicates. To date, chlorides have not been identified within any of the larger craters discussed in section 6.1.

[69] A few locations on the intercrater plains of northwest Sirenum do contain Al-phyllosilicates. Figure 27 enumerates eight intercrater sites at which a ~2.2 μm absorption is found in multispectral and/or hyperspectral CRISM data. All except site 8 have been imaged by HiRISE, revealing a range of exposure types. At sites 1 and 4 (Figures 31a and 31b), CRISM detects kaolin group phyllosilicates in the ejecta of small impact craters (D ~700 m and 600 m, respectively). The site 4 crater appears relatively unmodified (i.e., young), with bright rays visible in THEMIS nighttime IR images and abundant meter-scale blocks on the rim and proximal ejecta. This crater's proximal ejecta contain Fe/Mg-phyllosilicates (Figure 31a), which may underlie kaolinite-bearing materials in the subsurface here. Sites 2 and 7 each contain a cluster of small craters with kaolinite-bearing ejecta (Figures 31c and 31d); the largest of these craters exposes light-toned strata in its upper walls (Figure 31e) that may be the source of the kaolinite. At site 6, a D ~1.4 km crater exposes light-toned materials in its rim (Figure 30b). All of these craters are probably too small to have initiated long-lived hydrothermal activity to form phyllosilicates [*Rathbun and Squyres*, 2002], and given the general paucity of evidence for phyllosilicate formation in post-Noachian terrains [*Poulet et al.*, 2005; *Bibring et al.*, 2006; *Mustard et al.*, 2008], we infer that they likely excavated preexisting Al-phyllosilicates from the shallow subsurface.

[70] At intercrater Al-OH site 5, only a single hectometer-scale exposure of Al-phyllosilicate is identified in CRISM HRL00011D66, but adjacent light-toned layered deposits (Figure 30c) are spread across an area tens of km wide on the plains northwest of crater E. Similar to crater E's floor deposits, the layered deposits at site 5 have a relatively strong ~3 μm band as their only distinguishing feature in CRISM data. These deposits provide evidence that the sedimentation and aqueous processes that occurred in the large craters of northwest Terra Sirenum were not restricted to these locations but also affected at least some portions of the intercrater plains.

[71] At intercrater site 3 (the only 2.2 μm site south of Columbus and Cross craters) the ~2.2 μm band identified in CRISM mapping data is not primarily due to Al-OH, but instead to Si-OH. Although this site's relationship to the Columbus crater deposits is unclear, we describe it here in the interest of fully exploring the region's aqueous history.

[72] At this location (167.45°W, 33.15°S), a mound ~3 km by 5 km wide protrudes ~100 m from the surrounding plains (Figure 32a). The central mound has a weak spectral signature consistent with hydrated silica (i.e., opal), with stronger signatures present on its flanks and on the adjacent plains. Hydrated silica is distinguished from Al-phyllosilicates by its broader 2.2 μm band with an asymmetric long-wavelength edge extending to 2.3 μm or beyond [*Milliken et al.*, 2008; *Ehlmann et al.*, 2009]. In well-hydrated opaline silica this band is in fact a doublet with minima at 2.21 and 2.26 μm. Removal of H_2O from opal at moderate temperature or low relative humidity causes the 2.26 μm band to disappear, weakens the 1.9 μm H_2O band, and "shifts" the Si-OH overtone absorption from

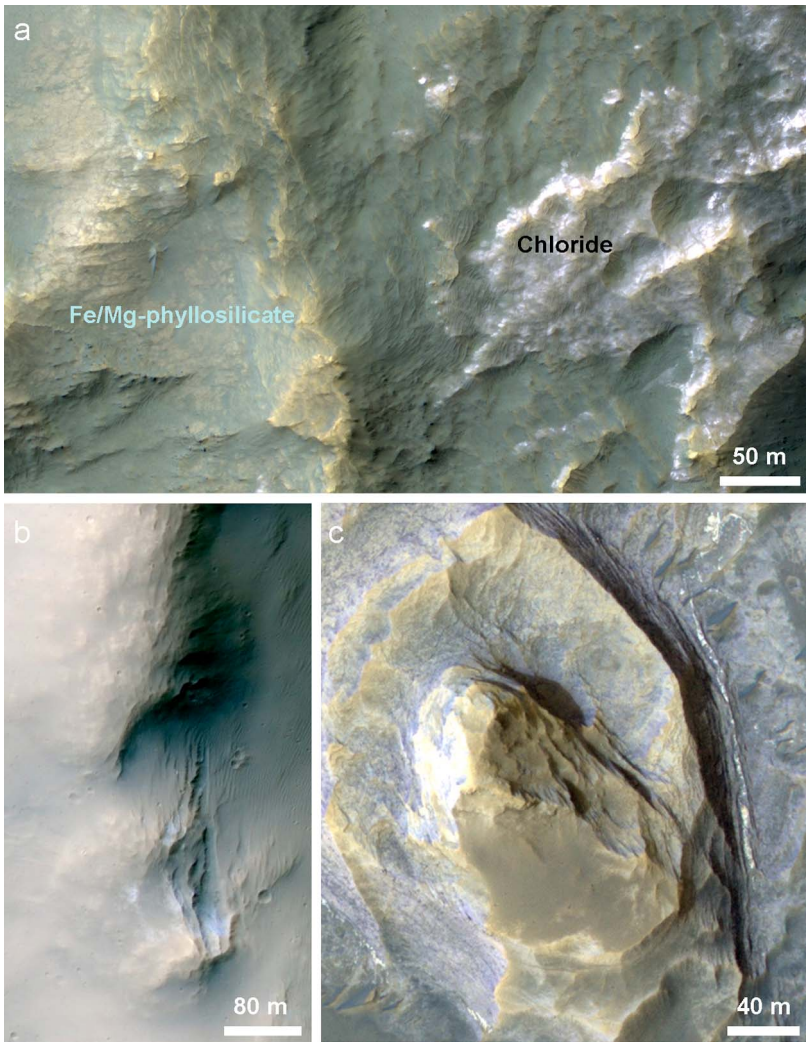

Figure 30. Light-toned deposits on the intercrater plains of Terra Sirenum. (a) Sample chloride/phyllosilicate exposure ~60 km east of Columbus crater; from HiRISE ESP_016162_1495. Context shown in Figure 27. (b) Light-toned, relatively blue outcrops exposed in crater rim corresponding to Al/Si-OH site 6 in Figure 27; from ESP_016030_1560. (c) Layered mesa near Al-OH site 5 in Figure 27; from ESP_012562_1545.

1.41 μm to 1.38 μm [*Anderson and Wickersheim*, 1964; *Milliken et al.*, 2008; *Cloutis et al.*, 2009; *Ehlmann et al.*, 2009]. Hydroxylated glasses have similar features, but their single 2.2 μm absorption is more symmetric and commonly centered at a slightly longer wavelength of 2.22–2.23 μm, and their ~1.4 μm overtone does not shift upon dehydration [*Milliken et al.*, 2008].

[73] Spectra observed on and around the mound at site 3 are most consistent with opaline silica with variable degrees of hydration (Figure 33a). H_2O-poor silica is found in bright materials (Figure 33b) on the plains around the mound, whereas more fully hydrated silica occurs on the mound itself and in some intermediate-toned exposures on the plains (Figure 32a). These spectral differences are observed even when the same denominator is used for all ratio spectra in the scene. There is no obvious stratification or zoning pattern of the hydration states. The presence of variably hydrated materials in close proximity may suggest differences in formation temperature or a dehydration process driven by local thermal gradients rather than atmospheric humidity, consistent with a hydrothermal environment for silica formation; alternatively, varying physical properties could have made some silica-bearing materials more susceptible to dehydration than others. Parts of the mound and surrounding plains have a narrower 2.16/2.20 μm doublet consistent with a kaolin group clay (Figure 33a), providing a possible mineralogic link to the kaolinite-bearing materials identified elsewhere in northwest Sirenum. Finally, a relatively strong low-calcium pyroxene signature is observed in plains several km distant from the mound, but the broader geologic context (Figure 32c) suggests no obvious connection between the mound and the pyroxene-bearing unit; the latter appears to be a more widespread underlying unit.

[74] We propose three alternative hypotheses for this topographic mound associated with opaline silica: it could be (1) an erosional remnant mesa, (2) a siliceous spring mound [e.g., *Guidry and Chafetz*, 2003], or (3) a volcanic construct that has been aqueously altered, possibly under

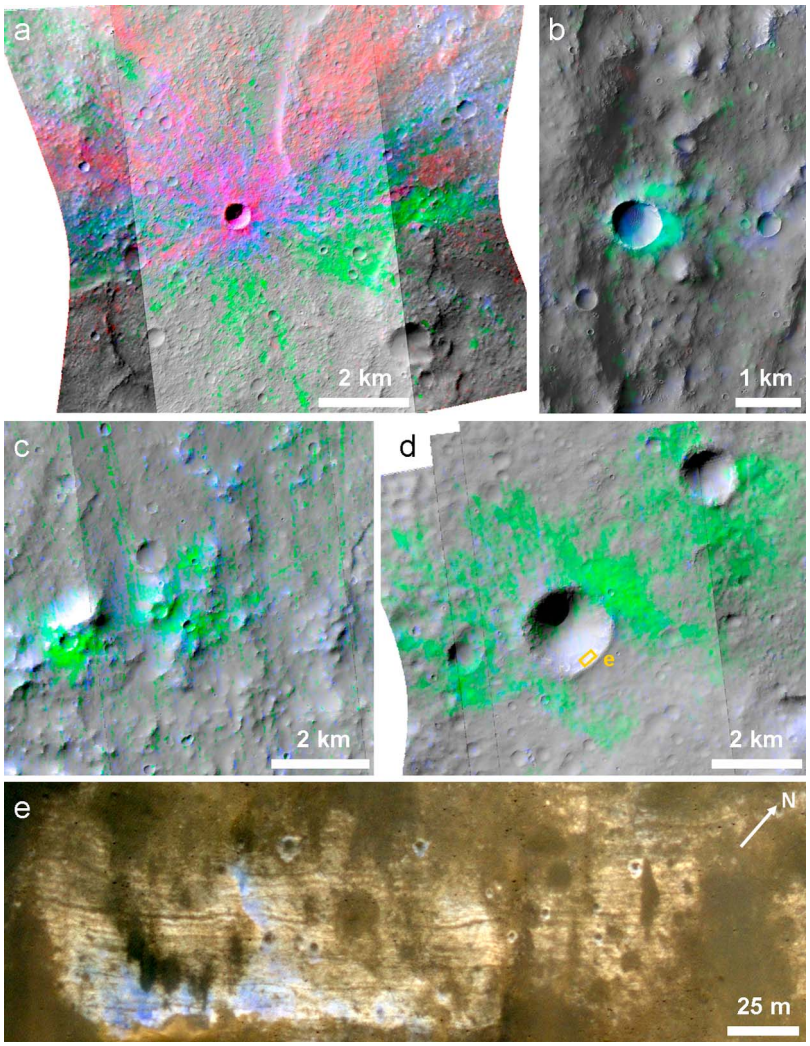

Figure 31. Craters in northwest Terra Sirenum with Al-phyllosilicate-bearing ejecta. Red is D2300 [*Pelkey et al.*, 2007], green is BD2200, and blue is BD1900H [*Ehlmann et al.*, 2009]; these map Fe/Mg-phyllosilicates, Al-phyllosilicates, and hydrated minerals, respectively. (a) Site 4 from Figure 27; CRISM FRT00009D7E parameters overlain on IR albedo and HiRISE PSP_008290_1565. (b) Site 1; CRISM HRL00009C1F on HiRISE ESP_016149_1550. (c) Site 2; FRT000176BD on ESP_017138_1525. (d) Site 7; FRT00017199 on ESP_016953_1540 and ESP_017164_1540. (e) Layers exposed in crater wall at site 7; from ESP_017164_1540.

acidic conditions [e.g., *Seelos et al.*, 2010]. Opaline silica has previously been identified adjacent to volcanic mounds both in the Columbia Hills of Gusev crater [*Squyres et al.*, 2008] and in the Nili Patera caldera of Syrtis Major [*Skok et al.*, 2010]. The Nili Patera mound is quite similar to our site 3 in lateral scale and in the localization of its partially dehydrated silica to bright outcrops adjacent to the mound. However, the Nili mound is ~3 times taller than ours, is texturally massive, and sheds abundant meter-scale boulders (see HiRISE ESP_013582_1895). Fewer boulders are visible on the flanks of the mound at site 3, suggesting the material is friable and thus consistent with a sedimentary nature; the mound's lower profile, constituent silica, and bedded or terraced morphology (Figure 32d) are more consistent with silica-cemented sediments or a spring mound than with a volcanic construct. Also unlike the Columbia Hills and Nili Patera, there are no other obvious volcanic features in the vicinity of site 3; whereas pyroxene and olivine-bearing ridged materials adjacent to the Nili mound are likely lava flows [*Skok et al.*, 2010], the pyroxene-bearing outcrops near our site 3 have a fractured texture (Figure 32b) uncharacteristic of typical Martian lavas. If site 3 is a siliceous spring mound, its size would rival the largest known spring mounds on Earth [*Crumpler*, 2003], but would be 1–2 orders of magnitude smaller than many Martian crater and canyon mounds that have previously been proposed as spring mounds [*Rossi et al.*, 2008]. Alternatively, this mound could simply be an erosional remnant of a previously more widespread deposit, possibly sediments that have been cemented by silica precipitating out of groundwater. If the kilometer-wide depression near the mound's summit is a degraded impact crater, then it may have made this portion of the deposit more resistant to erosion (e.g., by armoring the sur-

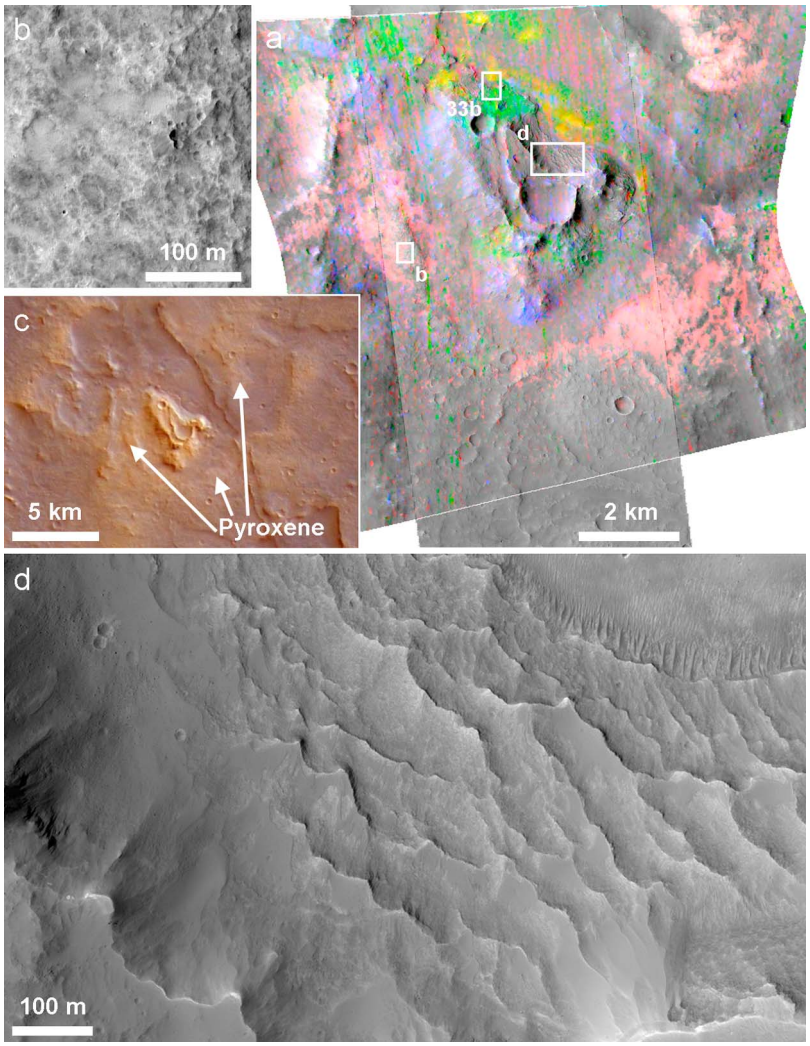

Figure 32. Intercrater Al/Si-OH site 3 from Figure 27. (a) Mineralogy of mound and surrounding plains. Red is LCPINDEX [*Pelkey et al.*, 2007], green is BD2200, and blue is BD1900H [*Ehlmann et al.*, 2009]; yellow is a parameter tracking wide 2.2 μm absorptions due to Si-OH. We have confirmed that red areas correspond to low-calcium pyroxene, blue to hydrated silica, yellow to partially dehydrated opal or altered glass, and green to kaolinite. Background is HiRISE ESP_011903_1465 and CRISM FRT00010EC5 IR albedo. (b) Surface texture of pyroxene-bearing materials. (c) Broader context of the mound and surrounding plains, from HRSC h0538_0000. (d) Exposure showing the mound's layered or terraced structure.

face with its ejecta). In this scenario, the process of silica formation would be poorly constrained.

7. Regional Hydrologic Modeling

[75] The diverse hydrated minerals found in Terra Sirenum (a region in which surface valley networks are relatively sparse [*Carr*, 1995; *Fassett and Head*, 2008b; *Hynek et al.*, 2010]) motivate consideration of a groundwater-dominated hydrology to explain the aqueous deposits. Global-scale hydrological models representing the groundwater evolution of early Mars can explain the distribution of sulfate-rich evaporite deposits in Meridiani Planum and surrounding regions [*Andrews-Hanna et al.*, 2007]. In those models, the region west of Tharsis (i.e., northern Terra Sirenum) is also a preferred location for a shallow water table and evaporite formation at smaller scales, driven by a combination of groundwater flow from the nearby high topography of Tharsis and the presence of a shallow topographic trough surrounding the rise [*Phillips et al.*, 2001]. Ejection of water from aquifers buried deep beneath Tharsis may also play a role [*Andrews-Hanna et al.*, 2007].

[76] In Terra Sirenum, hydrological activity in the vicinity of Columbus crater should be encouraged by a confluence of factors. These include its location roughly equidistant from the dichotomy boundary and a middle-sized basin to the south, each of which should act to draw down the water table in their immediate vicinity (so, by comparison, the water table would be relatively high near Columbus crater). Farther south, the water table drops deeper beneath the surface as a result of the southern limit of the low-latitude precipitation belt in the models and regional drawdown of

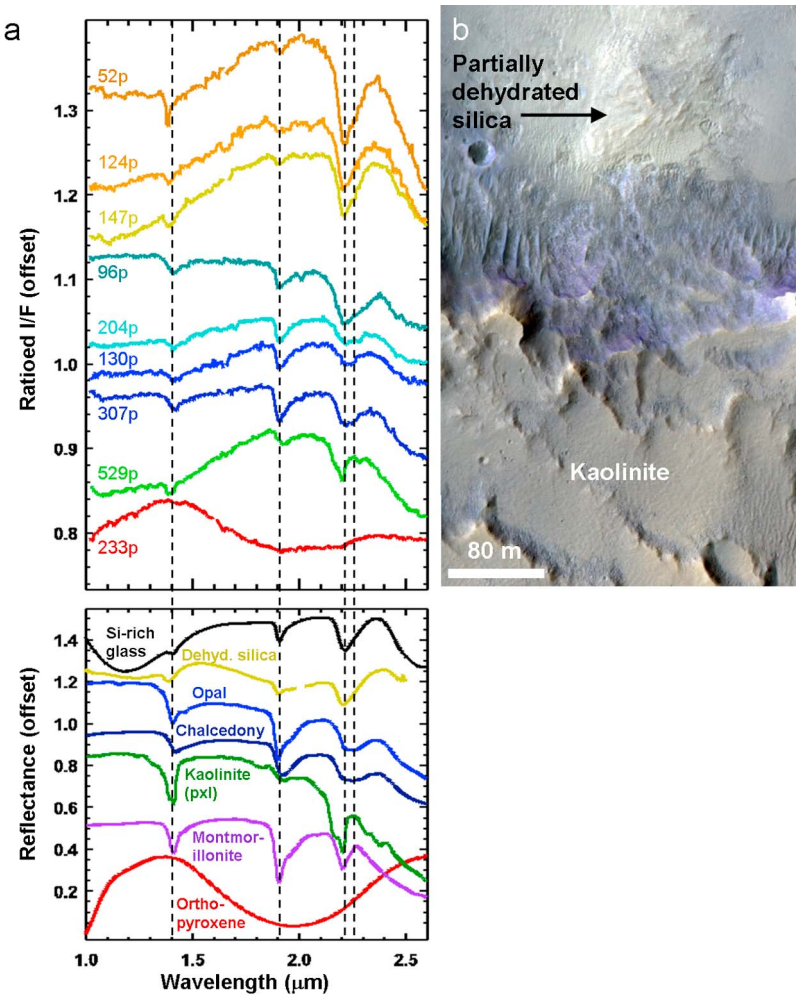

Figure 33. (a) CRISM spectra from mound at Sirenum intercrater at site 3 (top) and relevant lab spectra (bottom); format similar to Figure 11. All CRISM spectra are from FRT000010EC5. Si-rich glass is obsidian JB578 (scaled ×10 for ease of comparison) from *McKeown et al.* [2010]. Dehydrated silica is altered (silica coated) glass measured at Mars-like pressure and temperature (scaled ×20 for comparison) from *Milliken et al.* [2008]. Opal is sample TM8896, chalcedony (cryptocrystalline silica) is CU91–6A, poorly crystalline (pxl) kaolinite is KGa-2, and montmorillonite is SWy-1 from *Clark et al.* [2007]. Orthopyroxene is sample CBSB52 from CRISM spectra library. (b) Sample of mound texture (including kaolinite-bearing area) and adjacent light-toned materials containing partially dehydrated silica; from HiRISE ESP_011903_1465.

the water table in high southern latitudes by the Hellas and Argyre impact basins [*Andrews-Hanna et al.*, 2008]. For the detailed distribution of predicted evaporites in Sirenum, we turn to regional hydrologic modeling.

[77] We have run high-resolution (0.25 degree per pixel, corresponding to ~15 km at the equator) local hydrological models of the region west of Tharsis, using the precipitation rates and hydrologic head from the global simulations [*Andrews-Hanna et al.*, 2008, 2010] as boundary conditions. The precipitation is set to follow a cosine distribution between ±45° latitude, to approximately match the distribution of valley networks. The local model extends from 180° to 230°E and from 50°S to 10°N, boundaries sufficiently far from the region of interest (Figure 27) to avoid significantly affecting the results. The model assumes that groundwater evaporates upon reaching the surface, resulting in the formation of evaporites and evaporite-cemented sediments that can accumulate to substantial thickness in some regions. There is a dynamic coupling between the groundwater flow and the surface topography, in which groundwater-mediated sedimentation modifies the surface topography, which in turn modifies the paths and rates of groundwater flow. Ponding of emergent groundwater (e.g., in a crater lake) would affect the local hydrology in the same way as sediment accumulation would. The models assume a ratio between evaporated water column height and resulting sediment thickness of 50 to 1, consistent with evaporation of deep groundwater with salinity comparable to seawater and a 40% volumetric contribution from nonevaporitic sediments [*Handford*, 1991; *Möller et al.*, 1997; *Andrews-Hanna et al.*, 2007]. Higher or lower rates of deposit formation could result from increased or decreased sediment flux and fluid salinities. However, because the

surface topography evolves slowly relative to the fluid flow, the system is in a state of quasi-equilibrium at any one time, and the impact of different sedimentation rates can be achieved by simply scaling the time scale for evolution. Similarly, changing the mean crustal permeability primarily changes the rate of water cycling through the hydrologic system without altering the gross distribution and flow paths of water. The model results should, therefore, yield insights into the spatial distribution of relative evaporite thicknesses even if their absolute thicknesses are poorly constrained.

[78] As found in the global models [*Andrews-Hanna et al.*, 2008, 2010], the water table initially intersects the surface only within scattered impact craters and other topographic lows. The intersection of the water table with major impact craters can be clearly seen in maps of the hydraulic head at the beginning of the simulation (Figure 34b). As the simulation evolves, shallower craters fill with sediments resulting in a concomitant decrease in the rate of groundwater upwelling. In most cases, this trend progresses until the crater depth reaches some minimum value at which the groundwater flux to the surface terminates. The water table follows a smoothed approximation of the topography (Figure 34b), with the shorter-wavelength structure diminishing as the smaller craters are filled with sediments, resulting in the dominance of longer-wavelength flow paths (Figures 34f, 34j, and 34n). Nevertheless, Columbus crater still features prominently as a locus of groundwater upwelling and evaporation after the groundwater flux into many of the smaller craters has ceased (Figures 34i–34l). Although the models assume that groundwater evaporates immediately upon reaching the surface, this groundwater flux could support the formation of either playas or deeper lakes depending on the local climatic conditions.

[79] These models have used the present-day topography of Mars as a starting condition, though the current topography is the end product of 4.5 billion years of evolution. Although it is not possible to recreate the surface of Mars at any one time in its history, we can infer the effects of changes to the surface topography over time. It is noteworthy that the older craters in the region (Dejnev, Columbus, Cross, and others) typically contain hydrated minerals and/or layered deposits, whereas younger craters do not (Figure 27 and section 6.1). For example, the relatively fresh D ~80 km crater approximately 300 km east of Columbus ("X" in Figure 34q) is predicted to be a site of significant groundwater inflow, but no mineralogical evidence of such hydrological activity is seen. This would be expected if this crater postdated the active hydrological cycle, as is suggested by the lack of erosion of its ejecta blanket, raised crater rim, and central peak. Ignoring this crater, the remaining craters in Figure 27 with the greatest predicted evaporite thicknesses are Columbus and Cross (Figure 34q), consistent with our identification of hydrated sulfates exclusively in these two craters to date.

[80] Nevertheless, the true complexity of the Martian hydrologic cycle cannot be captured in these simple models. For example, the depth of the craters present during the active hydrological cycle is uncertain; many Martian craters appear to have experienced substantial erosion in the Noachian Period, resulting in flat-floored, shallow craters without raised rims [*Craddock and Howard*, 2002]. Some craters may have already been substantially eroded and infilled by the time active sulfate deposition occurred in the Late Noachian to Early Hesperian, while others may have been significantly deeper than their current state. Hydrological activity may have spanned a period of hundreds of millions of years, as evidenced by the presence of large craters interstratified within the Meridiani sulfate deposits [*Edgett and Malin*, 2002], but might not have been continuous. Craters formed during the period of hydrological activity west of Tharsis would have intersected and drawn down the water table in their immediate vicinity, possibly cutting off groundwater flow into nearby craters. In addition, many large craters west of Tharsis (including Columbus) are crossed by graben radial to Tharsis, some of which may date to the Noachian [*Anderson et al.*, 2001]. The faults underlying these graben would have channeled fluids along strike down the slope of the Tharsis rise, potentially enhancing groundwater flux into the craters they intersect, in contrast with the homogeneous and isotropic hydraulic properties assumed in the models. Therefore, the actual sequence of hydrological activity would have been much more complicated than the simple monotonic evolution predicted by the models.

[81] Although our study region west of Tharsis is a preferred location for evaporite formation, the model results suggest that intracrater hydrated mineral deposits should be relatively common in large Noachian-aged craters across much of Mars. In particular, Figures 34h, 34l, and 34p show that evaporite formation is predicted beyond the specific subregion of Terra Sirenum in which we identify hydrated minerals. The restricted distribution observed by CRISM may indicate that the hydrologic-climatic environment in northwest Sirenum was particularly amenable to formation of such deposits, or alternatively conditions here may simply favor the preservation or exposure of deposits that were originally more widespread. Specifically, pervasive dust cover north of ~20°S in this longitude range [*Ruff and Christensen*, 2002] may obscure the bedrock mineralogy north of the area in Figure 27. Likewise, south of ~30°S the Amazonian ice-dust mantle described by *Mustard et al.* [2001] obscures older deposits. West of our study region, a group of larger, interconnected basins experienced a distinct hydrologic history that has been considered in detail elsewhere [*Irwin et al.*, 2002; *Noe Dobrea et al.*, 2008b]. The circum-Tharsis trough to the east has been completely resurfaced by Hesperian lava flows, which would have buried any older evaporites.

[82] In summary, both the general concentration of aqueous deposits in northwest Terra Sirenum and the specific subset of craters with sulfates detected from orbit are consistent with groundwater upwelling predicted by tested hydrologic models, although postdepositional modification of the aqueous deposits has surely also affected their observed distribution. We note that although these models have focused on deposition of evaporitic sulfates, such groundwater activity may also have altered the Noachian crust to form phyllosilicates.

8. Discussion

[83] In this section, we present several hypotheses to explain the observations described above. We focus on Columbus crater but also discuss observations from else-

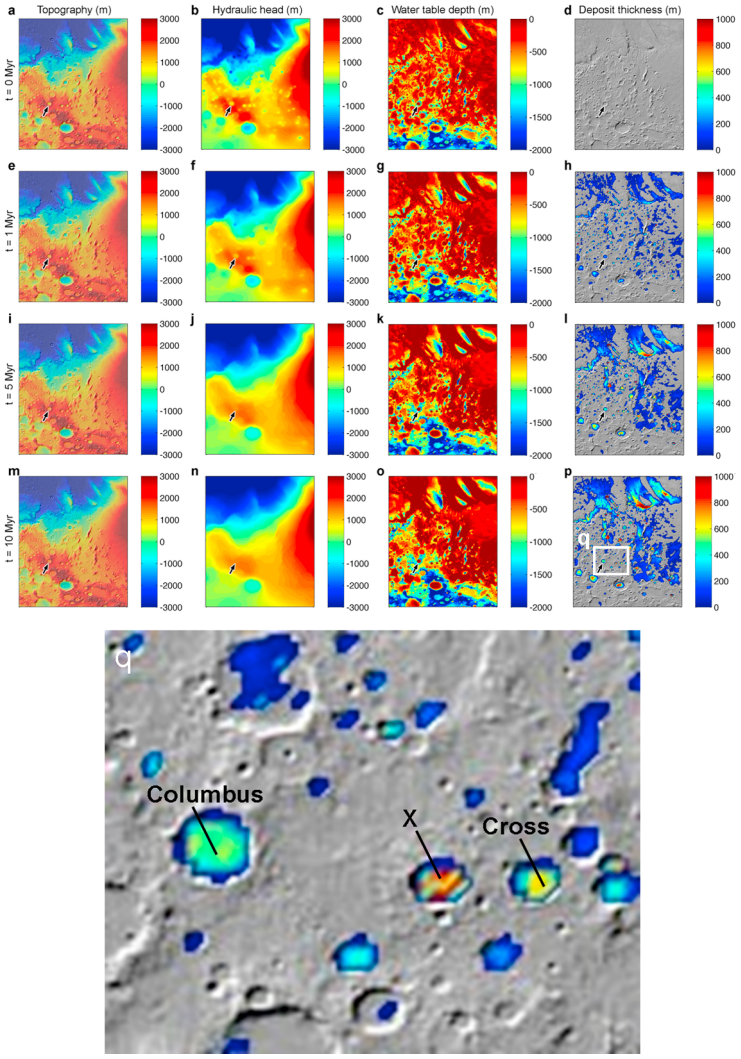

Figure 34. (a–p) Topography, hydraulic head (the elevation of the water table relative to an equipotential), the depth to the water table, and the predicted deposit thickness as a function of time in the hydrological simulations. Results are shown after 0, 1, 5, and 10 Ma of elapsed model time. Columbus crater is indicated by the arrow in each panel. (q) A zoomed view of predicted deposit thicknesses after 10 Ma across the approximate area of northwest Terra Sirenum shown in Figure 27. Crater "X" is predicted to be a site of significant groundwater inflow, but appears morphologically fresh and is interpreted to postdate regional aqueous activity, explaining its lack of observed hydrated minerals.

where in northwest Terra Sirenum. We begin with a summary of key findings and their general implications.

[84] Columbus crater is a Middle-to-Late Noachian-aged crater in a Middle Noachian-aged terrain. It contains layered deposits with diverse hydrous minerals, as do at least ten neighboring craters and small areas of the plains surrounding those craters. These deposits appear to date to the Late Noachian, an epoch during which significant groundwater upwelling and evaporation is predicted in this region, with Columbus being a location of especially significant modeled evaporite deposition. Based on the 50-to-1 water-to-evaporite volume ratio assumed in our hydrologic models (section 7), forming the ~10–20 m thickness of aqueous deposits on the walls and floor of Columbus crater (sections 2.2 and 5) via evaporation would have required ~500–1000 m total depth of water in the crater, integrated over time; this is similar to the ~900 m elevation difference between the modern crater floor and the sulfate ring around the crater walls.

[85] Thermal infrared measurements suggest that the light-toned deposits of Columbus are highly altered, with phyllosilicate and sulfate abundances in the tens of percent by volume. Visual evidence for ongoing physical weathering and erosion of these deposits (Figure 6b and 6d) argues for pervasive alteration throughout the deposits rather than a surficial alteration rind. The specific minerals observed indicate that pH, water activity (a_{H2O}), and possibly redox conditions of the alteration environment varied in space and/or time: Fe/Mg-smectites typically form at circumneutral pH [e.g., *Chevrier et al.*, 2007], whereas localized deposits of jarosite and alunite suggest pH < 3–4 at least locally, based on terrestrial analogs [*Bigham et al.*, 1996; *Fernández-Remolar et al.*, 2005; *Benison et al.*, 2007]. Gypsum on

Mars precipitates at water activity exceeding that of terrestrial seawater (0.98), whereas monohydrated Mg-sulfate precipitates at $a_{H2O} \sim 0.5$ [*Tosca et al.*, 2008a]. Szomolnokite (suggested in section 3.5 to constitute at least part of Columbus's monohydrate) is a ferrous sulfate, whereas ferric sulfates (including jarosite) and oxides/hydroxides are observed elsewhere in Columbus, implying variable redox conditions. Columbus is also one of the few known locations on Mars with interbedded phyllosilicates and sulfates, suggesting episodic changes in environmental conditions or sediment source regions. Whereas most Martian phyllosilicates are detected in apparent isolation from the salts that must have formed with them [*Milliken et al.*, 2009], Columbus crater (perhaps like Gale crater [*Milliken et al.*, 2010]) may retain its full alteration assemblage.

[86] Terrestrial lab experiments require moderate temperatures to convert polyhydrated Mg-sulfate into monohydrate [*Freeman et al.*, 2007] or to form $Fe(OH)SO_4$ from hydrated Fe-sulfates [*Milliken et al.*, 2008; *Swayze et al.*, 2008a; *Morris et al.*, 2009; *Lichtenberg et al.*, 2010]. Therefore it is intriguing that the strongest monohydrate and $Fe(OH)SO_4$ signatures in Columbus crater correspond to one of the freshest ~200 m impact craters on its light-toned deposits (Figure 17a), whose impact event could have provided the heat needed for these mineralogic transitions. However, other monohydrate-bearing outcrops on Columbus's floor have no obvious connection to impact craters; possible origins for these monohydrates are discussed in sections 8.2 and 8.4.

[87] A possible geochemical analog for the deposits of northwest Sirenum is provided by Western Australian acid saline lakes and groundwaters [e.g., *Benison et al.*, 2007; *Baldridge et al.*, 2009; *Story et al.*, 2010]. These playa lakes precipitate halite, gypsum, kaolinite, and ferric oxides, while associated groundwaters precipitate the same minerals in addition to jarosite, alunite, and Fe-bearing phyllosilicates. All of these minerals are identified in Columbus crater, with the single exception of halite, which (like other anhydrous chlorides) has no diagnostic infrared spectral absorptions, and therefore may be difficult to identify unless it occurs in high abundance over large areas [see *Osterloo et al.*, 2008]. The Mg-sulfates likely present in Columbus are missing from many Western Australian lakes, but this could be readily explained by a difference in primary compositions: the bedrock of Western Australia is granitic and gneissic [*Benison et al.*, 2007], whereas the plains outside Columbus (like much of Mars) appear to be basaltic (section 4) and thus more Mg-rich. Terrestrial acid-saline lakes and groundwaters typically exhibit substantial geochemical gradients over relatively short spatial scales, leading to variations in the precipitated minerals reminiscent of those found in Columbus crater [*Baldridge et al.*, 2009].

[88] Although acid-saline lakes precipitate kaolinite directly, elsewhere on Mars kaolinite formation has been attributed to top-down (possibly acid rainfall-driven) weathering [e.g., *Ehlmann et al.*, 2009; *Noe Dobrea and Swayze*, 2010], and some of the intercrater kaolinite in northwest Sirenum may have formed in this way (e.g., Figure 31a). If this weathering predated sulfate formation in Columbus crater (which may have occurred under acidic conditions as proposed for Late Noachian/Early Hesperian Mars globally [*Bibring et al.*, 2006]) then kaolinite could have survived these conditions more effectively than other phyllosilicates (e.g., smectites) due to its greater stability at lower pH [e.g., *Altheide et al.*, 2010b] and its comparatively slow dissolution rate [*Zolotov and Mironenko*, 2007]. However, the finding of kaolinite associated with a possible spring mound or silica-cemented sediments (section 6.2) supports a groundwater- (not surface weathering-) related origin for some Al-phyllosilicates in this region if these clays are authigenic. Indeed, the bright fracture fill observed in some kaolinite-bearing materials in Columbus crater (Figure 7) likely reflects mineralization from subsurface fluids migrating through the fractures [*Okubo et al.*, 2009]. Alteration may have been greatest within the impact craters labeled in Figure 27, in which emergent groundwater could have ponded. The region's Al-phyllosilicates may thus have formed via multiple processes over a range of time.

[89] We will consider the origin of the Sirenum layered deposits in more detail below; for now, we make only the general point that thin, conformable, laterally continuous beds (as are found in Columbus crater; see section 2.2) are commonly cited as evidence for deposition from suspension [e.g., *Wilson et al.*, 2007; *Grant et al.*, 2008], either as marine/lacustrine or air fall sediment. In the case of Holden crater, the additional characteristic of a restricted elevation distribution (as is also observed for Columbus's polyhydrate ring) has been argued to support subaqueous deposition [*Grant et al.*, 2008]. The polygonal fracture patterns observed on sulfate-bearing outcrops in Columbus crater are similar to fracture polygons observed on sulfate-bearing rocks in Meridiani Planum [*McLennan et al.*, 2005], and on chloride- [*Osterloo et al.*, 2008, 2010] and phyllosilicate-bearing [e.g., *Wray et al.*, 2008, 2009b] outcrops across much of Mars. Their preferential occurrence in materials containing aqueous minerals suggests that these polygons formed via desiccation of sediments and/or dehydration of constituent minerals.

[90] Also during the Late Noachian Epoch, groundwater upwelling and evaporation on the other side of Mars may have produced the aqueous deposits in Meridiani Planum [*Andrews-Hanna et al.*, 2007]. These materials share many mineralogic characteristics with those in Columbus crater, including significant abundances of Mg/Ca/Fe-sulfates and secondary aluminosilicates with minor crystalline ferric oxide and possibly Fe-phyllosilicates [*Clark et al.*, 2005; *Glotch et al.*, 2006]. The deposits in both regions also appear to lack carbonates. An apparent difference between Meridiani and Terra Sirenum is the presence of Al-phyllosilicates and Al-sulfates in the latter. Although modest amounts of kaolinite or alunite cannot be excluded by rover analyses of Meridiani rocks [*Clark et al.*, 2005], there is no evidence for either in remote sensing data [e.g., *Poulet et al.*, 2008a]. The dearth of these Al-bearing secondary phases in Meridiani and much of the rest of Mars has been cited as evidence for low water-to-rock ratios in the alteration environments [*Hurowitz and McLennan*, 2007]. The distinctive mineralogy of northwest Sirenum could reflect higher water-to-rock conditions, perhaps facilitated by the presence of large craters in which upwelling groundwater could pond. Similar conditions may have initially been present in Meridiani Planum, with the evidence now buried beneath the extensive younger playa deposits [*Andrews-Hanna et al.*, 2010].

[91] We now consider several hypotheses for the particular sedimentary processes that may have emplaced the layered deposits of northwest Sirenum, with an emphasis on the sulfate-bearing ring around the walls of Columbus crater. We find that most hypotheses conflict with at least some of our observations and/or with other knowledge of Martian geology, with the possible exception of the deep lake hypothesis (section 8.4).

8.1. Hypothesis 1: Columbus Ring as a Preexisting Layer

[92] In general, layered materials at roughly constant elevation around the walls of a crater could indicate impact exposure of preexisting layers in the subsurface. In the case of Columbus crater, we feel this hypothesis is untenable for several reasons.

[93] First, as described in section 5, a degraded D ~17 km crater superposed on Columbus's southwest wall contains polyhydrated sulfate-bearing layered deposits on its floor (Figure 10). These deposits are essentially contiguous with the polyhydrate ring on this portion of the crater wall, implying that the 17 km crater was present before the ring was emplaced. This in turn implies that Columbus crater predates the polyhydrate ring.

[94] Second, impact crater formation affects the geometry of strata exposed in crater walls and rims. Specifically, uplift of a crater rim and subsequent terrace formation via wall slumping along listric faults both cause preexisting strata to be back-tilted (i.e., to dip away from the crater interior) relative to their preimpact geometries [*Melosh*, 1989]. As an example, back-tilted strata are observed in the rim of Endeavour crater in Meridiani Planum, where they are inferred to predate that crater [*Wray et al.*, 2009b]. By contrast, the beds within Columbus crater's polyhydrate ring show the opposite trend, with an average dip direction almost exactly toward the crater interior and no beds observed to dip away from the crater (section 2.2). In addition to these quantitative measurements, images such as Figure 12 give the qualitative impression that the sulfate-bearing beds onlap the crater wall.

[95] Additional shortcomings of the preexisting layer hypothesis include the nondetection of this layer (or any polyhydrated sulfates) at similar (or any) elevations within adjacent craters, and the hypothesis' inability to account for the layered deposits with diverse hydrated minerals on the floors of Columbus and its neighboring craters, which must postdate these craters. Because of these numerous weaknesses, we discard this hypothesis for the sulfate-bearing ring of Columbus crater, while noting that some (but probably not all) kaolinite-bearing materials in Columbus and its neighboring craters might predate these craters.

8.2. Hypothesis 2: Columbus Ring as an Erosional Remnant

[96] Another explanation for the ring planform of polyhydrate-bearing deposits in Columbus crater is that this ring is the erosional remnant of beds that once spanned the entire crater. A variety of processes may have emplaced these beds, although we have argued that their morphologic features in orbital images appear most consistent with deposition from suspension. In this hypothesis, hydrated mineral formation may or may not be coeval with sedimentation; i.e., the sulfates and phyllosilicates could have formed (1) elsewhere and been transported into these craters, (2) during subaqueous sedimentation, or (3) subsequently via diagenesis. A combination of these alternatives is also possible; for comparison, evaporite minerals in the Meridiani Planum sediments are inferred to have formed elsewhere, been modified during deposition in playa lakes, and later experienced multiple episodes of diagenetic overprinting [*McLennan et al.*, 2005].

[97] If hydrated mineral formation predated deposition in the Sirenum craters, then the alteration environment is unknown. However, there is no known plausible source for these sulfates and Al-phyllosilicates elsewhere in the southern highlands [*Wray et al.*, 2009a]. Alunite in particular has been identified nowhere else on Mars to date.

[98] Alternatively, the aqueous minerals in these craters could have formed via diagenesis of layered deposits, which could have initially been composed of relatively unaltered mineral grains. Diagenesis (which likely occurred here, whether or not it produced most of the hydrated minerals) could account for Columbus's trend of polyhydrated sulfate at higher elevations on the crater walls versus monohydrated sulfate below on the crater floor. If all the sulfates were originally polyhydrated, then increased temperatures during burial diagenesis could have enabled conversion to monohydrate in the lowermost layers; this mechanism is one of several proposed to explain the stratification of polyhydrated over monohydrated sulfates in Candor Chasma and other canyons of Valles Marineris [*Murchie et al.*, 2009a]. However, diagenetic formation of all hydrated minerals in Columbus seems unlikely given the alternating kaolinite and sulfate-bearing beds seen in some locations (section 3.2), which are difficult to explain unless these beds originally had strikingly different primary compositions, porosities or permeabilities.

[99] The third possibility (that the hydrated minerals formed in shallow playa lakes coeval with sediment deposition) would be consistent with the playa environments of Meridiani Planum and Western Australia that we have cited as analogs. If Columbus crater was once filled with evaporitic sediments to at least the level of its polyhydrate ring, then these ~900 m of evaporites would have required tens of km total equivalent depth of water to evaporate in the crater over time, according to our model assumptions.

[100] Late Noachian sediments filling Columbus crater would have needed to be almost entirely removed by the Early Hesperian (the age of the probable lava now spanning the crater floor), requiring average erosion rates of at least a few μm/yr. These rates are modest by terrestrial standards, but have not existed globally on Mars since the Noachian, during which they have been attributed to precipitation-driven fluvial processes [e.g., *Craddock and Maxwell*, 1993; *Hynek and Phillips*, 2001]. Such processes could not have removed sediments from Columbus crater, which has no outlet; aeolian erosion and transport is the only conceivable mechanism for sediment removal. Aeolian erosion may be much more efficient for light-toned layered deposits than for typical basaltic surface materials on Mars [*Malin and Edgett*, 2000], and post-Noachian rates up to ~2 μm/yr have indeed been estimated from the lack of small craters on many such deposits [*McEwen et al.*, 2005], although this may overestimate the steady state rate if erosion is accel-

erated following impacts [*Golombek et al.*, 2010]. There is evidence for at least some erosion of light-toned layered deposits on Columbus's floor (Figure 26a and associated discussion in section 5), but the inferred eroded thickness is only a few tens of meters, over an order of magnitude less than that needed to fill the crater to the level of its wall ring.

[101] More broadly, there is strong evidence for substantial erosion of crater-filling layered deposits across Mars; in fact, enough examples are known that an evolutionary sequence can be defined [*Malin and Edgett*, 2000]. It appears that erosion typically begins along the crater walls and then proceeds inward, such that incomplete removal leaves behind intracrater mounds such as those found in Gale and Henry craters [*Malin and Edgett*, 2000]. To our knowledge, no Martian crater other than Columbus exhibits a remnant sedimentary ring along the crater walls instead of a central mound. Therefore, while our understanding of the erosional process(es) is sufficiently poor that we cannot rule out this scenario, it would make Columbus unusual or possibly unique among Martian craters.

8.3. Hypothesis 3: Springline "Tufas"

[102] If the sulfate ring at Columbus is not an erosional remnant of crater-filling sediments, but rather was deposited originally as a ring, then it could be an evaporitic deposit formed when groundwater emerged along an impermeable layer exposed in the crater walls. Carbonate deposits formed in this way on Earth are called perched springline tufa or travertine, where the latter term applies to thermal springs and the former to ambient temperature precipitates [e.g., *Ford and Pedley*, 1996]. In principle, similar processes could occur with sulfate-rich solutions on Mars. Given our interpretation of relatively low formation temperatures for jarosite in Columbus crater and alunite in Cross crater (section 3.6), we adopt the term tufa for the remainder of this discussion.

[103] Terrestrial springline tufas exhibit distributary channels and discontinuous distal fan-shaped deposits, as well as rimmed terraces in the proximal deposits where water has ponded and evaporated [*Pedley*, 1990; *Ford and Pedley*, 1996; *Fouke et al.*, 2000]. None of these features is evident in images of Columbus's light-toned deposits. It is also unclear how the perched springline model could account for the other craters of northwest Sirenum that have laterally continuous hydrated beds spread across their floors, but no preserved ring structures on their walls. Finally, the observation most difficult to reconcile with the springline tufa hypothesis is the presence of light-toned layered deposits in Columbus crater at the summit of the hills near its center, ~700 m above the crater floor (Figures 8c and 8d). CRISM data indicate that these deposits contain polyhydrated sulfates similar to those identified in the beds ringing the crater walls.

[104] Although we cannot rule out a more complex scenario combining springline tufa with other sedimentation and diagenetic processes on the Sirenum crater floors, we now turn to a single hypothesis that could account for all aqueous deposits in Columbus crater.

8.4. Hypothesis 4: Deep Lake(s)

[105] A deep lake filling Columbus crater to at least the level of its preserved sulfate ring could account for sediments deposited on both the crater walls and floor, including the (submerged) hills in Figure 8c. It would explain the lateral continuity and conformability of the intracrater beds, as well as the observed mineralogic sequence of polyhydrated sulfates on the crater walls versus monohydrated on the floor: the latter would have been precipitated after evaporation or freezing had lowered the lake level and yielded a concentrated brine. The observed alternation of clay versus sulfate-bearing beds could reflect alternating periods of lake level rise followed by evaporation. Highly localized deposits of jarosite and possibly alunite on the crater floor could have formed during the final stage of lake evolution in shallow ponds of highly concentrated fluid (Figure 6c may show another example of this), and/or via subsequent diagenesis as in the Western Australian acid saline systems [*Benison et al.*, 2007].

[106] Terrestrial saline lakes and playas commonly display "bathtub ring" patterns of evaporite deposition, with less soluble minerals (e.g., carbonates and/or polyhydrated sulfates) precipitating early on the lake margins and soluble salts (e.g., chlorides) later on the lakebed during the final stages of evaporation [e.g., *Baldridge et al.*, 2004]. Chlorides have not yet been identified on Columbus's floor, but this may be due to (1) the lack of diagnostic infrared spectral absorptions for anhydrous chlorides, (2) burial by younger sediments and Early Hesperian lavas, and/or (3) dissolution during later aqueous or diagenetic episodes. Indeed, multiple aqueous episodes in Columbus are suggested by the intimate association of Ca- and Mg/Fe-sulfates in its polyhydrate ring (section 3.3); in a monotonically evaporating lake, Ca-sulfate would be expected to precipitate early, and Mg/Fe-sulfates later at lower a_{H2O} [*Tosca et al.*, 2008a]. The fact that some outcrops in Columbus with gypsum appear as rugged, relatively high-standing masses compared to adjacent outcrops with only Mg/Fe-sulfate (Figure 6b) could indicate that more soluble Mg/Fe-sulfate has been dissolved from the upper beds during a later aqueous episode, leaving relict gypsum. In general, the minerals identified in Columbus agree reasonably well with those predicted by geochemical models to form in a deep lake on Mars [*Altheide et al.*, 2010a], although widespread kaolinite (if precipitated from lake water) and possible alunite suggest greater dissolved aluminum than is typically assumed for Martian solutions.

[107] The minimum ~900 m depth of the hypothesized Columbus paleolake is equivalent to that required by our hydrologic models (section 7) to form evaporite deposits of the thickness (~10–20 m) observed on the crater walls and floor. This could indicate that the lake was flooded to this level only once; alternatively, the lake may have been maintained or refilled if the salinity and/or clastic sediment fraction were lower than assumed in section 7. For a crater of Columbus's size, this depth implies a paleolake volume of ~6000 km^3, fractionally larger than Earth's Lake Michigan or the inferred Holden crater paleolake on Mars [*Grant et al.*, 2008], although the depth of the Columbus lake would have been several times greater than either. Assuming evaporation (or freezing and sublimation) as the dominant water loss process, Columbus's greater depth would have given it longer life than the Holden paleolake. For a rough estimate of Martian paleolake lifetime, several

authors have assumed terrestrial evaporation rates of ~1–10 m/yr [e.g., *Lewis and Aharonson*, 2006; *Grant et al.*, 2008; *Orofino et al.*, 2009], giving a minimum lifetime of several centuries for Columbus if the lake were filled only once. However, evaporation rates can be lowered by a factor of ~20 for highly concentrated sulfate brines [*Chevrier and Altheide*, 2008], which could greatly prolong the final stages of lake evaporation.

[108] Alternatively, the hypothesized lake in Columbus crater may have been capped by ice. If the Late Noachian climate was similar to that of modern Mars, the surface of a lake would freeze very rapidly; even if emergent groundwater were initially warm, freezing would occur within a few years [*Kreslavsky and Head*, 2002]. Permafrost conditions might have posed challenges for recharge of the groundwater aquifers that we favor as a source of lake water, but a relatively thin, latitudinally restricted, and/or temporary permafrost layer would be consistent with the groundwater model. Pure water lakes on modern Mars would freeze to a depth of hundreds of meters, but under (for example) a 300 mbar atmosphere the ice cover could have been only tens of meters thick [*Squyres*, 1989]. Saline water (as inferred from Columbus's sulfates) would remain liquid at lower temperature, allowing thinner ice in any climate. Water would be lost via ice sublimation at rates typically ~10–100 times slower than evaporation of liquid water [*McKay et al.*, 1985; *Squyres*, 1989], although these rates are strongly temperature-dependent. Detailed thermal models of lakes initially ~1000 m deep yield estimated lifetimes of ~10^5–10^6 years under present Martian conditions [*Moore et al.*, 1995; *Rivera-Valentin et al.*, 2010]; of course, Noachian Mars could have been quite different [e.g., *Craddock and Howard*, 2002].

[109] A deep lake in Columbus crater could have produced concentrated nearshore deposits of sulfate-bearing sediment in several ways. On Earth, lacustrine tufas form near the margins of large, deep lakes; *Zimbelman et al.* [2009] have noted the potential utility of such tufas for identifying the level of Martian paleoshorelines. On Earth these structures (sometimes termed "freshwater reefs") appear to be largely biogenic in origin [*Pedley*, 1990], but abiotic salt precipitation may also be enhanced in shallow water near the shore. In Columbus, crater wall profiles (Figure 4) typically have surface slopes <10° at the elevation of the sulfate ring and up to 20–30° below this level. Evaporites may have accumulated on a shallow water topographic "platform" here when the lake level was just above this point. Greater input of clastic sediment along the lake margins (e.g., from mass wasting or slope wash off the steep upper crater walls) may also have led to thicker and/or more resistant deposits forming there. This effect would have been strongest if the lake were ice covered: many lakes in the Antarctic dry valleys experience summer melting in a narrow "moat" around the lake margins [e.g., *Nedell et al.*, 1987]. Evaporation (and evaporite deposition) would then be limited to this melted zone. Of course, some light-toned layered deposits did also form on Columbus's central floor.

[110] Historically, large paleolakes on Mars have been identified almost exclusively via morphologic criteria, such as inlet or outlet channels, fan/delta deposits, and/or possible shoreline features such as wave-cut terraces [e.g., *Cabrol and Grin*, 1999; *Fassett and Head*, 2008b]. For Columbus crater (and possibly some of the neighboring craters) we propose a groundwater-fed lake, which would not require inlet channels or deltas. As for a shoreline, the break in slope observed at the elevation of Columbus's polyhydrate ring (Figure 4) could be interpreted as an imperfectly preserved shoreline, and the lack of other paleoshorelines recording lower lake levels would be consistent with terrestrial experience that only the high-standing shoreline is well preserved in some paleolakes [*Zimbelman et al.*, 2009]. Of course, terraces are common features of impact craters even on dry bodies such as the Moon (although such slump terraces typically do not have a constant elevation around the crater walls), and where shorelines have been identified previously on Mars, this interpretation is generally not unique [e.g., *Malin and Edgett*, 1999; *Leverington and Maxwell*, 2004]. Furthermore, laboratory experiments [*Lorenz et al.*, 2005] and modeling results [*Kraal et al.*, 2006] suggest that waves needed for shoreline development could not form in the tenuous atmosphere of modern Mars. And if the hypothesized lake in Columbus crater was covered by ice, then terrestrial polar beach analogs suggest that many traditional shoreline morphologies would never have developed [*Rice*, 1994]. Ice push ramparts might have developed at the lake margins, but these are rarely preserved in paleolakes [*Gilbert*, 1890, p. 72].

[111] Even if beach morphologies were once more apparent in Columbus crater, they have been attacked by gradational processes for over three billion years. Columbus is 5 orders of magnitude older than terrestrial paleolakes such as Bonneville [*Gilbert*, 1890] and Lahontan [*Russell*, 1885] to which we often appeal as morphologic analogs. Columbus crater has experienced volcanic resurfacing, tectonics, impacts by ~km-scale bolides, aeolian erosion, and mass wasting since its period of aqueous activity. In contrast, there is little remote sensing evidence for widespread mineralogic alteration (i.e., formation of hydrous minerals) outside the north polar region during much of this time [*Bibring et al.*, 2006; *Murchie et al.*, 2009b]. Therefore, it is not entirely unsurprising that evidence for Noachian/Hesperian paleolakes might be better preserved in their mineralogic stratigraphy than in their morphologic features.

8.5. Astrobiological Implications

[112] If a deep, groundwater-fed paleolake did exist in Columbus crater (or anywhere else on ancient Mars) then such an environment may have been promising for habitability and fossilization of prospective Martian life forms. The detection of gypsum in Columbus crater indicates a high water activity during part of its aqueous history, although other identified salts are consistent with a lower water activity that may have been detrimental to life [*Tosca et al.*, 2008a]. Temperatures might have been low, but hypersaline environments on Earth host organisms capable of growth at temperatures below 0°C [*Niederberger et al.*, 2010]. The acid saline lakes in Western Australia to which we have appealed as possible geochemical analogs are not only inhabited, but contain diverse microbial populations [*Mormile et al.*, 2009]. These lakes preserve microfossils and organic matter within crystals of gypsum and halite [*Benison et al.*, 2008], and similar preservation has been

observed in Mg-sulfate crystals precipitated from groundwater-fed lakes in British Columbia [*Foster et al.*, 2010].

[113] The thick ice covers that may have been present on Martian paleolakes would have presented a challenge for photosynthetic life, as opaque aeolian materials accumulating on the ice would substantially reduce light flux into the lake. Under this scenario, chemosynthetic life may have been more plausible in Martian paleolakes, and from this perspective groundwater-fed lakes may be more promising than those fed by surface runoff. In Earth's Lake Huron, for example, redox gradients between oxygenated lake water and anoxic waters emergent from sinkhole plumes are exploited by sulfate-reducing chemoautotrophs living at depths of <100 m [*Biddanda et al.*, 2006]. Redox gradients between groundwater and the surface/atmosphere have been proposed for ancient Mars [*Hurowitz et al.*, 2010], and terrestrial experience suggests that the interface between these two volatile reservoirs can be a source of chemical energy for life.

8.6. Future Investigations

[114] Future work will enable additional tests of the hypotheses described above. The Mars Odyssey spacecraft has recently transitioned to an early afternoon orbit that will enable higher SNR observations for THEMIS, potentially yielding stronger constraints on the mineralogy of light-toned deposits in Columbus and other Sirenum craters. Expanded CRISM coverage may also lead to the identification of additional minerals; this is especially true for the nine craters other than Columbus and Cross craters marked in Figure 27, which have minimal coverage to date. Our work described here has focused on Columbus crater but has benefited greatly from consideration of the regional context. Future orbital studies of comparable detail focused on craters such as Dejnev or crater E (Figure 27) may lead to evolution of some interpretations made here. Ongoing geochemical and physical modeling of Columbus crater [*Altheide et al.*, 2010a; *Rivera-Valentin et al.*, 2010] will further inform our interpretations.

[115] Many questions about the deposits in Columbus crater could be most effectively answered by a landed mission. High-resolution imaging on the surface could resolve sedimentary textures, stratigraphic contacts and mineralogic boundaries, providing new insights into the depositional and diagenetic history of the light-toned layered deposits. The diverse secondary minerals identified from orbit would allow a rover or sample return mission to probe a range of chemical conditions and explore variations in ancient habitability over space and time.

[116] More broadly, the mere possibility that Columbus crater once hosted a groundwater-fed lake highlights the value of mineralogy for identifying Martian paleolakes. Previous studies have focused on morphologic indicators such as channels and deltas that may provide more definitive evidence for ponded water but that cannot be used to identify groundwater-fed paleolakes. As the CRISM global mapping data set nears completion, broader searches for evaporites in paleolakes will be possible. Exploring the range of evaporites in Martian paleolakes could reveal not only how lake chemistry varied in space and time, but it may also constrain the composition of the ancient Martian atmosphere [e.g., *Moore et al.*, 2010; *Wray et al.*, 2009c].

9. Conclusions

[117] Columbus crater in the Terra Sirenum region of Mars contains light-toned layered deposits with diverse secondary minerals. Gypsum and polyhydrated Mg/Fe-sulfate are found in a discrete ring around the crater walls, and in some locations these sulfates are interbedded with kaolinite. Modeling of thermal emission spectra suggests that abundances of these minerals are in the tens of percent by volume. Crystalline ferric oxide/hydroxide also appears to be eroding from the crater wall ring deposit. Light-toned outcrops on the crater floor contain additional minerals, including monohydrated sulfates, jarosite, and possibly alunite. Additional Al and Fe/Mg phyllosilicates are found in scattered outcrops on the crater walls and floor.

[118] Beds in Columbus's sulfate-bearing ring dip gently toward the crater interior and appear to postdate the crater itself. Some bed surfaces exhibit polygonal fracture patterns, consistent with desiccation or dehydration of constituent minerals. Crater counts suggest that these and the other light-toned deposits in Columbus formed during the Late Noachian Epoch; subsequently, the crater floor was largely resurfaced by a darker, rough-textured deposit that we interpret as Early Hesperian lava flows.

[119] We have surveyed the region surrounding Columbus crater and found that ~10 nearby middle-sized craters also contain layered deposits and/or Al-phyllosilicates, although sulfates have only been found in one of these to date [*Swayze et al.*, 2008b]. The intercrater plains of the region also contain scattered exposures of Al-phyllosilicates and one isolated mound with opaline silica, in addition to more common Fe/Mg-phyllosilicates with chloride salts. The scarcity of fluvial dissection in this region (and around craters such as Columbus in particular) suggests a groundwater origin for the region's aqueous deposits. Regional hydrologic modeling results reported here confirm that Late Noachian groundwater upwelling is a plausible explanation for the evaporites found in Columbus and Cross craters.

[120] Based on these observations, we suggest that a lake of at least ~900 m depth may have occupied Columbus crater during the Late Noachian and that some of the observed minerals may have precipitated out of solution during evaporation or freezing. Geochemical gradients in this hypothesized lake may have been capable of supporting putative chemosynthetic life forms at some point in its existence. Alternatively, the sulfate ring around Columbus's walls could be a springline tufa/travertine-like deposit, or an erosional remnant of layered deposits that once filled the crater, although each of these hypotheses has shortcomings. The possibility of a deep groundwater-fed lake on ancient Mars motivates future spectroscopy-based searches for evaporite deposits in other Martian craters, which would be targets well suited for future in situ investigation.

[121] **Acknowledgments.** We thank S. Mattson and A. Dumke for their efforts producing HiRISE and HRSC DEMs, respectively. Early reviews by J. K. Crowley, G. A. Desborough, and S. A. Wilson Purdy as well as discussions with J. F. Mustard, M. P. Golombek, N. A. Cabrol, J. A.

Grant, D. J. Des Marais, V. F. Chevrier, T. S. Altheide, and S. Karunatillake improved the paper. We thank R. P. Irwin III and an anonymous reviewer for their thorough attention to the manuscript. J.J.W. thanks the Fannie & John Hertz Foundation and the NSF Graduate Research Fellowship for support. We thank the HiRISE and CRISM science and operations teams for acquiring the data most critical to our observations and interpretations.

References

Altheide, T. S., V. F. Chevrier, E. G. Rivera-Valentin, and J. J. Wray (2010a), Geochemical modeling of the evaporation of an ancient paleolake in Columbus crater, Terra Sirenum, Mars, *Lunar Planet. Sci.*, *XLI*, Abstract 2479.

Altheide, T. S., V. F. Chevrier, and E. Noe Dobrea (2010b), Mineralogical characterization of acid weathered phyllosilicates with implications for secondary Martian deposits, *Geochim. Cosmochim. Acta*, *74*, 6232–6248, doi:10.1016/j.gca.2010.08.005.

Anderson, J. H., Jr., and K. A. Wickersheim (1964), Near infrared characterization of water and hydroxyl groups on silica surfaces, *Surf. Sci.*, *2*, 252–260, doi:10.1016/0039-6028(64)90064-0.

Anderson, R. C., J. M. Dohm, M. P. Golombek, A. F. C. Haldemann, B. J. Franklin, K. L. Tanaka, J. Lias, and B. Peer (2001), Primary centers and secondary concentrations of tectonic activity through time in the western hemisphere of Mars, *J. Geophys. Res.*, *106*, 20,563–20,585, doi:10.1029/2000JE001278.

Andrews-Hanna, J. C., R. J. Phillips, and M. T. Zuber (2007), Meridiani Planum and the global hydrology of Mars, *Nature*, *446*(7132), 163–166, doi:10.1038/nature05594.

Andrews-Hanna, J. C., M. T. Zuber, and R. J. Phillips (2008), Early Mars hydrology: Valley networks and evaporites, *Lunar Planet. Sci.*, *XXXIX*, Abstract 1993.

Andrews-Hanna, J. C., M. T. Zuber, R. E. Arvidson, and S. J. Wiseman (2010), Early Mars hydrology: Meridiani playa deposits and the sedimentary record of Arabia Terra, *J. Geophys. Res.*, *115*, E06002, doi:10.1029/2009JE003485.

Ansan, V., et al. (2010), Stratigraphy, mineralogy, and origin of layered deposits inside Terby crater, Mars, *Icarus*, doi:10.1016/j.icarus.2010.09.011, in press.

Arvidson, R. E., F. P. Seelos IV, K. S. Deal, W. C. Koeppen, N. O. Snider, J. M. Kieniewicz, B. M. Hynek, M. T. Mellon, and J. B. Garvin (2003), Mantled and exhumed terrains in Terra Meridiani, Mars, *J. Geophys. Res.*, *108*(E12), 8073, doi:10.1029/2002JE001982.

Baker, V. R. (1982), *The Channels of Mars*, Univ. of Tex. Press, Austin.

Baldridge, A. M., and P. R. Christensen (2006), Detection of the hydration phase of Martian sulfates using emission spectroscopy of magnesium and calcium sulfates, *LPI Contrib.*, *1331*, Abstract 7041.

Baldridge, A. M., J. D. Farmer, and J. E. Moersch (2004), Mars remote-sensing analog studies in the Badwater Basin, Death Valley, California, *J. Geophys. Res.*, *109*, E12006, doi:10.1029/2004JE002315.

Baldridge, A. M., S. J. Hook, J. K. Crowley, G. M. Marion, J. S. Kargel, J. L. Michalski, B. J. Thomson, C. R. de Souza Filho, N. T. Bridges, and A. J. Brown (2009), Contemporaneous deposition of phyllosilicates and sulfates: Using Australian acidic saline lake deposits to describe geochemical variability on Mars, *Geophys. Res. Lett.*, *36*, L19201, doi:10.1029/2009GL040069.

Bandfield, J. L., V. E. Hamilton, and P. R. Christensen (2000), A global view of Martian surface compositions from MGS-TES, *Science*, *287*, 1626–1630, doi:10.1126/science.287.5458.1626.

Barlow, N. G., and C. B. Perez (2003), Martian impact crater ejecta morphologies as indicators of the distribution of subsurface volatiles, *J. Geophys. Res.*, *108*(E8), 5085, doi:10.1029/2002JE002036.

Bell, J. F., III, W. H. Farrand, J. R. Johnson, and R. V. Morris (2002), Low abundance materials at the Mars Pathfinder landing site: An investigation using spectral mixture analysis and related techniques, *Icarus*, *158*, 56–71, doi:10.1006/icar.2002.6865.

Benison, K. C., B. Beitler Bowen, F. E. Oboh-Ikuenobe, E. A. Jagniecki, D. A. LaClair, S. L. Story, M. R. Mormile, and B.-Y. Hong (2007), Sedimentology of acid saline lakes in southern Western Australia: Newly described processes and products of an extreme environment, *J. Sediment. Res.*, *77*, 366–388, doi:10.2110/jsr.2007.038.

Benison, K. C., E. A. Jagniecki, T. B. Edwards, M. R. Mormile, and M. C. Storrie-Lombardi (2008), "Hairy blobs:" Microbial suspects preserved in modern and ancient extremely acid lake evaporites, *Astrobiology*, *8*(4), 807–821, doi:10.1089/ast.2006.0034.

Bibring, J.-P., et al. (2006), Global mineralogical and aqueous Mars history derived from OMEGA/Mars Express data, *Science*, *312*, 400–404, doi:10.1126/science.1122659.

Bibring, J.-P., et al. (2007), Coupled ferric oxides and sulfates on the Martian surface, *Science*, *317*, 1206–1210, doi:10.1126/science.1144174.

Biddanda, B. A., D. F. Coleman, T. H. Johengen, S. A. Ruberg, G. A. Meadows, H. W. Van Sumerem, R. R. Rediske, and S. T. Kendall (2006), Exploration of a submerged sinkhole ecosystem in Lake Huron, *Ecosystems*, *9*, 828–842, doi:10.1007/s10021-005-0057-y.

Bigham, J. M., U. Schwertmann, S. J. Traina, R. L. Winland, and M. Wolf (1996), Schwertmannite and the chemical modeling of iron in acid sulfate waters, *Geochim. Cosmochim. Acta*, *60*, 2111–2121, doi:10.1016/0016-7037(96)00091-9.

Bishop, J. L., and E. Murad (2002), Spectroscopic and geochemical analyses of ferrihydrite from springs in Iceland and applications to Mars, in *Volcano-Ice Interactions on Earth and Mars*, edited by J. L. Smellie and M. G. Chapman, *Geol. Soc. Spec. Publ.*, *202*, 357–370.

Bishop, J. L., and E. Murad (2005), The visible and infrared spectral properties of jarosite and alunite, *Am. Mineral.*, *90*, 1100–1107, doi:10.2138/am.2005.1700.

Bishop, J. L., A. Banin, R. L. Mancinelli, and M. R. Klovstad (2002a), Detection of soluble and fixed NH_4^+ in clay minerals by DTA and IR reflectance spectroscopy: A potential tool for planetary surface exploration, *Planet. Space Sci.*, *50*, 11–19, doi:10.1016/S0032-0633(01)00077-0.

Bishop, J. L., E. Murad, and M. D. Dyar (2002b), The influence of octahedral and tetrahedral cation substitution on the structure of smectites and serpentines as observed through infrared spectroscopy, *Clay Miner.*, *37*, 617–628, doi:10.1180/0009855023740064.

Bishop, J. L., M. D. Dyar, M. D. Lane, and J. F. Banfield (2004), Spectral identification of hydrated sulfates on Mars and comparison with acidic environments on Earth, *Int. J. Astrobiol.*, *3*(4), 275–285, doi:10.1017/S1473550405002259.

Bishop, J. L., M. D. Lane, M. D. Dyar, and A. J. Brown (2008), Reflectance and emission spectroscopy of four groups of phyllosilicates: Smectites, kaolinite-serpentines, chlorites, and micas, *Clay Miner.*, *43*, 35–54, doi:10.1180/claymin.2008.043.1.03.

Bishop, J. L., et al. (2009), Mineralogy of Juventae Chasma: Sulfates in the light-toned mounds, mafic minerals in the bedrock, and hydrated silica and hydroxylated ferric sulfate on the plateau, *J. Geophys. Res.*, *114*, E00D09, doi:10.1029/2009JE003352.

Bishop, J. L., H. D. Makarewicz, W. P. Gates, N. K. McKeown, and T. Hiroi (2010), Beidellites: Spectral properties and importance for Mars, *Lunar Planet. Sci.*, *XLI*, Abstract 2080.

Bridges, N. T., et al. (2010), Aeolian bedforms, yardangs, and indurated surfaces in the Tharsis Montes as seen by the HiRISE Camera: Evidence for dust aggregates, *Icarus*, *205*, 165–182, doi:10.1016/j.icarus.2009.05.017.

Bullock, M. A., and J. M. Moore (2004), Aqueous alteration of Mars-analog rocks under an acidic atmosphere, *Geophys. Res. Lett.*, *31*, L14701, doi:10.1029/2004GL019980.

Burns, R. G. (1993), *Mineralogical Applications of Crystal Field Theory*, 2nd ed., 551 pp., Cambridge Univ. Press, Cambridge, U. K., doi:10.1017/CBO9780511524899.

Cabrol, N. A., and E. A. Grin (1999), Distribution, classification, and ages of Martian impact crater lakes, *Icarus*, *142*, 160–172, doi:10.1006/icar.1999.6191.

Carr, M. C. (1995), The Martian drainage system and the origin of valley networks and fretted channels, *J. Geophys. Res.*, *100*, 7479–7507, doi:10.1029/95JE00260.

Chevrier, V., and T. S. Altheide (2008), Low temperature aqueous ferric sulfate solutions on the surface of Mars, *Geophys. Res. Lett.*, *35*, L22101, doi:10.1029/2008GL035489.

Chevrier, V., F. Poulet, and J.-P. Bibring (2007), Early geochemical environment of Mars as determined from thermodynamics of phyllosilicates, *Nature*, *448*, 60–63, doi:10.1038/nature05961.

Chojnacki, M., and B. M. Hynek (2008), Geological context of water-altered minerals in Valles Marineris, Mars, *J. Geophys. Res.*, *113*, E12005, doi:10.1029/2007JE003070.

Christensen, P. R., et al. (2000), Detection of crystalline hematite mineralization on Mars by the Thermal Emission Spectrometer: Evidence for near-surface water, *J. Geophys. Res.*, *105*, 9623–9642, doi:10.1029/1999JE001093.

Christensen, P. R., et al. (2001a), Mars Global Surveyor Thermal Emission Spectrometer experiment: Investigation description and surface science results, *J. Geophys. Res.*, *106*, 23,823–23,871, doi:10.1029/2000JE001370.

Christensen, P. R., R. V. Morris, M. D. Lane, J. L. Bandfield, and M. C. Malin (2001b), Global mapping of Martian hematite mineral deposits: Remnants of water-driven processes on early Mars, *J. Geophys. Res.*, *106*, 23,873–23,885, doi:10.1029/2000JE001415.

Christensen, P. R., et al. (2004a), The Thermal Emission Imaging System (THEMIS) for the Mars 2001 Odyssey Mission, *Space Sci. Rev.*, *110*, 85–130, doi:10.1023/B:SPAC.0000021008.16305.94.

Christensen, P. R., et al. (2004b), Mineralogy at Meridiani Planum from the Mini-TES experiment on the Opportunity rover, *Science*, *306*, 1733–1739, doi:10.1126/science.1104909.

Clark, B. C., et al. (2005), Chemistry and mineralogy of outcrops at Meridiani Planum, *Earth Planet. Sci. Lett.*, *240*, 73–94, doi:10.1016/j.epsl.2005.09.040.

Clark, R. N. (1999), Spectroscopy of rocks and minerals, and principles of spectroscopy, in *Manual of Remote Sensing*, vol. 3, *Remote Sensing for the Earth Sciences*, edited by A. N. Rencz, pp. 3–58, John Wiley, New York.

Clark, R. N., T. V. V. King, M. Klejwa, G. A. Swayze, and N. Vergo (1990), High spectral resolution reflectance spectroscopy of minerals, *J. Geophys. Res.*, *95*, 12,653–12,680, doi:10.1029/JB095iB08p12653.

Clark, R. N., G. A. Swayze, K. E. Livo, R. F. Kokaly, S. J. Sutley, J. B. Dalton, R. R. McDougal, and C. A. Gent (2003), Imaging spectroscopy: Earth and planetary remote sensing with the USGS Tetracorder and expert systems, *J. Geophys. Res.*, *108*(E12), 5131, doi:10.1029/2002JE001847.

Clark, R. N., et al. (2007), USGS digital spectral library splib06a, *Digital Data Ser.*, *231*, U.S. Geol. Surv., Reston, Va.

Cloutis, E. A., and J. F. Bell III (2000), Diaspores and related hydroxides: Spectral-compositional properties and implications for Mars, *J. Geophys. Res.*, *105*, 7053–7070, doi:10.1029/1999JE001188.

Cloutis, E. A., et al. (2006), Detection and discrimination of sulfate minerals using reflectance spectroscopy, *Icarus*, *184*, 121–157, doi:10.1016/j.icarus.2006.04.003.

Cloutis, E. A., M. S. Rice, J. F. Bell III, S. A. Mertzman, D. L. Bish, and R. Renaut (2009), Spectral reflectance diversity of silica-rich materials: Insights into structure and petrogenesis and implications for Mars, *LPI Contrib.*, *1482*, Abstract 4002.

Craddock, R. A., and A. D. Howard (2002), The case for rainfall on a warm, wet early Mars, *J. Geophys. Res.*, *107*(E11), 5111, doi:10.1029/2001JE001505.

Craddock, R. A., and T. A. Maxwell (1993), Geomorphic evolution of the Martian highlands through ancient fluvial processes, *J. Geophys. Res.*, *98*, 3453–3468, doi:10.1029/92JE02508.

Crowley, J. K. (1991), Visible and near-infrared (0.4–2.5 μm) reflectance spectra of playa evaporite minerals, *J. Geophys. Res.*, *96*, 16,231–16,240, doi:10.1029/91JB01714.

Crowley, J. K., D. E. Williams, J. M. Hammarstrom, N. Piatak, I.-M. Chou, and J. C. Mars (2003), Spectral reflectance properties (0.4–2.5 μm) of secondary Fe-oxide, Fe-hydroxide, and Fe-sulphate-hydrate minerals associated with sulphide-bearing mine wastes, *Geochem. Explor. Environ. Anal.*, *3*, 219–228, doi:10.1144/1467-7873/03-001.

Crumpler, L. (2003), Physical characteristics, geologic setting, and possible formation processes of spring deposits on Mars based on terrestrial analogs, in *Sixth International Conference on Mars, July 20–25, 2003, Pasadena CA* [CD-ROM], *LPI Contrib.*, *1164*, Abstract 3228.

Dehouck, E., N. Mangold, S. Le Mouélic, V. Ansan, and F. Poulet (2010), Ismenius Cavus, Mars: A deep paleolake with phyllosilicate deposits, *Planet. Space Sci.*, *58*, 941–946, doi:10.1016/j.pss.2010.02.005.

Delamere, W. A., et al. (2010), Color imaging of Mars by the High Resolution Imaging Science Experiment (HiRISE), *Icarus*, *205*, 38–52, doi:10.1016/j.icarus.2009.03.012.

Edgett, K. S., and M. C. Malin (2002), Martian sedimentary rock stratigraphy: Outcrops and interbedded craters of northwest Sinus Meridiani and southwest Arabia Terra, *Geophys. Res. Lett.*, *29*(24), 2179, doi:10.1029/2002GL016515.

Ehlmann, B. L., J. F. Mustard, C. I. Fassett, S. C. Schon, J. W. Head, D. J. Des Marais, J. A. Grant, and S. L. Murchie (2008a), Clay minerals in delta deposits and organic preservation potential on Mars, *Nat. Geosci.*, *1*, 355–358, doi:10.1038/ngeo207.

Ehlmann, B. L., et al. (2008b), Orbital identification of carbonate-bearing rocks on Mars, *Science*, *322*, 1828–1832, doi:10.1126/science.1164759.

Ehlmann, B. L., et al. (2009), Identification of hydrated silicate minerals on Mars using MRO-CRISM: Geologic context near Nili Fossae and implications for aqueous alteration, *J. Geophys. Res.*, *114*, E00D08, doi:10.1029/2009JE003339.

Farmer, J. D., and D. J. Des Marais (1999), Exploring for a record of ancient Martian life, *J. Geophys. Res.*, *104*, 26,977–26,995, doi:10.1029/1998JE000540.

Farrand, W. H., T. D. Glotch, J. W. Rice Jr., J. A. Hurowitz, and G. A. Swayze (2009), Discovery of jarosite within the Mawrth Vallis region of Mars: Implications for the geologic history of the region, *Icarus*, *204*, 478–488, doi:10.1016/j.icarus.2009.07.014.

Fassett, C. I., and J. W. Head III (2005), Fluvial sedimentary deposits on Mars: Ancient deltas in a crater lake in the Nili Fossae region, *Geophys. Res. Lett.*, *32*, L14201, doi:10.1029/2005GL023456.

Fassett, C. I., and J. W. Head III (2008a), The timing of Martian valley network activity: Constraints from buffered crater counting, *Icarus*, *195*(1), 61–89, doi:10.1016/j.icarus.2007.12.009.

Fassett, C. I., and J. W. Head III (2008b), Valley network-fed, open-basin lakes on Mars: Distribution and implications for Noachian surface and subsurface hydrology, *Icarus*, *198*, 37–56, doi:10.1016/j.icarus.2008.06.016.

Feely, K. C., and P. R. Christensen (1999), Quantitative compositional analysis using thermal emission spectroscopy: Application to igneous and metamorphic rocks, *J. Geophys. Res.*, *104*, 24,195–24,210, doi:10.1029/1999JE001034.

Fergason, R. L., P. R. Christensen, and H. H. Kieffer (2006), High-resolution thermal inertia derived from the Thermal Emission Imaging System (THEMIS): Thermal model and applications, *J. Geophys. Res.*, *111*, E12004, doi:10.1029/2006JE002735.

Fernández-Remolar, D. C., R. V. Morris, J. E. Gruener, R. Amils, and A. H. Knoll (2005), The Río Tinto Basin, Spain: Mineralogy, sedimentary geobiology, and implications for interpretation of outcrop rocks at Meridiani Planum, Mars, *Earth Planet. Sci. Lett.*, *240*, 149–167, doi:10.1016/j.epsl.2005.09.043.

Ford, T. D., and H. M. Pedley (1996), A review of tufa and travertine deposits of the world, *Earth Sci. Rev.*, *41*, 117–175, doi:10.1016/S0012-8252(96)00030-X.

Forsythe, R. D., and C. R. Blackwelder (1998), Closed drainage basins of the Martian highlands: Constraints on the early Martian hydrologic cycle, *J. Geophys. Res.*, *103*, 31,421–31,431, doi:10.1029/98JE01966.

Foster, I. S., P. L. King, B. C. Hyde, and G. Southam (2010), Characterization of halophiles in natural $MgSO_4$ salts and laboratory enrichment samples: Astrobiological implications for Mars, *Planet. Space Sci.*, *58*, 599–615, doi:10.1016/j.pss.2009.08.009.

Fouke, B. W., J. D. Farmer, D. J. Des Marais, L. Pratt, N. C. Sturchio, P. C. Burns, and M. K. Discipulo (2000), Depositional facies and aqueous-solid geochemistry of travertine-depositing hot springs (Angel Terrace, Mammoth Hot Springs, Yellowstone National Park, U.S.A.), *J. Sediment. Res.*, *70*, 565–585, doi:10.1306/2DC40929-0E47-11D7-8643000102C1865D.

Freeman, J. J., A. Wang, and B. L. Jolliff (2007), Pathways to form kieserite from epsomite at mid to low temperatures, with relevance to Mars, *Lunar Planet. Sci.*, *XXXVIII*, Abstract 1298.

Garvin, J. B., S. E. H. Sakimoto, and J. J. Frawley (2003), Craters on Mars: Global geometric properties from gridded MOLA topography, in *Sixth International Conference on Mars, July 20–25, 2003, Pasadena CA* [CD-ROM], *LPI Contrib.*, *1164*, Abstract 3277.

Gendrin, A., et al. (2005), Sulfates in Martian layered terrains: The OMEGA/Mars Express view, *Science*, *307*, 1587–1591, doi:10.1126/science.1109087.

Gilbert, G. K. (1890), *Lake Bonneville*, *Monogr. U.S. Geol. Surv.*, vol. 1, 438 pp., U.S. Gov. Print. Off., Washington, D. C.

Glotch, T. D., J. L. Bandfield, P. R. Christensen, W. M. Calvin, S. M. McLennan, B. C. Clark, A. D. Rogers, and S. W. Squyres (2006), Mineralogy of the light-toned outcrop at Meridiani Planum as seen by the Miniature Thermal Emission Spectrometer and implications for its formation, *J. Geophys. Res.*, *111*, E12S03, doi:10.1029/2005JE002672.

Glotch, T. D., J. L. Bandfield, L. L. Tornabene, H. B. Jensen, and F. P. Seelos (2010), Distribution and formation of chlorides and phyllosilicates in Terra Sirenum, Mars, *Geophys. Res. Lett.*, *37*, L16202, doi:10.1029/2010GL044557.

Golombek, M., K. Robinson, A. McEwen, N. Bridges, B. Ivanov, L. Tornabene, and R. Sullivan (2010), Constraints on ripple migration at Meridiani Planum from Opportunity and HiRISE observations of fresh craters, *J. Geophys. Res.*, *115*, E00F08, doi:10.1029/2010JE003628.

Grant, J. A., et al. (2008), HiRISE imaging of impact megabreccia and sub-meter aqueous strata in Holden Crater, Mars, *Geology*, *36*, 195–198, doi:10.1130/G24340A.1.

Grant, J. A., S. A. Wilson, E. Noe Dobrea, R. L. Fergason, J. L. Griffes, J. M. Moore, and A. D. Howard (2010), HiRISE views enigmatic deposits in the Sirenum Fossae region of Mars, *Icarus*, *205*, 53–63, doi:10.1016/j.icarus.2009.04.009.

Greeley, R., and P. D. Spudis (1981), Volcanism on Mars, *Rev. Geophys.*, *19*(1), 13–41, doi:10.1029/RG019i001p00013.

Grotzinger, J. P., et al. (2005), Stratigraphy and sedimentology of a dry to wet eolian depositional system, Burns formation, Meridiani Planum, Mars, *Earth Planet. Sci. Lett.*, *240*, 11–72, doi:10.1016/j.epsl.2005.09.039.

Guidry, S. A., and H. S. Chafetz (2003), Anatomy of siliceous hot springs: Examples from Yellowstone National Park, Wyoming, USA, *Sediment. Geol.*, *157*, 71–106, doi:10.1016/S0037-0738(02)00195-1.

Hamilton, V. E., and P. R. Christensen (2005), Evidence for extensive, olivine-rich bedrock on Mars, *Geology*, *33*, 433–436, doi:10.1130/G21258.1.

Handford, C. R. (1991), Marginal marine halite: Sabkhas and salinas, in *Evaporites, Petroleum, and Mineral Resources*, edited by J. L. Melvin, pp. 1–61, Elsevier, New York, doi:10.1016/S0070-4571(08)70259-0.

Hanley, J., V. F. Chevrier, B. L. Davis, T. S. Altheide, and A. Francis (2010), Reflectance spectra of low-temperature chloride and perchlorate hydrates and their relevance to the Martian surface, *Lunar Planet. Sci.*, *XLI*, Abstract 1953.

Hurowitz, J. A., and S. M. McLennan (2007), A ~3.5 Ga record of water-limited, acidic weathering conditions on Mars, *Earth Planet. Sci. Lett.*, *260*, 432–443, doi:10.1016/j.epsl.2007.05.043.

Hurowitz, J. A., W. W. Fischer, N. J. Tosca, and R. E. Milliken (2010), Origin of acidic surface waters and the evolution of atmospheric chemistry on early Mars, *Nat. Geosci.*, *3*, 323–326, doi:10.1038/ngeo831.

Hynek, B. M., and R. J. Phillips (2001), Evidence for extensive denudation of the Martian highlands, *Geology*, *29*, 407–410, doi:10.1130/0091-7613(2001)029<0407:EFEDOT>2.0.CO;2.

Hynek, B. M., M. Beach, and M. R. T. Hoke (2010), Updated global map of Martian valley networks and implications for climate and hydrologic processes, *J. Geophys. Res.*, *115*, E09008, doi:10.1029/2009JE003548.

Irwin, R. P., III, T. A. Maxwell, A. D. Howard, R. A. Craddock, and D. W. Leverington (2002), A large paleolake basin at the head of Ma'adim Vallis, Mars, *Science*, *296*, 2209–2212, doi:10.1126/science.1071143.

Jouglet, D., F. Poulet, R. E. Milliken, J. F. Mustard, J.-P. Bibring, Y. Langevin, B. Gondet, and C. Gomez (2007), Hydration state of the Martian surface as seen by Mars Express OMEGA: 1. Analysis of the 3 μm hydration feature, *J. Geophys. Res.*, *112*, E08S06, doi:10.1029/2006JE002846.

Karunatillake, S., J. J. Wray, S. W. Squyres, G. J. Taylor, O. Gasnault, S. M. McLennan, W. Boynton, M. R. El Maarry, and J. M. Dohm (2009), Chemically striking regions on Mars and Stealth revisited, *J. Geophys. Res.*, *114*, E12001, doi:10.1029/2008JE003303.

Kirk, R. L., et al. (2008), Ultrahigh resolution topographic mapping of Mars with MRO HiRISE stereo images: Meter-scale slopes of candidate Phoenix landing sites, *J. Geophys. Res.*, *113*, E00A24, doi:10.1029/2007JE003000.

Kirkland, L. E., K. C. Herr, and P. M. Adams (2003), Infrared stealthy surfaces: Why TES and THEMIS may miss some substantial mineral deposits on Mars and implications for remote sensing of planetary surfaces, *J. Geophys. Res.*, *108*(E12), 5137, doi:10.1029/2003JE002105.

Klingelhöfer, G., et al. (2004), Jarosite and hematite at Meridiani Planum from Opportunity's Mössbauer Spectrometer, *Science*, *306*, 1740–1745, doi:10.1126/science.1104653.

Kloprogge, J. T. (2006), Spectroscopic studies of synthetic and natural beidellites: A review, *Appl. Clay Sci.*, *31*, 165–179, doi:10.1016/j.clay.2005.10.003.

Kounaves, S. P., et al. (2010), Soluble sulfate in the Martian soil at the Phoenix landing site, *Geophys. Res. Lett.*, *37*, L09201, doi:10.1029/2010GL042613.

Kraal, E. R., E. Asphaug, J. M. Moore, and R. D. Lorenz (2006), Quantitative geomorphic modeling of Martian bedrock shorelines, *J. Geophys. Res.*, *111*, E03001, doi:10.1029/2005JE002567.

Kreslavsky, M. A., and J. W. Head (2002), Fate of outflow channel effluents in the northern lowlands of Mars: The Vastitas Borealis Formation as a sublimation residue from frozen ponded bodies of water, *J. Geophys. Res.*, *107*(E12), 5121, doi:10.1029/2001JE001831.

Kuzmin, R. O., M. V. Mironenko, and N. A. Evdokimova (2009), Spectral and thermodynamic constraints on the existence of gypsum at the Juventae Chasma on Mars, *Planet. Space Sci.*, *57*, 975–981, doi:10.1016/j.pss.2008.12.008.

Lane, M. D. (2007), Mid-infrared emission spectroscopy of sulfate and sulfate-bearing minerals, *Am. Mineral.*, *92*, 1–18, doi:10.2138/am.2007.2170.

Lane, M. D., J. L. Bishop, M. D. Dyar, P. L. King, M. Parente, and B. C. Hyde (2008), Mineralogy of the Paso Robles soils on Mars, *Am. Mineral.*, *93*, 728–739, doi:10.2138/am.2008.2757.

Langevin, Y., F. Poulet, J.-P. Bibring, and B. Gondet (2005), Sulfates in the north polar region of Mars, *Science*, *307*, 1584–1586, doi:10.1126/science.1109091.

Le Deit, L., S. Le Mouélic, O. Bourgeois, J.-P. Combe, D. Mège, C. Sotin, A. Gendrin, E. Hauber, N. Mangold, and J.-P. Bibring (2008), Ferric oxides in East Candor Chasma, Valles Marineris (Mars) inferred from analysis of OMEGA/Mars Express data: Identification and geological interpretation, *J. Geophys. Res.*, *113*, E07001, doi:10.1029/2007JE002950.

Leverington, D. W., and T. A. Maxwell (2004), An igneous origin for features of a candidate crater-lake system in western Memnonia, Mars, *J. Geophys. Res.*, *109*, E06006, doi:10.1029/2004JE002237.

Lewis, K. W., and O. Aharonson (2006), Stratigraphic analysis of the distributary fan in Eberswalde crater using stereo imagery, *J. Geophys. Res.*, *111*, E06001, doi:10.1029/2005JE002558.

Lichtenberg, K. A., et al. (2010), Stratigraphy of hydrated sulfates in the sedimentary deposits of Aram Chaos, Mars, *J. Geophys. Res.*, *115*, E00D17, doi:10.1029/2009JE003353.

Lorenz, R. D., E. R. Kraal, E. E. Eddlemon, J. Cheney, and R. Greeley (2005), Sea-surface wave growth under extraterrestrial atmospheres: Preliminary wind tunnel experiments with application to Mars and Titan, *Icarus*, *175*, 556–560, doi:10.1016/j.icarus.2004.11.019.

Madejová, J., M. Pentrák, H. Pálková, and P. Komadel (2009), Near-infrared spectroscopy: A powerful tool in studies of acid-treated clay minerals, *Vib. Spectrosc.*, *49*, 211–218, doi:10.1016/j.vibspec.2008.08.001.

Malin, M. C., and K. S. Edgett (1999), Oceans or seas in the Martian northern lowlands: High resolution imaging tests of proposed coastlines, *Geophys. Res. Lett.*, *26*(19), 3049–3052, doi:10.1029/1999GL002342.

Malin, M. C., and K. S. Edgett (2000), Sedimentary rocks of early Mars, *Science*, *290*, 1927–1937, doi:10.1126/science.290.5498.1927.

Malin, M. C., et al. (2007), Context Camera Investigation on board the Mars Reconnaissance Orbiter, *J. Geophys. Res.*, *112*, E05S04, doi:10.1029/2006JE002808.

Mangold, N., A. Gendrin, B. Gondet, S. LeMouelic, C. Quantin, V. Ansan, J.-P. Bibring, Y. Langevin, P. Masson, and G. Neukum (2008), Spectral and geological study of the sulfate-rich region of west Candor Chasma, Mars, *Icarus*, *194*, 519–543, doi:10.1016/j.icarus.2007.10.021.

Mangold, N., L. Roach, R. Milliken, S. Le Mouélic, V. Ansan, J.-P. Bibring, P. Masson, J. F. Mustard, S. Murchie, and G. Neukum (2010), A Late Amazonian alteration layer related to local volcanism on Mars, *Icarus*, *207*, 265–276, doi:10.1016/j.icarus.2009.10.015.

McCauley, J. F. (1973), Mariner 9 evidence for wind erosion in the equatorial and mid-latitude regions of Mars, *J. Geophys. Res.*, *78*, 4123–4137, doi:10.1029/JB078i020p04123.

McEwen, A. S., B. S. Preblich, E. P. Turtle, N. A. Artemieva, M. P. Golombek, M. Hurst, R. L. Kirk, D. M. Burr, and P. R. Christensen (2005), The rayed crater Zunil and interpretations of small impact craters on Mars, *Icarus*, *176*, 351–381, doi:10.1016/j.icarus.2005.02.009.

McEwen, A. S., et al. (2007), Mars Reconnaissance Orbiter's High Resolution Imaging Science Experiment (HiRISE), *J. Geophys. Res.*, *112*, E05S02, doi:10.1029/2005JE002605.

McEwen, A. S., L. Tornabene, J. Grant, J. Wray, and J. Mustard (2008), Noachian megabreccia on Mars, *Eos Trans. AGU*, *89*(53), Fall Meet. Suppl., Abstract P43D–03.

McEwen, A. S., et al. (2010), The High Resolution Imaging Science Experiment (HiRISE) during MRO's primary science phase (PSP), *Icarus*, *205*, 2–37, doi:10.1016/j.icarus.2009.04.023.

McGuire, P. C., et al. (2009), An improvement to the volcano-scan algorithm for atmospheric correction of CRISM and OMEGA spectral data, *Planet. Space Sci.*, *57*, 809–815, doi:10.1016/j.pss.2009.03.007.

McKay, C. P., G. D. Clow, R. A. Wharton Jr., and S. W. Squyres (1985), Thickness of ice on perennially frozen lakes, *Nature*, *313*, 561–562, doi:10.1038/313561a0.

McKeown, N. K., J. L. Bishop, E. Z. Noe Dobrea, B. L. Ehlmann, M. Parente, J. F. Mustard, S. L. Murchie, G. A. Swayze, J.-P. Bibring, and E. A. Silver (2009), Characterization of phyllosilicates observed in the central Mawrth Vallis region, Mars, their potential formational processes, and implications for past climate, *J. Geophys. Res.*, *114*, E00D10, doi:10.1029/2008JE003301.

McKeown, N. K., J. L. Bishop, E. Amador, J. Cuadros, S. Hillier, H. D. Makarewicz, M. Parente, and E. A. Silver (2010), Spectral mixtures of clays and their impact on CRISM mineral identifications, *Lunar Planet. Sci.*, *XLI*, Abstract 2510.

McLennan, S. M., et al. (2005), Provenance and diagenesis of the evaporite-bearing Burns formation, Meridiani Planum, Mars, *Earth Planet. Sci. Lett.*, *240*, 95–121, doi:10.1016/j.epsl.2005.09.041.

Melosh, H. J. (1989), *Impact Cratering: A Geologic Process*, 245 pp., Oxford Univ. Press, New York.

Metz, J. M., J. P. Grotzinger, D. Mohrig, R. Milliken, B. Prather, C. Pirmez, A. S. McEwen, and C. M. Weitz (2009), Sublacustrine depositional fans in southwest Melas Chasma, *J. Geophys. Res.*, *114*, E10002, doi:10.1029/2009JE003365.

Milliken, R. E. (2006), Estimating the water content of geologic materials using near-infrared reflectance spectroscopy: Applications to laboratory and spacecraft data, Ph.D. thesis, 404 pp., Brown Univ., Providence, R. I.

Milliken, R. E., and D. L. Bish (2010), Sources and sinks of clay minerals on Mars, *Philos. Mag.*, *90*, 2293–2308, doi:10.1080/14786430903575132.

Milliken, R. E., J. F. Mustard, F. Poulet, D. Jouglet, J.-P. Bibring, B. Gondet, and Y. Langevin (2007), Hydration state of the Martian surface as seen by Mars Express OMEGA II: H_2O content of the surface, *J. Geophys. Res.*, *112*, E08S07, doi:10.1029/2006JE002853.

Milliken, R. E., et al. (2008), Opaline silica in young deposits on Mars, *Geology*, *36*, 847–850, doi:10.1130/G24967A.1.

Milliken, R. E., W. W. Fischer, and J. A. Hurowitz (2009), Missing salts on early Mars, *Geophys. Res. Lett.*, *36*, L11202, doi:10.1029/2009GL038558.

Milliken, R. E., J. P. Grotzinger, and B. J. Thomson (2010), The paleoclimate of Mars as captured by the stratigraphic record in Gale Crater, *Geophys. Res. Lett.*, *37*, L04201, doi:10.1029/2009GL041870.

Möller, P., et al. (1997), Paleofluids and recent fluids in the upper continental crust: Results from the German Continental Deep Drilling Program (KTB), *J. Geophys. Res.*, *102*, 18,233–18,254, doi:10.1029/96JB02899.

Moore, J. M., and A. D. Howard (2005), Large alluvial fans on Mars, *J. Geophys. Res.*, *110*, E04005, doi:10.1029/2004JE002352.

Moore, J. M., G. D. Clow, W. L. Davis, V. C. Gulick, D. R. Janke, C. P. McKay, C. R. Stoker, and A. P. Zent (1995), The circum-Chryse region as a possible example of a hydrologic cycle on Mars: Geologic observations and theoretical evaluation, *J. Geophys. Res.*, *100*, 5433–5447.

Moore, J. M., A. D. Howard, W. E. Dietrich, and P. M. Schenk (2003), Martian layered fluvial deposits: Implications for Noachian climate scenarios, *Geophys. Res. Lett.*, *30*(24), 2292, doi:10.1029/2003GL019002.

Moore, J. M., M. A. Bullock, H. Newsom, and M. Nelson (2010), Laboratory simulations of Mars evaporite geochemistry, *J. Geophys. Res.*, *115*, E06009, doi:10.1029/2008JE003208.

Mormile, M. R., B.-Y. Hong, and K. C. Benison (2009), Molecular analysis of the microbial communities of Mars analog lakes in western Australia, *Astrobiology*, *9*(10), 919–930, doi:10.1089/ast.2008.0293.

Morris, R. V., et al. (2000), Mineralogy, composition, and alteration of Mars Pathfinder rocks and soils: Evidence from multispectral, elemental, and magnetic data on terrestrial analogue, SNC meteorite, and Pathfinder samples, *J. Geophys. Res.*, *105*, 1757–1817, doi:10.1029/1999JE001059.

Morris, R. V., D. C. Golden, D. W. Ming, T. G. Graff, R. E. Arvidson, S. M. Wiseman, K. A. Lichtenberg, and S. Cull (2009), Visible and near-IR reflectance spectra for smectite, sulfate and perchlorate under dry conditions for interpretation of Martian surface mineralogy, *Lunar Planet. Sci.*, *XL*, Abstract 2317.

Mueller, K., and M. Golombek (2004), Compressional structures on Mars, *Annu. Rev. Earth Planet. Sci.*, *32*, 435–464, doi:10.1146/annurev.earth.32.101802.120553.

Murchie, S., et al. (2007), Compact Reconnaissance Imaging Spectrometer for Mars (CRISM) on Mars Reconnaissance Orbiter (MRO), *J. Geophys. Res.*, *112*, E05S03, doi:10.1029/2006JE002682.

Murchie, S., et al. (2009a), Evidence for the origin of layered deposits in Candor Chasma, Mars, from mineral composition and hydrologic modeling, *J. Geophys. Res.*, *114*, E00D05, doi:10.1029/2009JE003343.

Murchie, S. L., et al. (2009b), A synthesis of Martian aqueous mineralogy after 1 Mars year of observations from the Mars Reconnaissance Orbiter, *J. Geophys. Res.*, *114*, E00D06, doi:10.1029/2009JE003342.

Murchie, S. L., et al. (2009c), Compact Reconnaissance Imaging Spectrometer for Mars investigation and data set from the Mars Reconnaissance Orbiter's primary science phase, *J. Geophys. Res.*, *114*, E00D07, doi:10.1029/2009JE003344.

Mustard, J. F., S. Murchie, S. Erard, and J. Sunshine (1997), In situ compositions of Martian volcanics: Implications for the mantle, *J. Geophys. Res.*, *102*, 25,605–25,615, doi:10.1029/97JE02354.

Mustard, J. F., C. D. Cooper, and M. K. Rifkin (2001), Evidence for recent climate change on Mars from the identification of youthful near-surface ground ice, *Nature*, *412*, 411–414, doi:10.1038/35086515.

Mustard, J. F., et al. (2008), Hydrated silicate minerals on Mars observed by the Mars Reconnaissance Orbiter CRISM instrument, *Nature*, *454*, 305–309, doi:10.1038/nature07097.

Nedell, S. S., D. W. Andersen, S. W. Squyres, and F. G. Love (1987), Sedimentation in ice-covered Lake Hoare, Antarctica, *Sedimentology*, *34*, 1093–1106, doi:10.1111/j.1365-3091.1987.tb00594.x.

Neukum, G., and R. Jaumann (2004), HRSC: The High Resolution Stereo Camera of Mars Express, in *Mars Express: The Scientific Payload*, edited by A. Wilson, *Eur. Space Agency Spec. Publ.*, *ESA-SP 1240*, 17–35.

Niederberger, T. D., N. N. Perreault, S. Tille, B. Sherwood Lollar, G. Lacrampe-Couloume, D. Andersen, C. W. Greer, W. Pollard, and L. G. Whyte (2010), Microbial characterization of a subzero, hypersaline methane seep in the Canadian High Arctic, *ISME J.*, *4*(10), 1326–1339, doi:10.1038/ismej.2010.57.

Noe Dobrea, E. Z., and G. Swayze (2010), Acid pedogenesis on Mars? Evidence for top-down alteration on Mars from CRISM and HiRISE data, *Lunar Planet. Sci.*, *XLI*, Abstract 2620.

Noe Dobrea, E. Z., F. Poulet, and M. C. Malin (2008a), Correlations between hematite and sulfates in the chaotic terrain east of Valles Marineris, *Icarus*, *193*, 516–534, doi:10.1016/j.icarus.2007.06.029.

Noe Dobrea, E. Z., J. Moore, A. Howard, D. Catling, and J. Grant (2008b), Spectral and geomorphic evidence for a past inland sea in Eridania Basin, Mars, *Eos Trans. AGU*, *89*(53), Fall Meet. Suppl., Abstract P32B–03.

Noe Dobrea, E. Z., et al. (2010), Mineralogy and stratigraphy of phyllosilicate-bearing and dark mantling units in the greater Mawrth Vallis/west Arabia Terra area: Constraints on geological origin, *J. Geophys. Res.*, *115*, E00D19, doi:10.1029/2009JE003351.

Okubo, C. H., R. A. Schultz, M. A. Chan, G. Komatsu, and HiRISE Team (2009), Deformation band clusters on Mars and implications for subsurface fluid flow, *Geol. Soc. Am. Bull.*, *121*, 474–482, doi:10.1130/B26421.1.

Orofino, V., J. Goldspiel, I. Carofalo, A. Blanco, S. Fonti, and G. A. Marzo (2009), Evaluation of carbonate abundance in putative Martian paleolake basins, *Icarus*, *200*, 426–435, doi:10.1016/j.icarus.2008.11.020.

Osterloo, M. M., V. E. Hamilton, J. L. Bandfield, T. D. Glotch, A. M. Baldridge, P. R. Christensen, L. L. Tornabene, and F. S. Anderson (2008), Chloride-bearing materials in the southern highlands of Mars, *Science*, *319*, 1651–1654, doi:10.1126/science.1150690.

Osterloo, M. M., F. S. Anderson, V. E. Hamilton, and B. M. Hynek (2010), The geologic context of proposed chloride-bearing materials on Mars, *J. Geophys. Res.*, *115*, E10012, doi:10.1029/2010JE003613.

Parente, M. (2008), A new approach to denoising CRISM images, *Lunar Planet. Sci.*, *XXXIX*, Abstract 2528.

Pedley, H. M. (1990), Classification and environmental models of cool freshwater tufas, *Sediment. Geol.*, *68*, 143–154, doi:10.1016/0037-0738(90)90124-C.

Pelkey, S. M., et al. (2007), CRISM multispectral summary products: Parameterizing mineral diversity on Mars from reflectance, *J. Geophys. Res.*, *112*, E08S14, doi:10.1029/2006JE002831.

Phillips, R. J., et al. (2001), Ancient geodynamics and global-scale hydrology on Mars, *Science*, *291*, 2587–2591, doi:10.1126/science.1058701.

Plescia, J. B., and R. S. Saunders (1982), Tectonic history of the Tharsis region, Mars, *J. Geophys. Res.*, *87*, 9775–9791, doi:10.1029/JB087iB12p09775.

Poulet, F., et al. (2005), Phyllosilicates on Mars and implications for early Martian climate, *Nature*, *438*, 623–627.doi:10.1038/nature04274.

Poulet, F., J.-P. Bibring, B. Gondet, Y. Langevin, J. Mustard, N. Mangold, V. Chevrier, and A. Gendrin (2007), Discovery, mapping and mineralogy of phyllosilicates on Mars by MEx-OMEGA: A reappraisal, *LPI Contrib.*, *1353*, Abstract 3170.

Poulet, F., R. E. Arvidson, C. Gomez, R. V. Morris, J.-P. Bibring, Y. Langevin, B. Gondet, and J. Griffes (2008a), Mineralogy of Terra Meridiani and western Arabia Terra from OMEGA/MEx and implications for their formation, *Icarus*, *195*, 106–130, doi:10.1016/j.icarus.2007.11.031.

Poulet, F., N. Mangold, D. Loizeau, J.-P. Bibring, Y. Langevin, J. Michalski, and B. Gondet (2008b), Abundance of minerals in the phyllosilicate-rich units on Mars, *Astron. Astrophys.*, *487*, L41–L44, doi:10.1051/0004-6361:200810150.

Presley, M. A., and P. R. Christensen (1997), Thermal conductivity measurements of particulate materials: 2. Results, *J. Geophys. Res.*, *102*, 6551–6566, doi:10.1029/96JE03303.

Putzig, N. E., and M. T. Mellon (2007), Apparent thermal inertia and the surface heterogeneity of Mars, *Icarus*, *191*, 68–94, doi:10.1016/j.icarus.2007.05.013.

Putzig, N. E., M. T. Mellon, K. A. Kretke, and R. E. Arvidson (2005), Global thermal inertia and surface properties of Mars from the MGS mapping mission, *Icarus*, *173*, 325–341, doi:10.1016/j.icarus.2004.08.017.

Ramsey, M. S., and P. R. Christensen (1998), Mineral abundance determination: Quantitative deconvolution of thermal emission spectra, *J. Geophys. Res.*, *103*, 577–596, doi:10.1029/97JB02784.

Rathbun, J. A., and S. W. Squyres (2002), Hydrothermal systems associated with Martian impact craters, *Icarus*, *157*, 362–372, doi:10.1006/icar.2002.6838.

Rice, J. W., Jr. (1994), Terrestrial polar beach processes: Martian paleolake analogs, *Lunar Planet. Sci.*, *XXV*, 1125–1126.

Rivera-Valentin, E. G., R. Ulrich, V. F. Chevrier, T. S. Altheide, and J. J. Wray (2010), Dynamic modeling of Martian paleolake stability, *Lunar Planet. Sci.*, *XLI*, Abstract 1446.

Roach, L. H., J. F. Mustard, S. L. Murchie, J.-P. Bibring, F. Forget, K. W. Lewis, O. Aharonson, M. Vincendon, and J. L. Bishop (2009), Testing evidence of recent hydration state change in sulfates on Mars, *J. Geophys. Res.*, *114*, E00D02, doi:10.1029/2008JE003245.

Roach, L. H., J. F. Mustard, G. Swayze, R. E. Milliken, J. L. Bishop, S. L. Murchie, and K. Lichtenberg (2010a), Hydrated mineral stratigraphy of Ius Chasma, Valles Marineris, *Icarus*, *206*, 253–268, doi:10.1016/j.icarus.2009.09.003.

Roach, L. H., J. F. Mustard, M. D. Lane, J. L. Bishop, and S. L. Murchie (2010b), Diagenetic hematite and sulfate assemblages in Valles Marineris, *Icarus*, *207*, 659–674, doi:10.1016/j.icarus.2009.11.029.

Rogers, A. D., J. L. Bandfield, and P. R. Christensen (2007), Global spectral classification of Martian low-albedo regions with Mars Global Surveyor Thermal Emission Spectrometer (TES) data, *J. Geophys. Res.*, *112*, E02004, doi:10.1029/2006JE002726.

Rossi, A. P., G. Neukum, M. Pondrelli, S. van Gasselt, T. Zegers, E. Hauber, A. Chicarro, and B. Foing (2008), Large-scale spring deposits on Mars?, *J. Geophys. Res.*, *113*, E08016, doi:10.1029/2007JE003062.

Ruff, S. W., and P. R. Christensen (2002), Bright and dark regions on Mars: Particle size and mineralogical characteristics based on Thermal Emission Spectrometer data, *J. Geophys. Res.*, *107*(E12), 5127, doi:10.1029/2001JE001580.

Ruff, S. W., P. R. Christensen, R. N. Clark, H. H. Kieffer, M. C. Malin, J. L. Bandfield, B. M. Jakosky, M. D. Lane, M. T. Mellon, and M. A. Presley (2001), Mars' "White Rock" feature lacks evidence of an aqueous origin: Results from Mars Global Surveyor, *J. Geophys. Res.*, *106*, 23,921–23,927, doi:10.1029/2000JE001329.

Russell, I. C. (1885), *Geological History of Lake Lahontan, A Quaternary Lake of Northwestern Nevada*, *Monogr. U.S. Geol. Surv.*, vol. 11, 288 pp., U.S. Gov. Print. Off., Washington, D. C.

Scott, D. H., and K. L. Tanaka (1986), Geologic map of the western equatorial region of Mars, *U.S. Geol. Surv. Misc. Invest. Map*, *I-1802-A*.

Seelos, K. D., R. E. Arvidson, B. L. Jolliff, S. M. Chemtob, R. V. Morris, D. W. Ming, and G. A. Swayze (2010), Silica in a Mars analog environment: Ka'u Desert, Kilauea Volcano, Hawaii, *J. Geophys. Res.*, *115*, E00D15, doi:10.1029/2009JE003347.

Segura, T. S., O. B. Toon, A. Colaprete, and K. Zahnle (2002), Environmental effects of large impacts on Mars, *Science*, *298*, 1977–1980, doi:10.1126/science.1073586.

Skok, J. R., J. F. Mustard, B. L. Ehlmann, R. E. Milliken, and S. L. Murchie (2010), Silica deposits in the Nili Patera caldera on the Syrtis Major volcanic complex on Mars, *Nat. Geosci.*, *3*, 838–841, doi:10.1038/ngeo990.

Smith, D. E., et al. (1999), The global topography of Mars and implications for surface evolution, *Science*, *284*, 1495–1503, doi:10.1126/science.284.5419.1495.

Smith, D. E., et al. (2001), Mars Orbiter Laser Altimeter: Experiment summary after the first year of global mapping of Mars, *J. Geophys. Res.*, *106*, 23,689–23,722, doi:10.1029/2000JE001364.

Soderblom, L. A., et al. (2004), Soils of eagle crater and Meridiani Planum at the Opportunity Rover landing site, *Science*, *306*, 1723–1726, doi:10.1126/science.1105127.

Squyres, S. W. (1989), Urey prize lecture: Water on Mars, *Icarus*, *79*, 229–288, doi:10.1016/0019-1035(89)90078-X.

Squyres, S. W., et al. (2004a), The Spirit Rover's Athena Science Investigation at Gusev Crater, Mars, *Science*, *305*, 794–799, doi:10.1126/science.3050794.

Squyres, S. W., et al. (2004b), In situ evidence for an ancient aqueous environment at Meridiani Planum, Mars, *Science*, *306*, 1709–1714, doi:10.1126/science.1104559.

Squyres, S. W., et al. (2006), Rocks of the Columbia Hills, *J. Geophys. Res.*, *111*, E02S11, doi:10.1029/2005JE002562.

Squyres, S. W., et al. (2008), Detection of silica-rich deposits on Mars, *Science*, *320*, 1063–1067, doi:10.1126/science.1155429.

Stockstill, K. R., J. E. Moersch, S. W. Ruff, A. Baldridge, and J. Farmer (2005), Thermal emission spectrometer hyperspectral analyses of proposed paleolake basins on Mars: No evidence for in-place carbonates, *J. Geophys. Res.*, *110*, E10004, doi:10.1029/2004JE002353.

Stockstill, K. R., J. E. Moersch, H. Y. McSween Jr., J. Piatek, and P. R. Christensen (2007), TES and THEMIS study of proposed paleolake basins within the Aeolis quadrangle of Mars, *J. Geophys. Res.*, *112*, E01001, doi:10.1029/2005JE002517.

Story, S., B. Beitler Bowen, K. C. Benison, and D. G. Schulze (2010), Authigenic phyllosilicates in modern acid saline lake sediments and implications for Mars, *J. Geophys. Res.*, *115*, E12012, doi:10.1029/2010JE003687.

Swayze, G. A. (2004), Using reflectance spectroscopy to evaluate minerals of environmental concern, in *Infrared Spectroscopy in Geochemistry, Exploration Geochemistry, and Remote Sensing*, edited by P. L. King et al., pp. 181–196, Mineral. Assoc. Can., London, Ont.

Swayze, G. A., R. N. Clark, S. J. Sutley, C. A. Gent, B. W. Rockwell, D. L. Blaney, J. L. Post, and B. P. Farm (2002), Mineral mapping Mauna Kea and Mauna Loa shield volcanos on Hawaii using AVIRIS data and the USGS Tetracorder spectral identification system: Lessons applicable to the search for relict Martian hydrothermal systems, in *Proceedings of the 11th JPL Airborne Earth Science Workshop*, edited by R. O. Green, *JPL Publ. 03–4*, 373–387.

Swayze, G. A., G. A. Desborough, K. S. Smith, H. A. Lowers, J. M. Hammarstrom, S. F. Diehl, R. W. Leinz, and R. L. Driscoll (2008a), Understanding jarosite—From mine waste to Mars, in *Understanding Contaminants Associated With Mineral Deposits*, edited by P. L. Verplanck, *U.S. Geol. Surv. Circ. 1328*, 8–13.

Swayze, G. A., et al. (2008b), Discovery of the acid-sulfate mineral alunite in Terra Sirenum, Mars, using MRO CRISM: Possible evidence for acid-saline lacustrine deposits?, *Eos Trans. AGU*, *89*(53), Fall Meet. Suppl., Abstract P44A–04.

Tanaka, K. L. (1986), The stratigraphy of Mars, *J. Geophys. Res.*, *91*, E139–E158, doi:10.1029/JB091iB13p0E139.

Tosca, N. J., S. M. McLennan, D. H. Lindsley, and M. A. A. Schoonen (2004), Acid-sulfate weathering of synthetic Martian basalt: The acid fog model revisited, *J. Geophys. Res.*, *109*, E05003, doi:10.1029/2003JE002218.

Tosca, N. J., S. M. McLennan, B. C. Clark, J. P. Grotzinger, J. A. Hurowitz, A. H. Knoll, C. Schröder, and S. W. Squyres (2005), Geochemical modeling of evaporation processes on Mars: Insight from the sedimentary record at Meridiani Planum, *Earth Planet. Sci. Lett.*, *240*, 122–148, doi:10.1016/j.epsl.2005.09.042.

Tosca, N. J., A. H. Knoll, and S. M. McLennan (2008a), Water activity and the challenge for life on early Mars, *Science*, *320*, 1204–1207, doi:10.1126/science.1155432.

Tosca, N. J., R. E. Milliken, and F. M. Michel (2008b), Smectite formation on early Mars: Experimental constraints, *LPI Contrib.*, *1441*, Abstract 7030.

Vaniman, D. T., D. L. Bish, S. J. Chipera, C. I. Fialips, J. W. Carey, and W. C. Feldman (2004), Magnesium sulphate salts and the history of water on Mars, *Nature*, *431*, 663–665, doi:10.1038/nature02973.

Weitz, C. M., M. D. Lane, M. Staid, and E. Noe Dobrea (2008), Gray hematite distribution and formation in Ophir and Candor chasmata, *J. Geophys. Res.*, *113*, E02016, doi:10.1029/2007JE002930.

Weitz, C. M., R. E. Milliken, J. A. Grant, A. S. McEwen, R. M. E. Williams, J. L. Bishop, and B. J. Thomson (2010), Mars Reconnaissance Orbiter observations of light-toned layered deposits and associated fluvial landforms on the plateaus adjacent to Valles Marineris, *Icarus*, *205*, 73–102, doi:10.1016/j.icarus.2009.04.017.

Wilson, S. A., A. D. Howard, J. M. Moore, and J. A. Grant (2007), Geomorphic and stratigraphic analysis of Crater Terby and layered deposits north of Hellas basin, Mars, *J. Geophys. Res.*, *112*, E08009, doi:10.1029/2006JE002830.

Wray, J. J., B. L. Ehlmann, S. W. Squyres, J. F. Mustard, and R. L. Kirk (2008), Compositional stratigraphy of clay-bearing layered deposits at Mawrth Vallis, Mars, *Geophys. Res. Lett.*, *35*, L12202, doi:10.1029/2008GL034385.

Wray, J. J., S. L. Murchie, S. W. Squyres, F. P. Seelos, and L. L. Tornabene (2009a), Diverse aqueous environments on ancient Mars revealed in the southern highlands, *Geology*, *37*, 1043–1046, doi:10.1130/G30331A.1.

Wray, J. J., E. Z. Noe Dobrea, R. E. Arvidson, S. M. Wiseman, S. W. Squyres, A. S. McEwen, J. F. Mustard, and S. L. Murchie (2009b), Phyllosilicates and sulfates at Endeavour Crater, Meridiani Planum, Mars, *Geophys. Res. Lett.*, *36*, L21201, doi:10.1029/2009GL040734.

Wray, J. J., R. Milliken, G. A. Swayze, B. L. Ehlmann, C. M. Dundas, A. M. Baldridge, J. C. Andrews-Hanna, and S. L. Murchie (2009c), Evaporites in Martian Paleolakes: Observations and implications, *Eos Trans. AGU*, *90*(52), Fall Meet. Suppl., Abstract P41B–06.

Wray, J. J., S. W. Squyres, L. H. Roach, J. L. Bishop, J. F. Mustard, and E. Z. Noe Dobrea (2010), Identification of the Ca-sulfate bassanite in Mawrth Vallis, Mars, *Icarus*, *209*, 416–421, doi:10.1016/j.icarus.2010.06.001.

Yen, A. S., et al. (2008), Hydrothermal processes at Gusev Crater: An evaluation of Paso Robles class soils, *J. Geophys. Res.*, *113*, E06S10, doi:10.1029/2007JE002978.

Zimbelman, J. R., W. B. Garry, and R. P. Irwin III (2009), Precision topography of pluvial features in western Nevada as analogs for possible pluvial landforms on Mars, *Lunar Planet. Sci.*, *XL*, Abstract 1370.

Zolotov, M. Y., and M. V. Mironenko (2007), Formation and fate of phyllosilicates on the surface of Mars: Geochemical modeling of aqueous weathering, *LPI Contrib.*, *1353*, Abstract 3365.

J. C. Andrews-Hanna, Department of Geophysics, Colorado School of Mines, Golden, CO 80401, USA.

A. M. Baldridge, Jet Propulsion Laboratory, California Institute of Technology, Pasadena, CA 91109, USA.

J. L. Bishop, SETI Institute, 189 Bernardo Ave., Ste. 100, Mountain View, CA 94043, USA.

M. Chojnacki, Department of Earth and Planetary Sciences, University of Tennessee, Knoxville, TN 37996, USA.

R. N. Clark and G. A. Swayze, U.S. Geological Survey, Denver, CO 80225, USA.

C. M. Dundas, Lunar and Planetary Laboratory, University of Arizona, Tucson, AZ 85721, USA.

B. L. Ehlmann, Institut d'Astrophysique Spatiale, Université Paris Sud, F-91405 Orsay, France.

R. E. Milliken, Department of Civil Engineering and Geological Sciences, University of Notre Dame, Notre Dame, IN 46556, USA.

S. L. Murchie and F. P. Seelos, Johns Hopkins University Applied Physics Laboratory, Laurel, MD 20723, USA.

S. W. Squyres and J. J. Wray, Department of Astronomy, Cornell University, Ithaca, NY 14853, USA. (jwray@astro.cornell.edu)

L. L. Tornabene, Center for Earth and Planetary Studies, National Air and Space Museum, Smithsonian Institution, PO Box 37012, Washington, DC 20024, USA.